STATE UNIVERSITY OF NEW YORK COLLEGE OF CERAMICS

at Alfred University
Alfred, New York

SEMICONDUCTING MATERIALS

Final Report

PART II
AN INVESTIGATION OF THE BORON-PHOSPHOROUS SYSTEM

Contract Nonr 1503(01)
Project NR 015 215

Office of Naval Research
Physics Branch (Code 421)
Washington, D. C.

SEMICONDUCTING MATERIALS

FINAL REPORT, PART II -- AN INVESTIGATION OF THE BORON-PHOSPHOROUS SYSTEM (G. I. Post)

15 January 1965

Alfred University, Alfred, New York

Personnel associated with this program are as follows:

1. Project Director, Thomas J. Gray, Professor of Physical Chemistry; Administrator, Office of Research, State University of New York College of Ceramics at Alfred University

2. Graduate Research Fellows:

   Glenn I. Post, B.S., M.S. (now with Martin Company, Baltimore, Maryland); will receive Ph.D. in June 1965.

   Lyle H. Slack, B.S. (now with Bell Telephone Laboratories, Murray Hill, New Jersey); will receive Ph.D. in June 1965.

   Donald Guile, B.S. (now with Corning Glass Works, Research Laboratories, Corning, New York); will receive Ph.D. in June 1965.

Graduate students who have earned their doctorates on this contract are:

1. John L. Stull, Associate Professor of Physics, Department of Physics, Alfred University, Alfred, New York.

2. Clyde E. McNeilly, Jr., Plutonium Fuels Research (GE), Hanford, Washington

3. George T. Lewis, National Aeronautics and Space Administration, Instrumentation and Electronic Systems Division, Houston, Texas.

This report was prepared under the sponsorship of the United States Navy through the Office of Naval Research, Contract Nonr 1503(01), Project NR 015 215.

TABLE OF CONTENTS

TABLE OF CONTENTS

TABLE OF CONTENTS

TABLE OF CONTENTS

TABLE OF CONTENTS

LIST OF TABLES

LIST OF TABLES

LIST OF FIGURES AND ILLUSTRATIONS

LIST OF FIGURES AND ILLUSTRATIONS

LIST OF FIGURES AND ILLUSTRATIONS

LIST OF FIGURES AND ILLUSTRATIONS

LIST OF FIGURES AND ILLUSTRATIONS

ABSTRACT

Hot-pressing of BP was used to prepare polycrystalline samples in the boron-phosphorous system. Hot-pressed samples containing up to 24% carbon were also prepared and their properties analyzed.

A study of the effect of hot-pressing variables on composition and properties was made. A comprehensive analysis was made of compounds, phases, compositions, grain size, and impurity content.

A series of compositions, including pure $B_{13}P_2$, was examined for Knoop hardness, electrical conductivity, activation energies, thermal conductivity, thermoelectric power, density, Hall effect, and magnetoresistance.

An extensive review of the literature relates the properties measured in the boron-phosphorous system to those of other $B_{12}A$, $B_{12}A_2$, and $B_{12}A_3$ type compounds where A equals one or more p-orbital elements including boron.

The value of hot-pressed samples in the boron-phosphorous-carbon system for thermoelectric applications was measured and reviewed.

The electrical conductivity in $B_{13}P_2$ was measured and a mechanism for conduction based on extrinsic levels and a surface effect is proposed. A theoretical model for understanding the physical aspects of this system is presented.

Sufficient evidence of the existence of $B_{10}P$ was obtained to warrant further study.

A correlation between composition and physical properties was established.

I. INTRODUCTION

A. Origin of the Problem

In February 1958, a sample of boron monophosphide (BP) was supplied by The Monsanto Company for hot-pressing. After several attempts, each at a higher temperature, very hard black compacts were obtained by hot-pressing at 2000°C. Ten pressings were made by the author. At first inspection, the hot-pressed product was very hard, had low electrical resistance, and could withstand temperatures above 1200°C.

A study of hot-pressed samples of a number of potentially valuable materials, including the boron monophosphide (BP) was started for The Monsanto Company in September 1958. Reports by Holden (87) on this work indicatedthat at least five more samples were prepared which had variable composition, color, and hardness. X-ray evidence indicated the presence of a phase, probably B_6P. One other sample proved later to be a mixture of boron phosphates (BPO_4).

Some samples seemed to be good thermoelectric sources and appeared to exhibit semiconducting characteristics, while other samples had almost metallic conductivity. The material proved to be a high temperature ceramic which evolved phosphorous below temperatures suitable for compaction.

Holden found that one of the samples had a Knoop (100 gram load) hardness value of 3200 kg/mm^2. The Monsanto Company reported that a value between 6500 kg/mm^2 and 7000 kg/mm^2 had been measured. Some of the samples were quite brittle, others were not.

Only a preliminary evaluation of boron phosphide was made by Holden since other materials were included in his study.

Subsequently, Buchanan (19) and Erikson (45) used some of the early samples for thermoelectric measurements. Exceptional thermoelectric figure of merit values were obtained because of an unusually large thermoelectric power which entered into the equation for figure of merit as a square term. These were so high as to be suspect.

The material produced by hot-pressing boron monophosphide (BP) was proposed as the subject of this study. The study was to be directed at solving some of the more obvious problems associated with the prior work.

Since both boron and boron monophosphide are known semiconductors with broad band gaps (B = 2.0 ev, BP = 5.9 ev), the introduction of impurities or polycrystallinity should produce modifications ranging from those having the full band gap to metallic conduction. With this possible range of conduction and of resulting properties, the products of decomposition of boron monophosphide are certainly worthy of investigation.

B. The Problem

The problem selected was that of the evaluation of compositions in the boron-phosphorous system as electrical conductors, thermoelectric elements, and abrasives with particular attention to the properties of pure boron subphosphide ($B_{13}P_2$) and the role of carbon as the major impurity.

In order to investigate the products of hot-pressed boron monophosphide, it was most efficient to identify smaller problems which could be handled invidually. These are presented next with an indication of the general approach used. These problems and the answers obtained are reconsidered in the section dealing with the Discussion of Results.

The investigation was begun with a review of previous work. Information on boron, the boron-carbon system, the boron-phosphorous system, and related higher borides was assembled, and an attempt was made to determine what to expect in the nature of compounds and their properties.

The specific contributions to understanding the properties of the boron-phosphorous system are:

1. Several series of hot-pressed samples were prepared by varying the pressing temperature, time, and phosphorous content. The analysis of what compounds, phases, and crystal structures were present in the hot-pressed compacts was made

by X-ray diffraction, chemical analysis, and microscopy. Both a reflecting microscope and an electron microscope were used. A description of arrangement, shapes, and sizes of the materials present was formulated.

2. The relationship between compositions and conditions of preparation was examined to learn how to ensure reproducible products. This had to be done in such a way as to control impurities and ensure maximum densities so that samples suitable for further testing could be produced.

3. Early hardness tests indicated that phosphide-containing compacts were extremely hard. Microhardness determinations were made to establish the relative hardness values of boron subphosphide and boron carbide. The results were analyzed and explained.

4. The products obtained by hot-pressing boron monophosphide were examined for possible use as a thermoelectric element. This was done by determining the figure of merit for the material. Prior figure of merit values were then evaluated on the basis of the results of this study.

5. The character of the electrical conductivity in the hot-pressed compacts was also a subject of study. Information available from other studies suggested a possible mechanism for the conductivity results.

6. A method suitable for the preparation of $B_{13}P_2$ with total impurities below 0.1% was found. Properties of the pure $B_{13}P_2$ were measured and compared to those of BP, $B_{13}C_2$, and $B_{12}C_3$.

The approach to these problems was fourfold, beginning with a study of preparation techniques. The study of composition and structure was followed by the measurement of thermal and electrical properties. The information gathered was correlated and suggestions made for subsequent investigations.

C. Conventions

At this point, a clarification of the compounds and the names used for them in this study is in order. The compound BP and the name boron monophosphide are used interchangeably. When speaking of an exact ratio in the boron-phosphorous system, the formula will be used. For example, $B_{13}P_2$ refers to a compound of that ratio. The name boron subphosphide will be used for a more inexact composition represented by $B_{13}P_{2-\alpha}$ or $B_{12}P_{\alpha}B_{\beta}$. The term boron subphosphide then represents a range of boron to phosphorous ratios around the ratio shown.

Similarly, with the boron-carbon system, the term boron subcarbide will represent the range $B_{13}C_{2-\alpha}$. The exact composition will be given as $B_{12}C$ or $B_{13}C_2$. Here, however, common usage dictates that the familiar name boron carbide be retained to designate the approximate ratio B_4C ($B_{12}C_3$).

The term, "borostitial", is employed to designate the combination of the B_{12} lattice and the inserted p-orbital elements. This combination forms interstitial boron compounds of inexact composition represented by $B_{12}A_{\alpha}B_{\beta}$ where B indicates that boron is also an interstitial element.

The term, "interstitial", is used throughout this study to refer to atoms placed in the interstices between the boron icosahedra. Three interstitial sites may be occupied in each unit cell by atoms which bond to the boron icosahedra and to each other. Variations in expected combining ratios indicate that vacant sites occur.

In preparing sample numbers, a convention was adopted to distinguish the source of the sample by its first letter. For example, R-21 indicates the twenty-first sample prepared by "reaction" from the elements. A designation, D-16 indicates the sixteenth "decomposition" of BP to give a boron subphosphide. A sample number P-70 would be the seventieth specimen prepared by "hot-pressing".

The A, B, C, or D at the end of a sample number indicates relative position in a reaction tube, decomposition furnace, or hot-press mold.

II. REVIEW OF THE LITERATURE

A. Materials Used in This Research

1. General Information. When boron monophosphide (BP) is hot-pressed at high temperature, a boron subphosphide with a reduced phosphorous content is produced. If carbon is introduced as the major impurity, boron carbide is produced at a slightly higher temperature. Such products also can be formed from the elements. In order to understand the properties of the reactants and products, a review of boron, phosphorous, the boron-phosphorous system, and the boron-carbon system is presented in this section.

Boron occurs in both the amorphous and crystalline forms. At least three crystal forms are recognized, and a number of additional variations have been proposed. The amorphous form of boron is of interest in this study as a starting material, while the simple rhombohedral form may be considered the parent member of the borostitials. The historical background on the forms and properties of boron is confused by the presence of borides such as AlB_{12} and $Al_3C_2B_{44}$ which have passed as "pure" boron. Much of the earlier information is suspect, and one must examine more recent articles on single crystal and ultrapure preparations to ensure valid data.

2. Amorphous Boron. The finely divided amorphous form of boron is highly reactive when heated with air, concentrated sulfuric acid, concentrated nitric acid, and strong aqueous sodium hydroxide.

Amorphous boron is usually obtained by the reduction of a boron salt or boric oxide by magnesium or other active metal as reported by Mikheeva (146) and Kroll (121) or as patented by Finn (50). It may also be prepared by electrolysis of fused oxide and boride baths, but this is really an active metal reduction since the active metal is released at the electrode in the bath. Extreme measures are needed to prepare a really pure amorphous boron. Extensive leaching of the reduced product is usually followed by a vapor purification. Vacuum fusion or firing (153) causes aluminum, copper, magnesium, and tin to vaporize completely. Iron, silicon, and titanium vaporize partially, but molybdenum, carbon, and tungsten are retained.

Instead of using an active metal reduction which inevitably requires removal of active metal impurities, two other gaseous techniques are proposed which eliminate this residue. The first was used by Johnstone (100) to prepare a quantity of amorphous boron for thermodynamic studies. He passed diborane vapor mixed with helium through a long quartz tube at 700°C. The diborane decomposed quantitatively to amorphous boron and hydrogen.

Niemyski (154) prepared "pure" amorphous boron for semiconductor investigations by a fractionation of pure boron trichloride. The trichloride was prepared by chlorinating the sintered product of carbon and orthophosphoric acid between 700°C and 900°C. The boron trichloride was reduced by hydrogen in a quartz tube at 1100°C to 1200°C to produce "pure" (99.999+%) amorphous boron.

Amorphous boron has been prepared by Talley (219) by the reduction of boron tribromide with hydrogen in the vicinity of an incandescent tungsten filament. The material formed as massive rods with considerable hardness, tensile strength, and flexibility. It could also be deposited on other heated shapes without marked evidence of crystallinity on an X-ray diffraction pattern. Deposition was slow below 1100°K, and crystallization began above 1500°K. Talley concluded that this material was "a rather perfectly formed glass."

3. Crystalline Boron. Pure crystalline boron, as contrasted with the amorphous variety, is much more inert. When heated in air, crystalline boron is more resistant to combustion than the powdered amorphous variety possibly due to the formation of a surface glaze. Crystalline boron is only slightly attacked in hot concentrated sulfuric acid. Fused sodium hydroxide at a temperature above 500°C attacks the crystalline form, but hot aqueous alkali does not.

Three crystal forms of boron are recognized. The tetragonal I form was first to have its structure established. Hoard (85) suggested it in 1951, and further clarified this structure (86) in 1958. The tetragonal I polymorph has a tetragonal structure of 50 atoms per unit cell with a density of 2.31 g/cm^3. Forty-eight boron atoms are arranged at the vertices of four nearly regular icosahedra. These icosahedra are linked together so that every boron atom of a group forms six bonds directed toward the corners of a pentagonal pyramid. Five bonds are directed to atoms within the same icosahedron or to one of the remaining atoms located between the icosahedra.

The boron icosahedron is a symmetrical three-dimensional figure containing twelve boron atoms. Each group of three adjacent boron atoms in an icosahedron forms a triangular face which creates the twenty-sided structure shown in Figure 1. This icosahedron is a closely packed structure in which each boron atom is adjacent to six other boron atoms. The polygonal structure approaches a sphere and can be considered as a twelve-membered building block common to many structures containing boron.

The boron icosahedron is found again and again in the borostitial-type structures in which it is located on the eight corners of a rhombohedral unit cell. The lines drawn through

the icosahedron in Figure 1 represent the edges of the rhombohedral unit cells meeting inside the icosahedral unit. An icosahedron at either vertex of the rhombohedral unit cell will contribute three boron atoms to the edges of that unit cell. Any of the other six icosahedra contributing to that cell will supply four boron atoms. Of these four, three are on the cell edges and one is internal.

The rhombohedral unit cell is represented in Figure 2 as belonging to the hexagonal system. This figure relates the hexagonal a and c parameters to the rhombohedral a and α values.

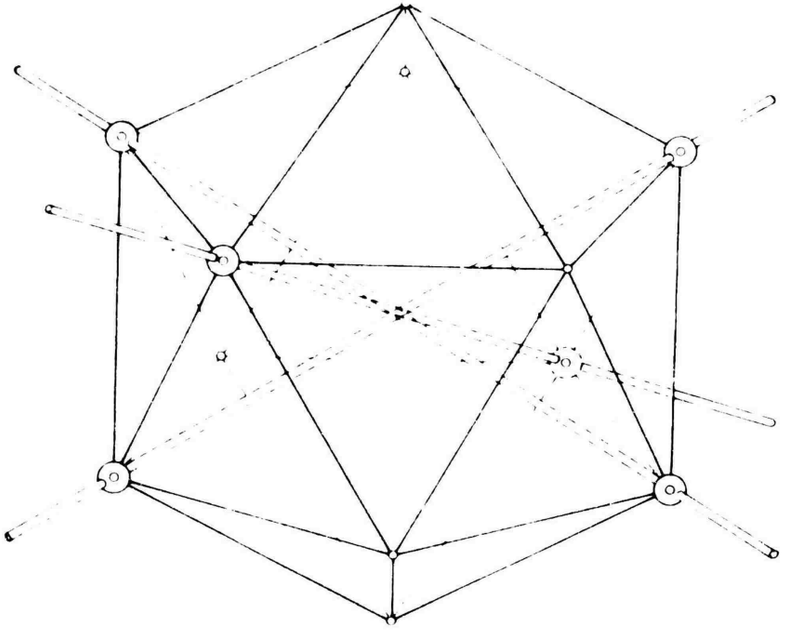

Figure 1. The Boron Icosahedron

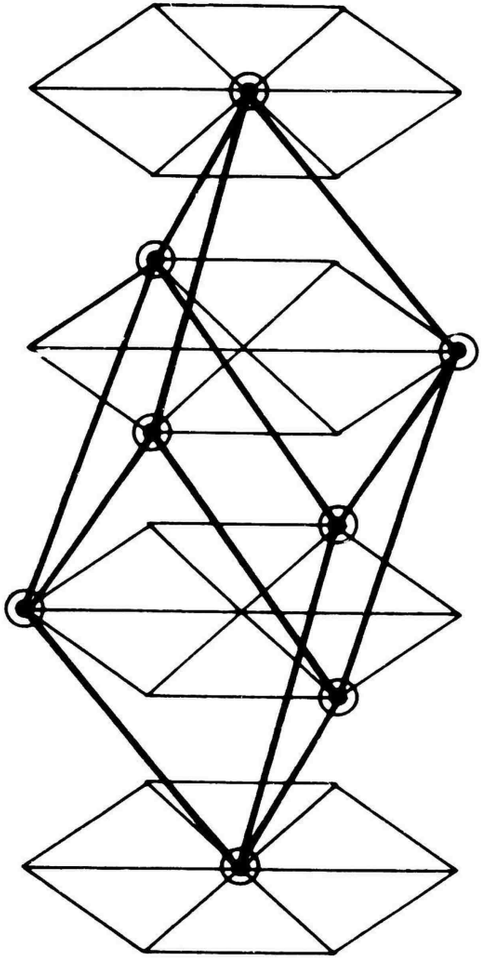

Figure 2. The Rhombohedral Unit Cell in Hexagonal Lattice

Tetragonal I boron has an experimental density of 2.31 g/cm^3 and contains four empty sites per unit cell with radii of 2.15 A. No evidence has been reported for the filling of these possible interstitial sites.

The most complicated confirmed crystal structure is that of β-rhombohedral boron with its 108 atoms per unit cell. This form is the stable form in the temperature region from 1500°C to the melting point of boron. It was readily formed from the melt as found by Sands (190) who identified it as a rhombohedral structure with a = 10.12 A and α = 65°28'. It had an experimental density of 2.35 g/cm^3 and to quote Sands, "There is no suggestion in the boron data of a pseudounit comparable in volume or obviously related in structure to the B_4C unit."

Crystals of β-rhombohedral boron were prepared by Gaule (56) by touching a heat-sink to the surface of a slightly supercooled melt. Two articles by Talley (216) and King (105) reported the preparation of pure single crystal β-rhombohedral boron. This material was prepared originally by chemical vapor-plating and was then zone refined to produce a high purity sample with a density of 2.345 g/cm^3.

An X-ray study by Hoard (84) of the polymorphism in boron pointed out that the β-rhombohedral form is to be expected from high temperature preparation with or without fusion. Above

1500°C, the β form is readily produced. Below 1000°C, α-rhombohedral boron is consistently obtained. Occasionally, β-rhombohedral boron will form at a temperature as low as 1100°C. A number of additional forms of boron have been proposed as being formed in the temperature region from 1000°C to 1500°C, but as yet, the stable and transient types have not been confirmed.

The α-rhombohedral form of boron is of particular interest because of its simple structure. It has 12 boron atoms per unit cell and a relatively high density of 2.46 g/cm^3. It was first prepared by McCarty (135) by pyrolysis of boron triiodide on a hot surface at 800°C to 1000°C. McCarty (134) then reported the procedure in detail. The α-rhombohedral boron was described as composed of units of nearly regular icosahedra in a slightly deformed cubic close-packing. Further support for the structure came from Decker (37) who reported it as being stable to 1200°C with transformation to the beta form at 1500°C. The α-rhombohedral unit cell dimensions were: a = 5.057 A and α = 58°06'. Decker pointed out that this structure may also be considered as derived from that of boron carbide by omission of the three center carbon atoms. Three-center or delta bonds were formed connecting three icosahedra instead of two to replace the boron to carbon bonds, and the icosahedra approached each other more closely.

The red color of the α-rhombohedral boron crystals reported by Horn (88) (90) may indicate both a more pure boron and a material with a larger band gap. These crystals were grown by slow freezing from a fifty atomic percent melt of boron and platinum at 1200°C.

In addition to the three crystals forms of boron established at this time, a number of others have been proposed. These have been reduced by McCarty (134) to three incompletely understood possibilities: tetragonal II boron (Z = 192 atoms) by Talley (218), hexagonal boron (Z = 90 atoms) by Rollier (177), and a tetragonal form (Z = 78 atoms) prepared by Naray-Szabo (152).

Since boron is used as a starting product and since its properties are so basically related to those of the hot-pressed material under study, a summary of reviews on boron is of interest. The proceedings of a conference on boron in 1960, as edited by Kohn (117), constitute a complete review of synthesis, structure, and properties. Four other authors, Laubengayer (130), Moss (148), Newkir (153), and Williams (242) have written brief reviews of preparations and properties. An extensive review of the polymorphic forms with their electrical and optical properties has been provided by Taylor (223).

4. Amorphous Phosphorous. Red amorphous phosphorous is more inert than the crystalline white form. The red variety sublimes at 416°C, and the vapor condenses into the white form. While ignition of the red phosphorous does not occur below 240°C, the white will ignite in dry air at 50°C. In moist air, excess phosphorous coming from a hot-pressing will form acid mixtures.

Commercially, red amorphous phosphorous is usually made by heating calcium phosphate with silica and carbon in an electric furnace at 1300°C forming calcium silicate and freeing carbon monoxide and phosphorous vapor.

5. The Boron-Phosphorous System. The boron-phosphorous system has the cubic boron monophosphide (BP) well established. A number of variations from B_6P_3, to B_6P and $B_{13}P_2$ and even to a ratio of $B_{40}P$ are reported for the subphosphide.

Preparation, crystal growth, and uses of the compounds in the boron-phosphorous system are reviewed. The relative position of the compound BP in the Group III-Group V families is then discussed.

Boron and phosphorous can form either a boron monophosphide or a boron subphosphide. The first compound has the exact composition BP while the second compound has been reported to have compositions of $B_{13}P_2$ or $B_{12}P_2$.

Cubic boron monosphosphide is a semiconductor material with a band-gap of approximately six electron volts. It is an extremely hard material, chemically inert, and stable to at least 1000°C. Three basic methods of preparation exist: the direct combination of elements; reactions involving borides, phosphides, or the elements; and pyrolysis of a volatile compound, usually upon a hot wire or hot surface. Pyrolysis usually involves the decomposition of an addition compound containing boron and phosphorous or the decomposition of the individual elements of the addition compound. In many cases, the distinction between reactions and pyrolysis is purely arbitrary.

Perhaps the most direct preparation of BP is the combination of boron and phosphorous vapor in a furnace at 800°C to 1500°C. This is covered by Williams' patent (243).

Direct combination of boron and phosphorous can also take place in a molten metal matrix. By adding either phosphorous or ferrophosphorous to molten ferroboron and cooling, a precipitate of boron monophosphide can be obtained. The technique was used by The Monsanto Company for the early preparation of the cubic BP used in this study. The precipitated phosphide was removed by leaching. Stone (207) indicates that molten metals such as copper, aluminum, silicon, iron,

manganese, or nickel are suitable solvents for the boron and phosphorous. According to Kirk (106), ferrophosphorous when used has a phosphorous content of 17 to 29%, and the principal impurities are silicon, titanium, and vanadium. Ferroboron has a boron content of between 10% and 24%. It may contain as much as 4% silicon and 3% carbon.

By using a slow cooling rate, the metal solvent method can be used to grow large single crystals which may be separated from the metal by leaching.

A variation on the first method was cited by Popper (168) and Rundqvist (180). This method used an evacuated, sealed silica tube which was filled with boron and red phosphorous and heated to 1100°C. The cooler end of this tube was kept at 450°C. Another variation of the same method was that proposed by Wood (252) in which the compounds were formed as a sinter by heating the elements to about 1100°C or 1200°C while maintaining a constant pressure of phosphorous at about one or two atmospheres. The implosive shock technique has also been used to prepare BP by direct combination. Engelke (43), by detonating an explosive in a sealed chamber, produced a shock wave of 2×10^6 atmospheres for a brief period of time. During this time, the temperature of the boron phosphorous mixture sealed in the chamber

reached several thousand degrees Kelvin. An impure boron monophosphide resulted. The reaction of gaseous phosphorous with a boron surface in the presence of hydrogen has been used by Williams (250) to produce a protective layer of boron monophosphide on rocket parts.

Williams (244) (248) produced boron phosphide by reacting a gaseous boron halide such as BCl_3 with aluminum phosphide AlP at 1000°C. A preparation was mentioned by Mellor (143) in which either the compound BPI_2 or BPI was reduced at 500°C in a stream of hydrogen. A reaction between boron suboxide (B_2O_2) from 600°C to 1200°C with elemental phosphorous in the gas phase produced boron phosphide in a method proposed by Stone (208). The boron suboxide was produced by heating equal parts of B_2O_3 and B with argon passing through the charge at 1400°C for 23 hours. Another preparation using zinc phosphide (Zn_3P_2) and boron was used by Peret (165) to produce boron monophosphide. The elements were compacted into pellets and dropped into a pre-heated reaction zone. The zinc was removed in the vapor phase. Nies (156) has prepared boron phosphide by the electrolysis of a melt containing an oxide or halide of phosphorous with B_2O_3, an alkali metal fluoride, usually a similar chloride, and optionally, an acid substance such as acid halide, boron fluoride, or

complex fluoride. BPO_4 is preferred to P_2O_5 as a source of phosphorous. Electrolysis takes place from 750°C to 800°C, and the product is easily removed from the cathode.

Boron monophosphide can be prepared by the decomposition of addition compounds containing boron and phosphorous. Vickery (231) prepared BP by decomposing the compound $BCl_3 \cdot PCl_5$ at 300°C in a sealed tube. Williams (247) also prepared boron phosphide in this manner. He did not prepare the addition compound first, but instead, reacted boron trichloride with phosphene at a temperature sufficient to form BP, 870°C to 1480°C. Pyrolysis on metal substrates heated inductively has been used by Schossberger (191) for the same preparation, as well as the reaction between phosphorous trichloride and boron trichloride in the presence of hydrogen at 1000°C. A common preparation parallels that used to prepare pure boron in that a hot filament is used for pyrolysis. Greiner (65) has used a tantalum filament heated to 1300°C in the presence of boron trichloride and phosphorous trichloride and hydrogen. A review of the addition compounds that may be used for this preparation was provided by Van Wazer (230) in his book on phosphorous and its compounds. He pointed out the possibility of forming analogous addition compounds with the trifluoride and tribromide.

Boron monophosphide can be grown into larger crystals in a process described by Ruehrwein (178) in which boron phosphide was heated in an atmosphere containing phosphorous. Stone (210)(211) has also found that an atmosphere of hydrogen halide vapor will cause single crystals of boron phosphide to form. Stone started with amorphous or crude boron phosphide and brought it into contact with a stream of hydrogen chloride or hydrogen bromide gas at a temperature between 800°C and 1200°C. When this carrier gas was passed through a zone of higher temperature, crystals of boron monophosphide were produced.

Boron subphosphide can easily be prepared by either of two methods, from the elements or by decomposition of boron monophosphide. Spinar (204) prepared $B_{13}P_2$ by heating BP to 1100°C to 1400°C in vacuum or argon until decomposition was apparently complete. The thermodynamic relationships of the dissociation reaction have been studied by Stone (212). Williams (243)(248) combined the elements as for the preparation of BP but raised the temperature above 1100°C under 1 mm pressure to produce B_6P. It would seem that any boron monophosphide preparation technique that can be carried out above 1100°C would also be a method of preparation for the subphosphide if held for sufficient time above that temperature.

Engelke (43) attempted to prepare B_6P by sealing boron monophosphide with the proper amount of boron in an evacuated, sealed quartz tube. The X-ray pattern of his product did not agree with that of the usual subphosphide material. Matkovich (140) prepared the low boron phosphide by decomposition of BP in graphite crucibles in a neutral atmosphere at temperatures of 1400°C to 1700°C. A second method used by Matkovich was the reaction of aluminum phosphide and amorphous boron powder to produce the boron subphosphide with aluminum phosphide and aluminum. The unwanted materials were removed with dilute hydrochloric acid.

One other boron phosphide was reported by Mellor (143). He stated that when boron monophosphide was heated to 1000°C in a current of hydrogen, B_6P_3 was formed. While this reference is found in many places in the literature, no later work is available on this compound.

The value of the boron phosphides can readily be seen from the uses to which they have already been put, and their future value can be seen from the uses suggested in some of the patent literature. Three patents assigned to Williams (244)(247)(250) of The Monsanto Chemical Company emphasized the value of the boron phosphides as coatings for rocket nozzles, as linings for rocket fuel tanks, as parts for jet

engines, and as general refractories. Two patents assigned to Gruber (71)(72) pointed out the abrasion and corrosion resistant properties of boron-phosphide-coated molybdenum, tungsten, or tantalum turbine bucket parts. One of these patents covered the stabilization of the boron phosphide surface so that it would be more useful in an oxygen-rich atmosphere. Boron subphosphide is currently being marketed by The Allis-Chalmers Corporation under the trade name, Cerac-3, as a fine powder abrasive material. Stone (209) mentioned that point-contact-rectification has been observed with both n-type and p-type BP. Rectification ratios of greater than 10^2 have been observed both at room temperature and at 400°C. A patent by Williams (249) described a method of preparation and the voltage current curves for point-contact diodes prepared from boron phosphide. Another report by Williams (245) carried this idea still further and suggested the use of boron phosphide to make transistors usable at 1000°C. Hill (82) has patented the possibility of using boron subphosphide as a thermoelectric element to 200°C. The patents by Williams (247) (250) mentioned a number of possible uses for the boron phosphides such as for nuclear reactor shields, hardening agents embedded in a metal base, and as coating materials for burners. Their chemical inertness suggests that they might be good for coating agitator arms or for making porous boron phosphide filters for

use in the chemical industry. Their optical transmission between 1850 A and 8000 A suggests that they might provide erosion resistance for the surface of a window passing light of this wave length. All of these actual and proposed uses only serve to underscore the valuable properties possessed by these materials.

Boron monophosphide can be thought of as a member of two Group III - Group V series. Little is known of the members of the boron series (BBi, BSb, BAs, BP and BN) except for the last two members. The phosphide series has received more attention. As one approaches boron phosphide going through indium, gallium, aluminum, to boron, the intrinsic activation energy increases (InP = 1.25 ev, GaP = 2.24 ev, AlP = 3.0 ev, BP = 5.9 ev). Indium phosphide has considerable electron and hole mobility (u_e = 5000 cm^2/vs, u_h = 700 cm^2/vs), gallium phosphide has a much lower pair of values (u_e = 110 cm^2, u_h = 75 cm^2/vs). Boron monophosphide, on the other hand, shows an increase with hole mobilities reported as 100 - 500 cm^2/vs. While not too much is known about these III-V series, the trends indicate that BP is clearly a large band-gap material with a moderately low mobility and with a tendency to form both n-type and p-type crystals. For one of the p-type crystals with a carrier concentration ranging from 1 - 5 x 10^{18} car/cm^3, the Hall coefficient is essentially constant from about

900°K down to 160°K. The thermoelectric power of this material, analyzed by Stone (209), is about 300 μv/°C for both the n-type and the p-type BP. General reviews of the III-V compounds including tables of properties are provided by Sizelove (201), Willardson (241), Lawson (131), Welker (235), and Hilsum (83). Bibliographies of the Group III - Group V semiconductor compounds have been compiled by Fredericks (52) and Esposito (46).

6. The Boron-Carbon System. Boron carbide (B_4C) is a hard but brittle, high-temperature material. It is readily prepared and is chemically very inert. Conduction properties vary from metallic to semiconductor conductivity. For the past ten years, considerable activity has been directed at determining the actual phases present around the so-called B_4C composition.

Commercial B_4C is prepared by heating a charge of boron anhydride (B_2O_3) with carbon black in a resistance furnace or an arc furnace. Boric acid (H_3BO_3) is frequently used as a source of boron. This process is patented by Atoda (8). A variation on this process prepares boron carbide in the gaseous phase. Formstecher (51) combined boron oxide and carbon in the presence of chlorine at 600°C to produce boron trichloride and carbon monoxide. These gases with a hydrogen carrier gas were decomposed on a hot molybdenum or tungsten filament to produce boron carbide. The methods of preparation of boron carbide were reviewed by Kranz (120).

In 1943, Clark (28) studied the crystal structure of B_4C. He established that it was rhombohedral with a = 5.19 A and $\alpha = 66°18'$. He suggested that the reported indications that commercial B_4C had a B to C ratio greater than four might be accounted for by the presence of a solid solution. Glaser (59) in 1953, noticed a wide range of homogeneity around the composition B_4C. Since the formation of B_4C was not observed, he suggested that this region may be described best as solutions of varying amounts of carbon in a slightly distorted boron lattice. Meyerson (144), in the same year, pointed out that B_4C melts with decomposition at 2250°C in a peritectic-type reaction. Allen (7) investigated the solid solution between boron and boron carbide, and Zhdanov (256) further investigated the solid solution region and suggested that it was a displacement-type solid solution. That is, that the carbon in the center of the three-carbon-chain was displaced by boron. Zhdanov found that the limiting formula for the boron to carbon ratio was $B_{6.5}C$. A second study by Zhdanov (257) suggested that the substitution of carbon atoms in the lattice by boron proceeded until the composition is $B_{13}C_2$. This was supported by hardness and X-ray measurements.

Epelbaum (44) identified a new phase after studying the region from 65 to 90% boron. This phase between $B_{13}C_2$ and $B_{13}C_2$ was also studied by Samsonov (189) who proposed a phase

diagram for the boron-carbon system. This work by Samsonov (185) was expanded in 1958, and a phase diagram given which showed that the compound $B_{13}C_2$ melted congruently at slightly above 2400°C. This system also contained the incongruently melting compound $B_{12}C_3$ which melted to form liquid and a beta prime phase and contained a gamma phase (B_nC_m) occurring at 69% carbon. The latter two compounds form an eutectic in the region 30 to 31% carbon.

An X-ray study with large angle scattering has been reported by Kudryavtsev (123) in which precision-lattice-parameter determinations of the boron-carbide system were made. Work by Zhuravlev (258) in 1961, confirmed the presence of a new boron-rich compound corresponding to $B_{12}C$. This new phase has been incorporated into the latest phase diagram by Samsonov (187) at about 8% carbon and is called a delta phase. This latest phase diagram for the boron-carbon system is reproduced in Figure 3.

B. Related Materials

1. General Information. Boron subphosphide and boron carbide are derivatives of α-rhombohedral boron. A study of other variations with the same basic boron structure including ternary systems should provide related information of value. Of particular interest are the B_4A, B_6A, $B_{12}A$ borides in which A is any p-orbital element.

In borides of the form Me_4B and Me_2B, the boron atoms are isolated from each other. In compounds with the form Me_3B_2,

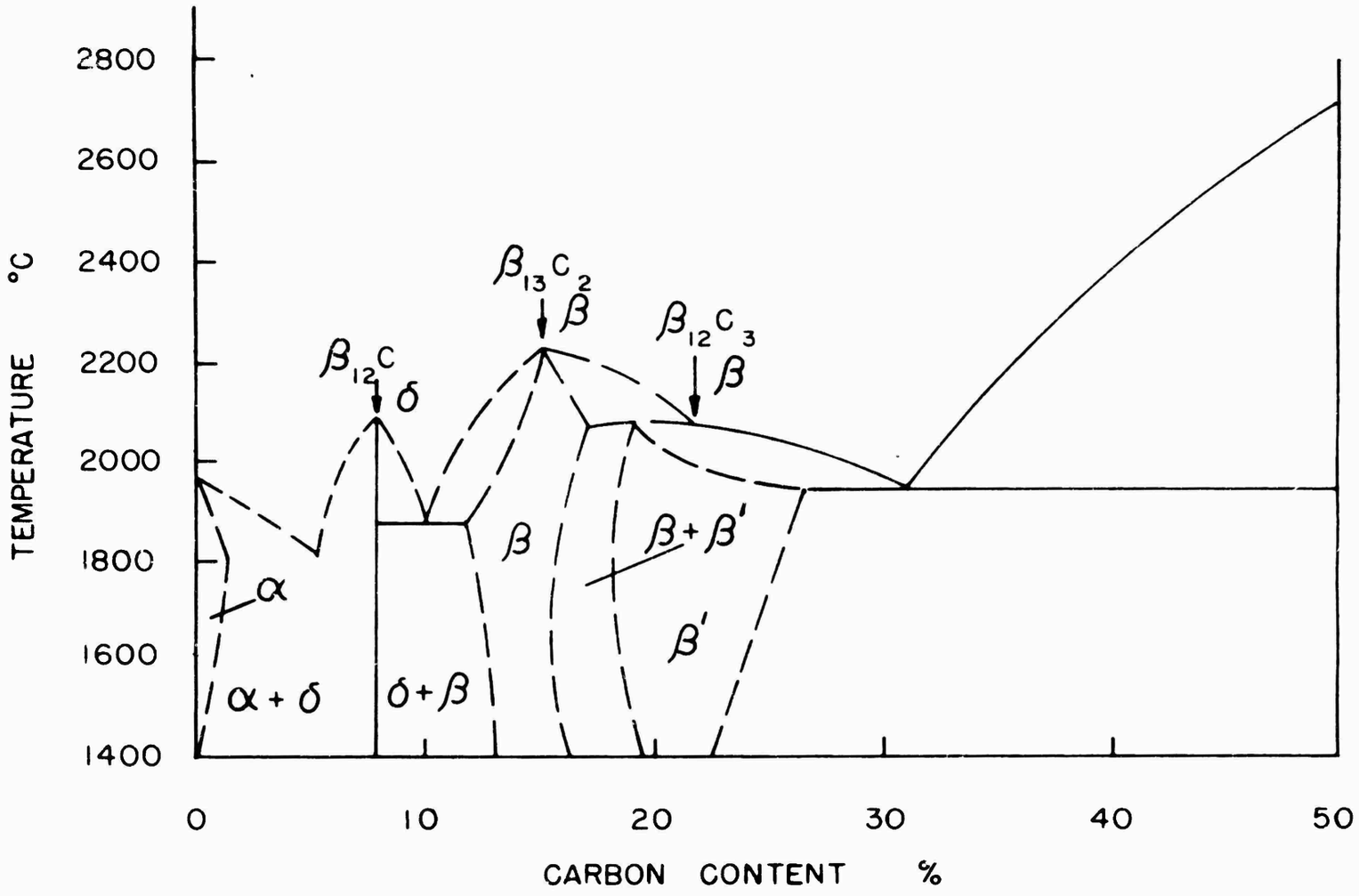

Figure 3. Phase Diagram for the Boron-Carbon System

the boron atoms are paired; while in the compound MeB, they form isolated zig-zag chains. Double chains are formed in the compound Me_3B_4, and networks are formed in borides of the form MeB_2. The borides of interest, however, are B_4Me, B_6Me, and $B_{12}Me$. In these borides, the boron atoms form three-dimensional networks which gain their strength from the strong bonds between the boron atoms. These materials are further strengthened by cross-bonding within the boron framework to the atoms situated in their pores.

Two conditions must be met for a compound to be called a borostitial compound: it must be a derivative of the B_{12} structure, and it must contain one or more interstitial atoms of the p-orbital elements. So far, three such materials have been reviewed. The first of these was the parent boron structure; the second, boron subphosphide; and the third consisted of $B_{13}C_2$ and $B_{12}C$ which are included in the general name boron subcarbide. A study of the literature reveals that more such compounds have been confirmed containing as the interstitial element: oxygen, aluminum, silicon, sulfur, and arsenic. Of the remaining possibilities, nitrogen, gallium, germanium, and tin will be considered as a group.

2. The Boron-Oxygen System . In 1959, Pasternak (163) published crystallographic evidence for the existence of B_7O. The actual formula given by Pasternak for the compound was $B_{8.6}O$. A simultaneous study by Rizzo (174) on the oxidation of boron in air between 400°C and 1300°C revealed the presence of B_7O. A review by Matkovich (139) in 1960, compared the hexagonal and rhombohedral cell parameters for the borostitial compounds. He recalculated the $B_{8.6}O$ as the compound $B_{13}C_2$ which fell nicely into a rhombohedral lattice. His table is reproduced in Table I. Matkovich remarked that the compounds in the table were arranged in increasing order of atomic size and noted that it is interesting that the expansion of the unit cell took place in the direction of the hexagonal a-axis only. He pointed out that at the same time the unit cell shrunk in the direction of the c-axis until a certain minimum value was reached at 11.5 A. From there, the expansion took place in all directions by a change in the rhombohedral angle. A further comparison of the $B_{13}A_2$ compounds was given by LaPlaca (129) in which the boron oxide compound was once again listed as $B_{13}O_2$, and its X-ray pattern compared with those of the $B_{13}A_2$ compounds.

Another report by Rizzo (175) in 1962, suggested that the formula should be B_6O. In the preceding studies, only the boron content was determined and the oxygen taken by difference. No

Table I.

X-ray Comparison of the Borostitials by Matkovich (139)

	Hexagonal cell			Rhombohedral cell	
	a	c	c/a	a	α
α-Boron	4.908	12.567	2.56	5.057	58°4'
$B_{13}O_2$	5.37	12.31	2.30	5.14	62°56'
$B_{12}C_3$ (B_4C)	5.60	12.12	2.17	5.175	65°18'
$B_{13}C_2$	5.67	12.19	2.15	5.218	65°49'
$B_{13}P_2$	5.984	11.850	1.98	5.248	69°31'
$B_{13}As_2$	6.142	11.892	1.935	5.319	70°32'
$B_{12}Si_3$ (B_4Si)	6.330	12.736	2.015	5.602	68°49'

estimate of impurities such as magnesium or silicon was made. In this study, Rizzo determined both the boron and oxygen content of the boron oxide. He further concluded, on the basis of density, that the compound must be B_6O and not B_7O or $B_{13}O_2$. The calculated X-ray density for $B_{13}O_2$ = 2.80 g/cm^3 while the calculated X-ray density for $B_{12}O_2$ or B_6O = 2.59 g/cm^3. Rizzo's measured density was 2.62 g/cm^3 with a maximum density for the hot-pressed product of 2.588 g/cm^3. While Rizzo mentioned the solubility of silicon in the hot-pressed product probably as SiB_6, he made no mention of the possible presence of carbon.

3. The Boron-Aluminum System. In the boron-aluminum system, five compounds are recognized. Kohn (112)(114)(116) has reviewed these and listed them as AlB_2, an hexagonal phase; $B_{10}Al$, an orthorhombic phase; alpha $B_{12}Al$, a tetragonal pseudocubic phase; beta $B_{12}Al$, an orthorhombic pseudo-tetragonal phase; and gamma $B_{12}Al$, also orthorhombic. These five phases are confirmed. A sixth reported phase, the monoclinic $B_{12}Al$, was found by Parthe (162) to be identical with a form of elementary boron. Kohn (112) stated that although the higher aluminum borides were closely related structurally among themselves and to the modifications of boron, their crystal structures have not yet been described fully. The relationship between the boron icosahedron with a diameter of 5.1 A and the

various phases of the higher aluminum borides was striking. Kohn pointed out that two times the diameter of the boron icosahedron, i.e., 10.2 A, is a value common to the a of alpha $B_{12}Al$, beta rhombohedral boron, and tetragonal II boron. This dimension is also common to the c of beta $B_{12}Al$ and alpha $B_{12}Al$. It is again related to 2a of alpha rhombohedral boron and approximately to 2a of boron carbide. Finally, the 2c value of tetragonal I boron is related to the 10.2 A unit. Among very recent work, an article by Will (240) comment on the crystal structure of $B_{10}Al$. Will propose a crystal structure based on an icosahedral arrangement of four boron icosahedra and four intericosahedral boron atoms per unit cell. Thiswas then made up of 52 boron atoms with the aluminum atoms distributed statistically over several sites. In spite of the marked similarity of the higher boron aluminides to the boron structures, no direct relationship with the rhombohedral form of $B_{13}A_2$ has yet been established. A recent report by Matkovich (142) is said to comment upon this relationship, but it has not yet been published. A phase diagram of the boron-aluminum system has been prepared by Serebryanskii (194)(195).

4. The Boron-Silicon System . Moissan (147) proposed the presence of two compounds, B_3Si and B_6Si, in the boron-silicon system. A number of years later, Gurevich (74) studied the boron-silicon system and concluded that B_3Si did not exist. The following year, the compound B_6Si was definitely established by Cline (31) and Adamsky (4). They found it to be orthorhombic and to contain 40 or 43 atoms per unit cell. In 1959, Cline (30) further investigated this compound, B_6Si. Matkovich (141) then established the crystal form for B_4Si. It had rhombohedral symmetry with an hexagonal unit cell. The compound was isomorphous with B_4C and transform to the orthorhombic B_6Si above 1350°C. The B_6Si phase has been studied thermodynamically by Knarr (109). Its preparation by hot-pressing, cold-pressing, and slip-casting were studied by Colton (33). Colton (34)(35) has also studied the B_4Si compound, as has Brosset (17). Colton has pointed out that the B_4Si and B_6Si compounds were not the only ones apparently present. Work along this line has been carried out by Adamsky (5) who announced the presence of $B_{12}Si$ and by Magnusson (138) who announced the $B_{2.89}Si$. Magnusson's compound was said to have a crystal structure like B_4C. It was clear that two phases were definitely established, B_6Si and B_4Si. The latter of these was similar to alpha rhombohedral boron in its structure. The possiblity of other phases

being present was clearly indicated. These phases too, as indicated by Magnusson's work, may follow the rhombohedral structure.

5. The Boron-Sulfur System. The reaction of amorphous boron and sulfur powder at 1600°C to 1700°C produced a new borostitial, the compound $B_{12}S$. This material, produced by Matkovich (139), is a brown powder which released sulfur upon further heating and turned black. Chemical analyses indicated a 12/1 and sometimes a 13/1 ratio, although the 13/1 ratio was probably explained by the presence of unreacted boron. The rhombohedral unit cell had a = 5.19 A and $\alpha = 67°56'$. The measured density was 2.40 g/cm^3 which was somewhat higher than the theoretical value of 2.33 g/cm^3 calculated from X-ray information.

6. The Boron-Arsenic System. One other borostitial compound was clearly established, $B_{13}As_2$. Perri (166) prepared cubic BP and BAs in a zinc-blend structure. Both of these decomposed when heated in air. In the presence of arsenic vapor, BAs was stable to 920°C. Above this temperature, according to Perri, it decompose to an orthorhombic form which was highly inert. Williams (246)(248) reacted arsenic vapor with crystalline or amorphous boron or boron halides from 700°C to 900°C for the preparation of boron monoarsenide. By increasing this temperature from 900°C to 1200°C, he prepared the boron

subarsenide. The subarsenide so prepared had the same orthorhombic structure as that obtained previously by Perri. By investigating the boron to arsenic ratio with a thermogravimetric technique, Williams concluded that the composition was between 6/1 and 7/1 and accordingly reported it as a nominal composition, B_6As. In Matkovich's article (139) on the interstitial compounds of boron, he pointed out that the orthorhombic claim for the structure of the subarsenide had been corrected by Post and now was stated as being $B_{13}As_2$ with a rhombohedral unit cell containing one molecule of the subarsenide. LaPlaca and Post (129) then republished their data in 1961, with a complete comparison of the elements of the other materials also possessing this basic boron carbide structure.

7. Other Borostitials. One compound is obviously missing from this collection of borostitials, the subnitride. No reported subnitride exists in the literature. Boron mononitride (BN) exists in the soft, hexagonal form, the analog to graphite and in the cubic, very hard BN form, the analog to diamond. Wentorf (236)(237) has prepared cubic BN with a zinc blend structure. When he heated a fragment of the cubic form to over 2000°C in vacuum, no change was obtained. Cubic BN or borazon, as it is called, was extremely stable, was prepared by high pressure and temperature, and was hard enough to

scratch diamond. Vickery (231) prepared a film of borazon by treating boron monophosphide with ammonia at 800°C. Nitrogen gas containing 5% ammonia was used.

Three other materials that are probably borostitials have been mentioned. In 1961, Chretien (27) reported that he had prepared $B_{12}Ga$ by heating gallium and boron to 1300°C in sealed tubes. He reported it to be in the tetragonal system with a density of 4.273 g/cm^3. A patent by Henderson (77) covered the possible thermoelectric element that could be prepared from germanium and boron or tin and boron. Such an element contains 0.05 to 45% germanium with boron or 0.05 to 45% tin with boron, and the thermoelectric device was said to generate power from 110°C to 925°C. No other borostitial compounds have been mentioned in the literature, although possibilities may exist. The most likely possibility seems to be the subnitride.

The higher borides that are not borostitial occur throughout the periodic table in the B_4A, B_6A, and $B_{12}A$ forms. Much information is available on such compounds prepared from the metals of the alkaline earths, the lanthanides, and the actinides. No such compounds are reported for Group I elements. Many transition metal elements also form the higher borides. In general, the face-centered cubic structure prevails. Most of these higher borides have high hardness, high melting points,

and are very inert. The preparations used for these are the same as for the borostitials. Tipton (225) indexed a number of the phase diagrams for the binary higher borides.

8. Ternary Systems. Since the material under study may be thought of as a boron-phosphorous-carbon ternary system, other ternary systems are of interest. Ternary work may be divided into that containing boron and two borostitials and that containing boron, a borostitial element, and another metal. In the first category, boron plus two other borostitial elements, the first work was done by Naray-Szabo (151) on the boron-aluminum-carbon system. This is the original work that was used to show that the so-called pure boron was not pure. Recent work by Rizzo (176) was directed at showing that the borostitial compound of boron and silicon could be protected at high temperatures by the formation of a boron-silicon-oxygen glass on the surface. Becher (12) has recently worked on the boron-beryllium-aluminum system. Most of the work, however, has been on the boron-silicon-carbon system with emphasis upon the combination of silicon carbide and boron carbide. This work has been carried out by Portnoi (169), Meyerson (145), Secrist (193), Kalinina (101), and Samsonov (184) (187).

The ternaries consisting of boron, another borostitial, and a metal, have been investigated by Stadelmaier (205) who studied the compounds of boron, borostitial elements, and cobalt or nickel. The borostitial elements were aluminum, gallium, tin, germanium, and indium. Nowotny (158) studied the boron-silicon-metal and boron-carbon-metal system where the metal was uranium, thorium, or molybdenum. Samsonov (187) studied the boron-silicon-metal system where the metal was titanium, vanadium, niobium, tantalum, chromium, molybdenum, tungsten, manganese, and iron, and the system boron-carbon tungsten. One other ternary system of interest was that of the boron-phosphorous-iron system studied by Rundqvist (181).

C. Hot-pressing

1. Procedure . Before using the hot-pressing technique, one should understand the mechanism and the essential elements of the process. A review of the process is followed by a clarification of the unusual features which characterize this particular hot-pressing problem.

The general concept of hot-pressing has been reviewed by Thomas (224), Jackson (96), and Murray (150). The essential elements of the process begin with the application of heat to a powder sample in a mold. Pressure is next applied to compress the particles and the time-at-temperature is controlled in order

to aid the sintering process and regulate grain growth. The effects of applied pressure on densification have been studied by Kingery (105). As heat is applied, one may think of plastic flow taking place in which pores are closed and density is increased. Such a model has been studied by McClelland (136). Hot-pressing is of value over ordinary sintering in that greater density is obtained in a shorter time, and a shorter time-at-temperature means a finer grain size which is quite desirable in many ceramic products. To the essential elements of heat and pressure and time-at-pressure, one must add temperature measurement and control.

The hot-pressing of boron subphosphide from boron monophosphide does have several special features to be considered. The most obnoxious problem is that of the evolution of copious quantities of phosphorous in the form of phosphorous oxides. This evolution of phosphorous gas serves both to hinder the sintering operation and to hinder the determination of proper temperatures. The application of vacuum pressing, as used by Eubank (47), for the preparation of boron compacts had the particular advantage of removing adsorbed gaseous impurities and thus permitting not only a pure compact but also a more rapid densification. Many compounds will not pressure-sinter

as long as adsorbed gas remains on the surface. In addition to the problem of egress of phosphorous, the problem of ingress of carbon remains a particularly challenging one in the pressing of phosphides. The first step in protecting against the incoming carbon is to use a boron nitride lining in the graphite mold. This was done by Eubank (47) in the pressing of boron. Once again, the volatility problem occured. Boron nitride, itself, cannot be pressed in the pure state. Jackson (96) and Samsonov (187) have pointed out that it was usually cemented together by boron oxide which was volatile between 1100°C and 1300°C. Not only was the lining evolving gas, but it was becoming more porous as the temperature increased. The temperature of hot-pressing in this study was above the 1650°C recommended as the maximum working temperature for solid boron nitride in an inert atmosphere. Jackson (96) also pointed out that boron, itself, cannot be pressed unless it is cemented. The cement for the boron powder is frequently boron carbide.

A device prepared by Ridgway (173) was essentially a multiple hot-pressing device using a plurality of minor plungers. This was very similar in principle to the technique used in this study, that of pressing sealing plugs above and below the sample to reduce the influx of volatile carbon compounds. The de-gassing of molds and linings as used in this study was also used by

Shilliday (200) who out-gassed his boron nitride containers for three to four hours at 1450°C to 1500°C.

Since reaction hot-pressing was used to prepare boron subphosphide, a brief review of this is included. It was found that Meyerson (145) used reaction hot-pressing to prepare compacts in the boron-silicon-carbon system. Specimens were obtained by hot-pressing powder mixtures of the elements at 2000°C to 2100°C. Another such study was made by Accary (3) who studied the mechanism of hot-pressing in the uranium-nitrogen and the uranium-silicon systems. In this work, reaction took place before densification.

A high flow rate of helium up through the optical sight path removed phosphorous vapor and made it possible to determine temperatures accurately with an optical pyrometer. It was then desirable to determine the correction needed to adjust the optically determined temperature to the actual sample temperature. This was done by means of a high temperature thermocouple. Many high temperature thermocouple materials have been suggested, among these carbides, carbon itself, borides, refractory metals, and oxides. In this study, a tungsten 3% rhenium vs. tungsten 25% rhenium thermocouple was used. Such thermocouple systems have been described by Lachman (124) and Slaughter (202).

2. The Hot-Pressing of the Borostitials. Hot-pressing has been applied to the borostitials and to the pressing of boron monophosphide. Boron monophosphide has been hot-pressed by Williams (244), and boron subphosphide has been hot-pressed by Peret (165). Boron has been pressed by Eubank (47) and Best (13). Rizzo's article (175) on B_6O mentioned a preparation by hot-pressing. Samsonov (186), Colton (33), and Feigelson (49) mentioned the hot-pressing of boron silicides. The commercial hot-pressing of boron carbide is quite common as outlined by Samsonov (187)(188). Tarasov (221) and Knowlton (111) discussed the hot-molding of boron carbide at temperatures to 2200°C in graphite molds. Both from the standpoint of solving the special problems involved in producing boron subphosphide and from using a well-developed technique of known applicability, hot-pressing seems to be the best technique for use in this study.

D. Structure and Bonding

1. Icosahedral Structures. The basic building block in the borostitial compounds is the boron icosahedron. As boron icosahedra are stacked at the corners of a rhombohedron, three interstitial sites are left empty in each unit cell. The compounds produced and the character of these interstitial compounds is reviewed.

The first step toward the clarification of the borostitial structure was the analysis of boron carbide by Zhdanov (255) in 1941. He proposed that the structure can be represented formally as an approximate sodium chloride-type of structure with a compact group of twelve boron atoms substituting for the sodium ion and a linear group of three carbon atoms for the chloride ion. He found that the twelve boron atoms were arranged at the vertices of a nearly regular icosahedron. Each boron atom had sixfold coordination being bonded to five others in the icosahedral group and to one other atom outside of the group. In the carbon chain, the two end carbon atoms had fourfold coordination, and the center one, twofold coordination. All of the boron atoms built the rigid framework of the rhombohedral structure.

Zhdanov's structure was confirmed by Clark (28) in 1943. In considering the continuous boron network which ran throughout the crystal, a coordination number of six for the boron atoms which have only three electrons meant that ordinary covalent bonding was impossible. A high degree of resonance, approaching metallic binding, was necessary to account for the high stability of the structure. This was supported by the high electrical conductivity of boron carbide. Clark proposed various types of electronic formulas for the C-C-C group and its immediate neighbors.

On the basis of the carbon to carbon separation, he proposed a superposition of such formulas to represent the actual structure. The work by Hoard (85) on tetragonal boron developed the idea of a basic structure of boron icosahedra with additional borons forming cross-links between the icosahedra. Hoard closed with the statement, "The linked icosahedra in boron and boron carbide give strong network structures in which suprisingly large holes are interspersed among the very compact icosahedral groups."

The theoretical investigation by Longuet-Higgins (133) in 1955, by the method of molecular orbitals provided a qualitative estimate of the probable electronic structure of the regular icosahedron. This report attempted to explain the structure in boron carbide, elementary boron, and decaborane. The idea of coordination polyhedra mentioned by Hume-Rothery (91) pointed out that 12 atoms can be close-packed around a twelvefold coordination site in any of three structures: the face-centered cubic, the cuboctahedral, and the icosahedral. The higher lanthanide borides occurred in the face-centered cubic structure. Transition metal higher borides, such as $B_{12}U$ and $B_{12}Z$, occur in the cuboctrahedral structure. The borostitials, of course, had the icosahedral structure. An attempt by Lipscomb (132) to systematize our understanding of the valence orbital structures

in the higher boron frameworks considered the compounds $B_{12}U$ and $B_{12}Zr$, boron, boron carbide, and the aluminum borides. Lipscomb pointed out the cuboctahedron in the compound $B_{12}Zr$ is stabilized by the presence of the zirconium orbitals and that, without these, it might be expected to revert to the more stable icosahedral arrangement.

Lipscomb went on to explain bonding schemes for rhombohedral and tetragonal boron forms. The alpha rhombohedral form of boron had boron-to-boron bonds among atoms of the icosahedra only. Ten electrons were required from each B_{12} group for the external bonds to other icosahedra. Twenty-six electrons were left for the intraicosahedral bond of each B_{12}. The 26 electrons just filled the bonding intraicosahedral molecular orbitals. In boron carbide, on the other hand, 26 electrons were required inside each icosahedron; 12 electrons for the 12 outward-pointing boron orbitals and six electrons for the six orbitals of the center C-C-C group. The central carbon atom had four electrons for bonding. An analysis of the aluminum borides by Lipscomb suggested that it might be possible to have aluminum atoms substitute for boron atoms and thus explain the unusual formula weights per unit cell. Such ratios as 14.4 atoms per unit cell for $B_{12}Al$ and 5.2 atoms per unit cell for $B_{10}Al$ cannot easily be explained with present knowledge. This attempt

to systematize and explain the central bonding in the higher borides is of interest in terms of the possible resonance structures which could be related to the conductivity of these materials. Canon (23) extended the work of Lipscomb on the compounds $B_{12}U$ and $B_{12}Zr$ and explained the tendency to form cuboctahedral bonding in these compounds.

Taylor (223) has reviewed the structures reported for alpha rhombohedral boron and tetragonal I boron and has begun the calculation of the band structure of the alpha rhombohedral boron form.

Matkovich (139) presented a model for the structure of boron compounds which explained another portion of the borostitial family. By analogy to the carbon-boron-carbon center chain in boron subcarbide, Matkovich identified the center chain in boron subphosphide as phosphorous-boron-phosphorous. The structure shown in Figure 4 represents $B_{13}P_2$. This rhombohedral unit cell has two boron atoms on each edge. The group of three boron atoms at each of the vertices belongs to a boron icosahedra. Groups of four boron atoms at each of the other six corners of the rhombohedra belongs to other icosahedra. Thus one icosahedron is located at each corner of the rhombohedral unit cell. Between these icosahedra are located three atoms. As seen in Figure 4, the central site is occupied by a boron atom with a phosphorous

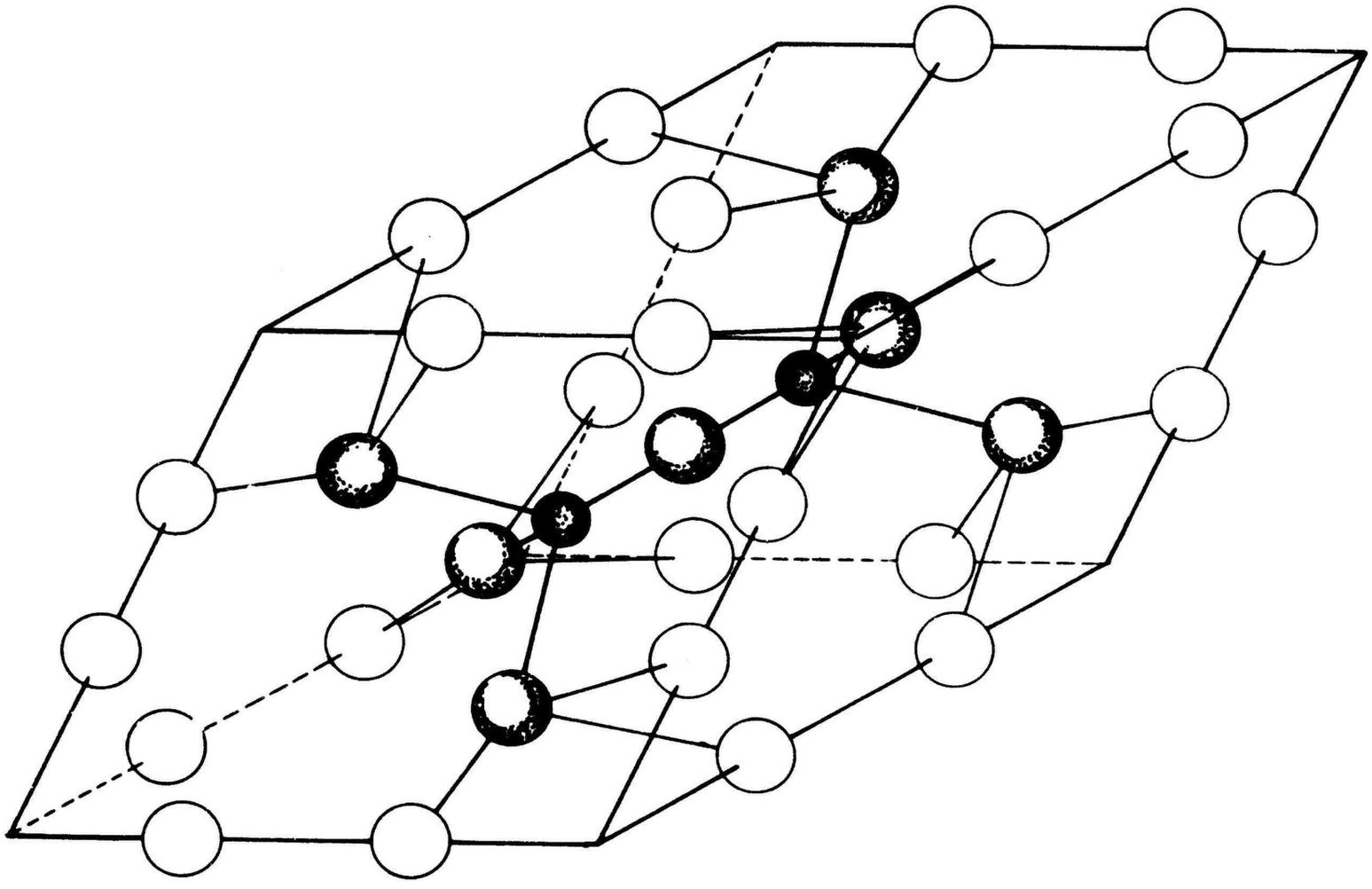

Figure 4. Rhombohedral Structure of $B_{13}P_2$.

atom located on either side of it. Each phosphorous atom is bonded to the central boron atom and to three boron atoms, each in a different icosahedron.

The icosahedral structure was shown previously in Figure 1. The lattice lines drawn through that icosahedra represent the edges of the rhombohedral unit cell. This figure shows how two corners of the rhombohedron contain three boron atoms each and six corners contain four boron atoms each.

Matkovich (139) produced the compound $B_{12}S$ which is analogous to $B_{12}C$. In these structures, the center atom was sulfur or carbon and the interstitial sites on either side of the central atom were unoccupied. Spinar (204) confirmed the structures of $B_{13}P_2$ and $B_{\sim 3}S$ and determined their atomic positions.

The concept of a boron carbide structure type or, as designated here, a borostitial material, was summarized by LaPlaca (129) who announced that a detailed single-crystal analysis of the boron subphosphide is now under way. LaPlaca stated, "There are indications that the assumed chemical formula may have to be modified as a result of X-ray findings. At the present stage of the analysis, we find only two phosphorous atoms, rather than two phosphorous atoms plus one boron atom arranged interstitially parallel to the threefold axis." He went on to state that the true formulas will not be firmly established until

detailed crystal structure determinations have been completed. Both Matkovich and LaPlaca pointed out that a boron subnitride would be extremely interesting if it could be prepared.

2. Interstitial Compounds. Many compounds fail to have definite combining proportions, and are known as Berthollide or nonstoichiometric compounds. Examples are the hydrides of cerium and vanadium; oxides of iron and titanium; sulfides, selenides, and tellurides of copper. The borostitials also appear to have this property. Lack of true stoichiometry is associated with defects in the crystal lattices. The two main types of such defect are the Frenkel defect in which sites are vacated and the atom is lodged in an interstitial position, and the Schottky defect in which sites are vacated and the atom is left on the surface. Detailed reviews of the types of defects and the way they affect the properties and materials are provided by Gray (61) and Van Bueren (229).

Hagg (76) systematized the structures of interstitial compounds formed between transition metals and hydrogen, boron, carbon, and nitrogen. His simple method of characterizing such structures described by Westgren (238). The more simple interstitial compounds had a radius ratio between 0.41 and 0.59. When it was over 0.59, complex structures result. If in this range, the usual structures were face-centered cubic or hexagonal or slight

distortions of these. In discussing this size effect, Hume-Rothery (91) made several points which can be adapted to this system. If the boron lattice is thought to be similar to the cubic structure discussed by Hagg, one may think of the insertion of atoms at the three central sites as causing a distortion of this basic lattice. This is just the distortion cited by Matkovich (139). As the c/a ratio was changed, the angle was changed for the basic rhombohedral structure. Hume-Rothery's second statement (91) was that the composition of interstitial phases were generally not definite but corresponded to a range of formulas in the boron-carbon system as noticed in the extensive solid-solution regions on the phase diagram. It was also readily observed in the boron-oxygen, boron-phosphorous, and boron-arsenic systems where one of the elements was volatile. The third point that Hume-Rothery made is that, as in the carbides and nitrides of the sodium chloride structure, the extent and type of interstitial insertion was determined not only by the size or radius ratio but also by the bonding. One could determine an effective radius ratio for these rhombohedral structures, but this alone would not be sufficient to determine the nature of the structure formed. The directed orbitals in the interior region of the three sites in the boron rhombohedron determine what will be accepted and how much. This interstitial character of

these materials has been shown by Van Buerен (229) to have a marked effect on the resistivity and thermal conductivity in metals.

E. Properties Related to Structure

1. X-ray Parameters. The X-ray parameters for boron and the borostitials are listed in Tables I and II. The compounds listed in Table I were arranged by Matkovich (139) in the order of increasing size of the interstitial atoms. The hexagonal unit cell expanded with larger additions in the direction of the a-axis. The c-axis shrunk at the same time to a minimum of 11.85 A and then also expanded. The angle of the rhombohedral unit cell changed as the cell expanded.

2. Densities and Melting Points. The densities and melting points for boron and the borostitials are reported in Table III. The letter "c" or "e" following many of the density figures indicates that that value is either calculated or experimental.

3. Hardness. The Knoop and Vickers hardness values for boron and the borostitials have been assembled in Table IV. Whenever possible, the load is given for each cited hardness value because hardness numbers without a load do not mean very much for hard, brittle materials. Some background is provided for understanding the nature of hardness and for interpreting curves of hardness number vs. load.

Table II.

X-ray Diffraction Parameters for Materials Having a Structure Based on the Boron Icosahedron

Material	(Z)	Form	a	b	c	α	Reference
B	(50)	tetr. I	8.75	-	5.06	-	(86)
B	(192)	tetr. II	10.12	-	14.14	-	(220)
B	(12)	α-rhomb.	5.057	-	-	58°06'	(37)
B	(12)	α-rh.(hex.)	4.908	-	12.567	-	(37)
B	(108)	β-rhomb.	10.12	-	-	65°18'	(190)
B	(108)	β-rh.(hex	10.95	-	23.73	-	(190)
$B_{12}C_3$		rh.(hex.)	5.61	-	12.07	-	(7)
$B_{6.66}C$		rh.(hex.)	5.65	-	12.15	-	(7)
B_7C		rh.(hex.)	5.67	-	12.19	-	(7)
$B_{12}C_3$		rhomb.	5.19	-	-	66°18'	(28)
$B_{5.07}C$		rh.(hex.)	5.606	-	12.148	-	(123)
$B_{5.29}C$		rh.(hex.)	5.616	-	12.166	-	(123)
$B_{8.75}C$		rh.(hex.)	5.630	-	12.194	-	(123)
$B_{12}C_3$		rhomb.	5.17	-	-	65°45'	(254)
$B_{12}C_3$		rhomb.	5.598	-	12.12	-	(183)
$B_{6.5}C$		rhomb.	5.630	-	12.19	-	(183)
$B_{13}P_2$		rhomb.	5.248	-	-	69°31'	(139)(140)
$B_{13}P_2$		rh.(hex.)	5.984	-	11.850	-	(139)(140)
$B_{12}S$		rhomb.	5.12	-	-	67°56'	(139)
$B_{12}S$		rh.(hex.)	5.80	-	11.90	-	(139)
$B_{12}Ga$		tetr.	12.93	-	4.84	-	(27)
$B_{13}As_2$		orthorh.	9.710	4.343	3.066	-	(166)
$B_{13}As_2$		rhomb.	5.319	-	-	70°32'	(139)
$B_{13}As_2$		rh.(hex.)	6.142	-	11.892	-	(139)
$B_{13}C_2$		rhomb.	5.218	-	-	65°49'	(139)
$B_{13}C_2$		rh.(hex.)	5.67	-	12.19	-	(139)
$B_{12}C_3$		rhomb.	5.175	-	-	65°18'	(139)
$B_{12}C_3$		rh.(hex.)	5.60	-	12.12	-	(139)
$B_{13}O_2$		rhomb.	5.14	-	-	62°56'	(139)
$B_{13}O_2$		rh.(hex.)	5.37	-	12.31	-	(139)
$B_{6.6}O$		orthorh.	8.20	5.35	5.13	-	(163)
$B_{12}O_2$		hex.	5.395	-	12.342	-	(175)
$B_{12}Si_3$		rhomb.	5.602	-	-	68°49'	(139)(141)
$B_{12}Si_3$		rh.(hex.)	6.330	-	12.736	-	(139)(141)
$B_{12}Si_2$	(40)	orthorh.	14.392	18.277	9.885	-	(4)
$B_{12}Si_3$		-	6.319	-	12.713	-	(17)
$B_{10}Al$	(5.2)	orthorh.	8.881	9.100	5.690	-	(240)
α-$B_{12}Al$		tetr.	10.28	-	14.30	-	(183)
β-$B_{12}Al$		orthorh.	12.34	12.631	10.162		(183)
BP		cubic	4.537	-	-	-	(244)
BN		cubic	3.615	-	-	-	(183)

Table III.

Densities and Melting Points for Borostitials and Related Materials

Material	Density g/cm³	Melting point °C	Reference
B tetr. I	2.31 e	-	(37)
B β-rh.	2.33 e	-	(37)
B α-rh.	2.46 e	-	(37)
B amorphous	2.354	1260 (trans.)	(219)
B tetr. II	2.364	-	(220)
B β-rh.	2.35	-	(190)
B β-rh.	2.3	2100	(115)
B_4C	2.51 e	-	(7)
$B_{5.85}C$	2.484 e	-	(7)
B_7C	2.47 e	-	(7)
$B_{8.5}C$	2.44	-	(183)
$B_{12}C$	2.48	-	(187)
$B_{13}C_2$	2.48	-	(187)
B_4C	2.53	-	(187)
B_4C	-	2250 (peritectic)	(144)
B_4C	2.519	2450	(22)
B	-	2370-2390	(232)
B_4C	-	2360	(232)
$B_{13}C_2$	-	2480	(232)
$B_{11}C_4$	2.496	-	(120)
BP cubic	2.97 c	-	(183)
BN cubic	3.49 c	-	(183)
$B_{13}P_2$	2.74 e,c	-	(140)
α-$B_{12}Al$	2.58	2100	(115)
β-$B_{12}Al$	2.60	-	(115)
$B_{10}Al$	2.54	2000-2100	(115)
$B_{10}Al$	2.537 c	-	(183)
$B_{12}Al$	2.79 c	-	(183)
$B_{12}Ga$	4.273 e	-	(27)
$B_{12}Ga$	4.130 c	-	(27)
$B_{12}O_2$	2.55-2.62 e	-	(175)(174)
$B_{12}O_2$	2.59 c	-	(175)(174)
$B_{13}O_2$	2.80 c	-	(129)
$B_{13}C_2$	2.64 e	-	(129)
$B_{6.6}O$	2.644 e	-	(163)
$B_{12}S$	2.40 e	-	(139)
$B_{12}S$	2.33 c	-	(139)
$B_{12}Si_3$	2.47 e	-	(141)
$B_{12}Si_2$	2.43	1950	(30)
$B_{12}Si$	-	2250	(5)
$B_{12}Si_2$	2.47	-	(187)
$B_{12}Si_3$	2.41	-	(187)

Table IV.

Comparative Hardness Values

Material	Knoop kgm/mm²	Vickers	Load gms.	Reference
B vac.h-p.up.	2410		100	(47)
B β-rh.sx.	2314		100	(57)
B β-rh.p..	2460		100	(57)
B		2950	100	(174)
B		3440	-	(144)
B		2410	100	(183)
B		3400	50	(183)
$B_{12}C$	6100		30	(187)
$B_{13}C_2$	5490		30	(187)
$B_{12}C_3$	6700		30	(187)
$B_{12}C_3$	2620		100	(57)
$B_{12}C_3$ h-p.	2755		100	(36)
$B_{11}C_4$ pure		8500	peak	(119)
$B_{12}C_3$		4950	30	(183)
$B_{12}C_2$		5600-5800	30	(183)
$B_{12}C$		4100	50	(183)
BP		3200	100	(183)
$B_{13}O_2$		3600	100	(174)(175)
$B_{12}O_2$		3820	100	(174)(175)
$B_{12}Si_3$		1830-2240	100	(183)
$B_{12}Si_2$		2470-2810	100	(183)
$B_{12}Si_2$	1910		100	(30)
$B_{12}Si_2$	1900		100	(47)
$B_{12}Si_2$	2350		100	(49)
$B_{12}Si_3$	2100		100	(49)
β-B_{12}Al sx.	2754		100	(36)
β-B_{12}Al sx.	2450,2525,2870*		100	(57)
α-B_{12}Al sx.	2445,2380,2210*		100	(57)
B_{10}Al sx.	2610,2785,2550*		100	(57)

*at various crystal orientations.

The technique of microindentation hardness testing was described by Knoop (110) in the Journal of Research of the National Bureau of Standards. This paper was reproduced in its entirety by Small (203). Small also presented a description of the Tukon Microhardness Tester. Specifications for the indenter and for the application of the load were included in this paper. A discussion of errors in the test and an experimental procedure were also included.

A book by Williams (251) discussed the theories and definitions of hardness. A background for understanding hardness was described by Mott (149), Kohn (113), and Grodzinski (68) (70). The region of the hardness curve of interest in this study was that section with a load below 100 grams. This was called the low-load hardness region as compared to the macrohardness region above 10 kilograms and the microhardness region below 200 grams. Analysis of the curves of hardness vs. load for the boron phosphide samples showed first, a horizontal area from 200 to 1000 grams; second, an area for which, as the load was decreased, the hardness increase ; third, a peak hardness occurred somewhere in the region of 25 to 50 grams; and fourth, a drop-off area at loads below the peak load. Many theories of hardness state that the microhardness region should follow a hyperbolic law in which hardness should

increase indefinitely as a minimum load is approached. This hyperbolic law does not allow for the drop-off region. Grodzinski (69) discussed the principal ways in which this had been accounted for by various authors. Shaw (196) predicted a variation in yield-stress with specimen size and stated that the apparent increase in hardness with the decreasing indenting load was actually due to the greater flow-stress that accompanies a decrease in thickness of the deformed zone. He called this the size effect. Shaw's work applied to metals that behave in a ductile fashion. A similar treatment was given by Weibull (233) for brittle materials. He suggested a flaw-concept in which the probability of finding a flaw decreased as the specimen size was decreased. The drop-off region was said by Schulze (192) to be a function of the inaccuracies in the device used for testing. Grodzinski (69) suggested that instead of these problems of size, flaw, and technique, one might consider the region in the crystal from a plastic-elastic deformation viewpoint. He pointed out that as the load is increased, one began with a purely elastic region, proceeded next to an elastic-plastic region, then to almost pure plastic deformation, and finally to a heavy fracture area. The elastic effect was found when at very low loads, an indentation was made and when the indenter was removed, no mark was found. If, as supposed by Grodzinski, the drop-off area at loads below the

peak load is caused by elastic-plastic deformation, then a method should be found to measure the effect of elastic recovery after indenting. Several techniques have been tried for coating the indenter with a thin film that will be left behind and thus mark the extreme points of the indent. Vapor-plated silver and flame-deposited carbon have been used with success. Indents in glass have also been observed through the glass at the point of maximum impression to obtain a measurement free of the elastic effect. Grodzinski's measurements established that the hardness of the uncoated material increased with smaller loads below 100 grams and that the coated-material hardness fell almost to zero at small loads.

Hardness is usually defined as either a stress (a load divided by the supporting area) as used in Knoop hardness or as the analog to the modulus of elasticity (the idea of a hardness modulus, i.e., stress per unit of deformation). Grodzinski (70) suggested that since the drop-off zone was related to elastic-plastic deformation, that a new definition of hardness should be given. He proposed that it be defined as the load necessary to produce a given deformation. When this definition is applied, the hyperbolic hardness rule follows. Grodzinski (67) developed an apparatus suitable for measuring hardness at low load in which the

loadwas increased continuously measuring at the same time the depth of the indentation. With automatic recording, load-depth curves and time-depth curves for studying creep and recovery processes could be plotted. In this way, the elastic and plastic properties of a material could be recorded and the hardness test could be made into a true rheological test.

A recent paper by Kranz (119) on the hardness of $B_{11}C_4$ cited an unusual hardness figure (Vickers 8500 kgm/mm^2) for this compound. High temperatures (2300°C) and pressure (120 atm) were used to prevent the precipitation of graphite which caused the hardness to drop sharply at high carbon to boron ratios.

F. Background of Conduction Measurements

1. Mechanisms Contributing to Electrical Conductivity.

In order to evaluate the electrical properties of the boron-phosphide-carbide compacts, some background on the nature of electrical conduction is necessary. Various conduction mechanisms of possible direct application in this study are investigated.

The first consideration in studying the electrical conductivity in the boron-phosphide-carbide compacts is that these samples are polycrystalline and provide several possible conduction paths. Each sample may be thought of as a number of branches

or legs comprising series-parallel circuits along which electrons and holes may flow. The first path to be considered is that developed by the bulk conductivity characteristic of the crystal body; conductivity within each grain then comes from the charge carriers released intrinsically. This intrinsic bulk-conductivity is further modified in two ways. Charge carriers are formed extrinsically at impurity sites, and if grains of different material exist (grains composed of other compounds or phases), each may provide an alternate path for the charge carriers. In such material, for instance, a little of one interstitial element properly distributed throughout the sample could determine the conductivity. In other words, the bulk conductivity is complicated not only by extrinsic sites but by nonhomogeneity within the polycrystalline body.

Books by Putley (170) and Ehrenberg (42) provided excellent reviews of the bulk semiconductor properties of crystal bodies. A review of the conductivity of boron was prepared by Taylor (223). The work of Shaw (198) on the conductivity of boron single crystals established the dependence of boron conductivity on donor impurity levels.

When hot-pressing a polycrystalline material of very fine grain structure, a high surface-to-volume ratio is obtained. Such a system of germanium particle aggregates was studied by Kmetko (108). He concluded that the conductivity was essentially a surface

property in this type of structure. A similar study of metallic films by Bonfiglioli (14) established the importance of enhanced contributions from surface states. In addition to bulk-conductivity and conductivity from surface states, the conductivity along grain boundaries may have a pronounced effect on the overall charge-carrying ability of the material. A study by Henisch (79) proposed a theoretical approach involving potential hills and crystallite boundaries. Two experimental studies, one by Tweet (227) and the other by Abeles (1), determined the effect of an increased number of grain boundaries on the semiconductor properties of the material. In comparing a single crystal with a polycrystalline material with the same number of impurity sites, the resistivity was usually higher in the polycrystalline material because of the barrier action common to grain boundary walls. Where resistance between grains was high, the resistivity fell off rapidly as the frequency of measurement of conductivity was increased because of the capacitive-shorting effect at higher frequencies.

The fourth possible mechanism that might control the electrical conductivity is a contribution from the defect structure of the crystal. The freedom of movement of the charge carriers may be chiefly a function of the amount of interstitial element that is absent from the crystal structure. It is even

possible that it might be a function of the amount of boron missing from the icosahedral structure. Van Bueren (229) pointed out that lattice imperfections scattered both electrons and phonons. Abeles (2) calculated theoretically the effect of lattice vacancies on the electrical resistance and thermoelectric power in metals and showed that resistance was appreciably increased. In Samsonov's work (189) on the boron-carbon system, he stated that the electronic conductance of alloys of the structure, $B_{13}C_2$, was dependent on the number of vacancies along the c-axis. In this study and several of his studies on the phase diagram for the boron-carbon system, he has used electrical resistivity to follow the various phases in the system.

The fifth mechanism which may control or contribute to the electrical conductivity in the borostitial structures is a crystal structure effect. In this effect, the more perfect the crystal structure, the easier the conduction. This may be due to the presence of a path of conjugate bonds in the form of chains or the presence of a general conjugate skeleton throughout the body. Such a conjugate system may be thought of as causing semimetallic conduction or semiionic conduction or both depending on the resonance structures which can exist. A study of the electrical properties of polycrystalline boron by

Uno (228) produced some evidence which showed that the conductivity at room temperature might not increase with the amount of impurities but depends, rather, on the difference in the crystal structure. The resonance idea was applied to boron carbide by Clark (28) who wrote various types of electronic formulas for the C-C-C group and its immediate neighbors. He described the three most probable resonance structures by allowing the double bond and the "no bond" to resonate among the various equivalent positions as required. Clark's proposed degree-of-resonance leads to a condition not far removed from metallic bonding. He suggested that the metallic appearance of the material indicated the presence of some free electrons. Hoard (86) mentioned the idea of a possible general conjugation existing throughout the boron and the interstitial structure.

In either case, the conjugate system would be closely related to organic semiconductors. A study by Aftergut (6) of the electronic properties of organic compounds attempted to relate the chemical structure of heterocyclic compounds to their electrical properties. Another study by Pohl (167) was an attempt to relate the extent of conjugation in semiconducting polymers to the enhancement of electronic properties. In both the work on the heterocyclic compounds and the conjugate polymeric compounds, a similarity to the borostitials was apparent.

Within the conjugated aromatic organic molecules, current flow is unimpeded. It is chiefly the jump from molecule to molecule that hinders the conduction process. The analogous step in polycrystalline materials is the "jumping" of the grain boundary and possibly a deep surface region. This, too, may be the controlling step in these polycrystalline materials if the bulk conductivity within the grain is high. No adequate theory exists to cover the transfer from one organic molecule to the next.

A review of organic semiconductors by Garrett (55) describe the theories that have been applied to conduction mechanisms in molecular crystals. One interesting concept ha been developed for electrons that had left their parent molecules but were not completely free to move as in a continuum of energy states. Under such circumstances, the perfect periodicity of the free case was distorted. As a result, the bands of allowed electron and hole states were expected to be very narrow (0.1 ev or less). If this were the case, it follows that the effective masses would tend to be quite large, and the mobility would accoridngly be lwo. When the mean free path was restricted to molecular (particle) dimensions, the mobiltiy like the carrier density, should show an exponential increase with temperature. The activation energy then represented the process of "hopping" from molecule to molecule.

All of these effects which might modify the electrical conductivity in the borostitials are related by basic semiconductor properties. One or more of them may contribute at various temperatures and with various borostitial compositions. The mutually dependent nature of these effects can be seen by supposing that the lattice defects of the sample were increased. In this case, the scatter of the electrons would increase and the conductivity would fall. One might also think that the increased lattice defects would decrease the order and therefore reduce the resonance of the system again causing the conductivity to fall.

2. Electrical Contacts. The second subject of importance which affects electrical conductivity is that of contacts and contact noise. Shaw (198) reported that one of the biggest difficulties encountered in measuring the Hall voltage of boron single crystals was that of electrical contact noise.

One really has three problems in making good contacts for conductivity and Hall effect measurements. The first is getting the contact there. Shaw (197) solved this for very small samples with a micromanipulator. Pelliekaan (164) solved the problem of attachment by developing an apparatus for fusing contacts to semiconductors. O'Connor (160) used sharpened tungsten wires held against the sample by spring action and secured in place by

Sauereisen cement. He also used conducting plastics, effective to 260°C, for attaching electrodes.

After mounting and attaching or securing the contact by spring action or cement, the third problem is that of making an ohmic contact. Putley (170) summarized the establishment of ohmic contacts to semiconductors. Many forms of solder such as indium and tin-lead were used, evaporated films were used, sputtered films were used, pressure contacts, welds, and chemical depositing agents were used. Such chemical agents as gold chloride and silver nitrate were reduced on semiconductor surfaces to give the free metal which produce an ohmic contact. A form of electroless contact applicable to silicon carbide or boron phosphide had been suggested by Raybold (171). He chemically plated nickel upon the sample after first treating it with stannous chloride and palladium chloride. An electrodeless measurement technique had been suggested by Jacobs (97) in which resistivity measurements of semiconductors were made at microwave frequencies without attaching any contacts. This reduced error caused by surface leakage or crystal imperfections in the semiconductor. Nyberg (159) also suggested an electrodeless technique for semiconductor measurements. His technique is applicable to Hall effect measurements.

3. The Hall Coefficient. When the conductivity (σ) of a semiconductor is determined, the value obtained is a function of the number of charge carriers (n_e for electrons and n_h for holes), the charge per carrier (e), and their freedom of motion or mobibility (μ_e for electrons and μ_h for holes).

$$\sigma = n_e e\mu_e + n_h e\mu_h \qquad (1)$$

This measurement, however, does not differentiate between a very few highly mobile charge carriers and many restricted charges which permit the same ultimate passage of current.

This separation can often be made by measuring the Hall voltage of the sample. If a current is passed longitudinally through a sample, a transverse magnetic field will deflect charge carriers along curved paths and cause a small potential to build up along the axis perpendicular to both the current direction and magnetic field direction. This potential, the Hall voltage (V), is related to the current (I), the magnetic field (B), and the specimen thickness along the magnetic axis (t), by:

$$V = R \frac{I B}{t} 10^{-8} \qquad (2)$$

The Hall coefficient (R) is a proportionality constant. When I is in amperes, B in gauss, t in centimeters, and V in volts, the insertion of 10^{-8} maintains the system of practical

units and thus produces R with the units cm^3/coulomb. The sign of the potential produced is an indicator of the carrier present in excess.

In a material with only electronic conduction, the Hall coefficient is:

$$/R/ = - \frac{1}{n\,e} \tag{3}$$

where n is the concentration of charge carriers and e is the charge per carrier.

This relationship between the Hall coefficient and the electron concentration means that the absolute value of the Hall coefficient is also the proportionality factor between conductivity and mobility.

$$R\ \sigma = \mu \tag{4}$$

A numerical factor enters into (4) as $\frac{3\pi}{8}$ for nondegenerate semiconductors. This factor approaches unity in either the case of degeneracy or in high magnetic fields. In any event, it rarely deviates very much from unity.

In weak magnetic fields, the Hall coefficient for semiconductors exhibiting mixed conduction is:

$$R = - \frac{3\pi}{8} \cdot \frac{n_e\mu_e^2 - n_h\mu_h^2}{(n_e\mu_e - n_h\mu_h)^2} \tag{5}$$

A review of the Hall effect including equations for other measurements in mixed conductors was provided by Putley (170). Putley also described the magnetoelectric effects. The Hall effect is but one of four interaction effects among electric current, thermal current, and magnetic field. In a perpendicular magnetic field, a longitudinal electric current may create a transverse Hall potential and the transverse thermal current of the Ettinghausen effect. If instead, a longitudinal thermal current flows in the same magnetic field, two other effects may be observed. They are a transverse Nernst potential and the transverse thermal current of the Righi-Leduc effect.

Clawson (29) has prepared a bibliography on the theory, design, and application of the Hall effect. The measurement of Hall effect has been the subject of a bibliography prepared by Kraft (118) for the period 1955 through April 1961.

4. Sign Reversal and Surface Effects. According to Putley (170), reversal of sign of the Hall potential was common for some materials such as tellurium, lead telluride, indium arsenide, and Mg_2Sn. Pure tellurium was p-type at low temperatures but change to n-type and began to conduct intrinsically between 200°K and 250°K. At 400°K, it again reverted to p-type The latter change was a true bulk property and was not affected by purity. This was thought to occur because the mobility ratio

of 1.3 fell with increasing temperature as a result of change in the effective masses of the carriers. The band picture was said to consist of two overlapping conduction bands one slightly above the other. The lower band had a larger electron mobility than hole mobility. The upper band had the reverse condition. As temperature was increased, the second choice higher band received a greater proportion of electrons, and the upper sign change was accounted for as bulk property.

Other possible ways of accounting for the upper sign change in tellurium are reviewed by Whelan (239). Among these were the possibility of p-type lattice defects with activation energies of 0.5 to 0.7 ev and a "single conduction-double valence" band model. Evidence so far seems to favor the double conduction band model.

The anomalous sign reversal for the Hall potential of indium arsenide was explained by Rupprecht (182) as a surface effect. The sign change could be created by grinding and removed by etching. Rupprecht also reported that the reversal in lead telluride could be produced by warming an n-type sample in an oxidizing atmosphere.

Welker (235) reported a double sign change for samples of InAs, first at 20°C and again at -100°C. The position of the

first sign change changed only slightly with composition, while the second was quite sensitive to the introduction of doping agents.

In crystals of Mg_2Sn, Frederickse (53) found conduction took place by a surface effect rather than by bulk or impurity-level-induced conduction. Conduction in the n-type material took place through a surface layer with the mobility reduced by a factor of 50-100 times the bulk mobility. This layer could be produced easily by the adsorption of oxygen on the surface. The wave functions of neighboring impurities were said to overlap thus forming a surface band able to carry current.

Channels or leakage paths in transistors can form and modify the interelectrode conductance. Dunlap (41) mentioned that p-type inversion layers have been produced on n-type germanium by an exposure to oxygen, ozone, or hydrogen peroxide. Channels might also be an n-type layer on an n-type base. Two sets of surface states in germanium are now accepted. The first is a group at the surface of the bulk germanium which is within 0.1 ev of the conduction band. The others are in or on an oxide surface layer found on nearly all germanium.

The mechanism of modifications of surface states by gas adsorption, while apparently quite common, is incompletely understood and has received only partial theoretical treatment as yet.

Tweet (227) found that a gold doped (n-type) germanium bicrystal with a relatively high resistivity (10^3 to 10^5 Ω cm) had a low resistance conduction path along the grain boundary. Iron doped germanium was found to show the same effect. The effect was explained by the presence of a number of acceptor levels localized in the grain boundary with energies near the valence band. Electrons from the valence band were trapped by these centers and the resulting holes were confined to a space charge layer surrounding the acceptor levels. Speculation as to the source of the acceptor levels led to either impurities trapped at the grain boundary or distorted and unsaturated valence forces.

5. Magnetoresistance. A semiconductor when placed in a magnetic field frequently exhibits increased resistivity and thus a decreased Hall coefficient. This magnetoresistive effect in metals was studied by Jan (98) and in semiconductors by Johnson (99). The latter work considered the effect of impurity scattering and mixed conduction in high temperature semiconductors. Existing theories predict smaller effects than were obtained experimentally, and Johnson's work increased the difference between experiment and theory rather than reduced it. It also established that a much greater magnetoresistive effect should be expected for intrinsic semiconductors than for extrinsic ones.

When a magnetic field is applied to a semiconductor, the moving charge carriers acquire curved trajectories. The component of motion in the direction of the primary current will be reduced as the magnetic field is increased thus making the resistance increase. The magnetoresistance is usually proportional to the square of the magnetic field at low strengths and linearly related at high fields.

Two unusual effects were reported by Carmichael (24) for vacuum fused polycrystalline boron prepared from zone refined samples. An increase in electrical conductivity was noted upon application of a magnetic field. This reverse magnetoresistance was unaffected by air or argon atmospheres. The samples were p-type to thermoelectric measurements. A charge storage effect was also reported. Current continued to flow after removal of an applied potential. When the potential was applied at very low temperatures, a thermal current release analogous to a thermal-glo curve was obtained upon warming.

6. Conductivity in Boron and the Borostitials . Shaw (197) prepared small crystals of boron from boron tribromide and hydrogen and found the purest to be p-type. He reported that these could be converted to n-type by heat treatment.

An extensive study of the electrical conductivity and Hall potential of single crystals of boron was made by Shaw (198).

The crystals were prepared by pyrolysis of BBr_3 in H_2 between 1300°C and 1600°C. The electrical conductivity of 28 crystals generally followed the same pattern. At high temperatures, they approached an intrinsic line with an activation energy of 1.58 ev. At low temperatures, the curves of logarithm of resistivity vs. reciprocal temperature almost all followed curved paths approaching activation energies between 0.06 ev and 0.25 ev. The deviation from straight-line conductivity was shown to arise from Joule heating. Changes in resistivity curves brought about by high temperature heating were permanent. Heat treatment was thought to introduce imperfections capable of contributing charge carriers.

Shaw (198) made Hall measurements on three boron crystals. Signals between 30 microvolts and 300 microvolts were detected with fields between 5000 gauss and 18,000 gauss. The first sample had a negative potential at 297°K, but at about 430°K changed to a positive sign. Since at high temperatures the number of positive and negative charge carriers must approach equality, this was thought to indicate that the mobility of holes is greater than the mobility of the electrons. This conclusion was verified by Shaw's thermoelectric measurements.

The change in sign occurred before the onset (600°K to 700°K) of intrinsic conduction. The suggestion was made that both acceptor and donor levels were present. The activation energy of the acceptor level was slightly greater than that for the donor but there were more acceptor levels.

The sample that changed resistivity on extensive heating apparently had a large number of ionized donor impurities or defects introduced. The resulting negative carriers lowered the resistivity and changed the sign of the Hall coefficient from plus to minus.

Mobilities for boron have been estimated by Shaw (198) by assuming that the Hall sign indicated charge carriers of only one sign. As a result, mobilities between 0.2 cm^2/vs and 0.9 cm^2/vs were obtained with hole mobilities slightly greater.

Bean (11) reported the preparation of a p-type boron film by pyrolysis of boron tribromide. This material was then purified by vacuum-float zone refining and formed into single crystals. The basic p-type material when melted with small amounts of tungsten remained p-type. If, on the other hand, tungsten were diffused into the single crystal for 12 hours at 1350°C, a 20 micron-deep n-type layer would be produced.

An ultrapure sample of boron was vacuum hot-pressed by Eubank (47), and its electrical conductivity vs. temperature compared with that of similarly prepared commercial boron.

Its resistivity curve was much closer to a straight line than the less pure commercial samples.

A pure boron prepared by Hagenlocher (75) by zone refining was n-type at room temperature and changed to p-type upon heating. Even the best material had a curved activation energy plot which approached an upper limit at $\Delta E = 1.50$ ev. All n-type samples changed sign on heating. The purest sample had a hole mobility of 55 cm^2/vs and an electron mobility of one cm^2/vs at room temperature.

A study by Gaule (56) of single crystal β-rhombohedral boron produced p-type samples with resistivity of 10^6 ohm-cm at room temperature. These samples all approached an intrinsic activation energy of 1.56 ev and leveled off at 0.02 ev in the region from 75°K to 125°K. Absorption measurements on the same samples indicated that crystalline boron could accommodate a large concentration of gaseous impurities. Gaule supported the optical results with unpublished resistivity measurements by Medcalf of samples heated in different gas atmospheres. Oxygen and nitrogen increased the resistivity by 200% while hydrogen decreased it by 35%.

Phosphorous was added to boron by Greiner (65) to prepare two low phosphorous alloys (0.0007% and 0.08%) and one high phosphorous alloy, $B_{6.8}P$ (14.7%). The phosphorous addition decreased

the electrical resistivity in the extrinsic conductivity range. The resistivity of the $B_{5.8}P$ alloy was significantly lower at low temperatures and higher at high temperatures than the low phosphorous alloys. It was also of a different crystal structure.

Electrical resistivities for boron and the borostitials are collected in Table V. Activation energies, both extrinsic and intrinsic, are compared in Table VI. Information available on Hall coefficient, Hall mobility, and concentration of charge carriers is assembled in Table VII.

G. Background of Thermoelectric Measurements

1. Thermoelectric Effects. One of the objectives of this study was to determine the thermoelectric value of the phosphide compacts. The thermoelectric power and thermal conductivity are combined with the electrical conductivity to determine the thermoelectric merit of this material. A discussion of each effect, a review of methods of measurement, and any special features applicable to the system studied are presented. Values of thermoelectric power are presented in Table VIII.

Table V.

Electrical Resistivities in Boron and the Borostitials

Material	Resistivity Ω cm	Temperature °C	Reference
B amorphous	1×10^{4}	RT	(219)
B argon	10^{6}	RT	(155)
B vacuum	10^{8}	RT	(155)
B 1000°C	0.1	RT	(10)(54)
B 1300°C	2700	RT	(10)(54)
B 1500°C	10^{6}	RT	(10)(54)
B β-rh.sx.	1.7×10^{6}	RT	(197)
B β-rh.	10^{11}	-160	(65)
B β-rh.	10^{6}	RT	(65)
B β-rh.	0.1	700	(65)
B up.px.	4×10^{6}	RT	(75)
B up.px.	5×10^{-2}	1950	(75)
B β-rh.sx.	10^{-3}	1775	(56)
B β-rh.sx.	10^{6}	RT	(56)
B β-rh.sx.	10^{11}	-175	(56)
B px.	200	RT	(228)
B sx.	1×10^{6}	RT	(199)
B sx.	below 1	550	(199)
B	1×10^{6}	RT	(65)
B	5×10^{10}	-150	(65)
B+0.0007%P	3×10^{5}	RT	(65)
B+0.0007%P	2×10^{9}	-150	(65)
B+0.08%P	2×10^{3}	RT	(65)
B+0.08%P	1×10^{6}	-150	(65)
B+14.7%P ($B_{13}P_2$)	3×10^{2}	RT	(65)
B+14.7%P ($B_{13}P_2$)	2×10^{3}	-150	(65)
$B_{13}P_2$ h-p.	1×10^{4}	RT	(165)
$B_{13}P_2$ h-p.	2.5	500	(165)
$B_{13}P_2$ sx.	10^{6}	RT	(208)
BP sx.	1	RT	(208)
$B_{12}C_3$	0.3-0.8	RT	(15)
$B_{12}C_3$	0.445	20	(172)
$B_{12}C$	5.6	RT	(187)
$B_{13}C_2$	0.05	RT	(187)
$B_{12}C_3$	1.6	RT	(187)
$B_{12}Si_2$	0.16	RT	(49)
$B_{12}Si_3$	4	RT	(49)
$B_{12}Si$	0.2-10	RT	(5)
$B_{12}Si_2$	0.2	RT	(5)

Table VI.

Comparison of Activation Energies

Material	Prepared from	Activation energy ev intrinsic	extrinsic	Reference
B argon	BCl_3	1.1		(155)
B vacuum	BCl_3		0.6-0.7	(155)
B	B_2H_6	1.2		(148)
B	B_2H_6	1.03	0.65-0.7	(148)
B 1000°C	B_2H_6		0.3	(10)(54)
B 1300°C	B_2H_6		0.86	(10)(54)
B 1500°C	B_2H_6	1.12		(10)(54)
B	BBr_3	1.55		(197)
B vac.h-p.up.		1.45		(47)
B commercial		1.27,1.18, 0.94		(47)
B up.px.		1.5	0.6 (Be)p	(75)
B up.px.		1.5	0.7 (C) n	(75)
B up.px.		1.5	0.5 (Si)n	(75)
B β-rh.sx.		1.56		(56)
B α-rh.sx.		2.00	+ shallow levels	(89)
B px.		1.39		(66)
B		1.2	0.03,0.06	(128)
B		-	0.44,0.64	(128)
B		1.5		(115)
$B_{12}C_3$		1.64		(258)
$B_{12}C_3$			0.7	(127)
$B_{12}C_3$		1.64	0.7	(184)(188)
BP		5.8		(249)
α-$B_{12}Al$		1.8-1.9		(115)
$B_{12}Al$		1.7		(126)
$B_{12}Al$		1.4,1.08, 1.22	+ shallow levels	(25)
$B_{12}Si_3$		2.0		(49)
$B_{12}Si_2$		1.2		(49)

Table VII.

Values of Hall Coefficient, Hall Mobility, and Concentrations of Charge Carriers for Boron and Boron Phosphide

Material	Measured values	Temperature	Reference
B p-type	$\mu_e = 0.7$ $\mu_h = 0.9$ cm^2/vs	RT	(197)
B sx.	$R_H = 400$ cm^3/coulomb $\mu = 0.1$ to 0.9 p-type predominates	RT	(198)
B px.	$\mu_e = 1$ $\mu_h = 55$ cm^2/vs	RT	(75)
BP n-type	$n = 10^{17}$ carriers/cm^3	RT	(208)
BP sx. p-type	$R\sigma$ = 10 to 100 cm^2/vs μ = 300 to 500 cm^2/vs $n = 5 \times 10^{18}$ carriers/cm^3	160°K-900°K	(209)

Table VIII.

Comparative Values of Thermoelectric Power

Material	α μv/°C	Temperature °C	Reference
B β-rh.sx.	500	RT	(56)
B	300-325	100-700	(155)
B_4C	280 700	RT 2200	(15)
$B_{12}C$	250	RT	(187)
$B_{13}C_2$	200	RT	(187)
B_4C	235	RT	(187)
BP	300	RT	(209)
B_6Si	80	RT	(187)
B-Si-C	50-300	RT	(169)

Relationships between heat flow and electrical-charge-carrier flow in a material are called thermoelectric effects. The first such effect occurs when two different materials are joined and the junction is heated. Charge carriers tend to diffuse from the hot junction to the colder unconnected ends. Since the degree of charge shift is different for the two materials comprising the couple, a net potential will exist between the two unconnected ends. This potential is proportional to the temperature difference (ΔT) between the junction and the open end. The Seebeck coefficient (α) is the proportionality constant between small changes in temperature and the small potentials created:

$$\alpha = \frac{E}{\Delta T} \tag{6}$$

Shorting the two unconnected ends causes a current to flow in the loop.

If a current is passed through the junction of two different conductors, heat is either released or absorbed at the junction. This heat is a linear function of current compared to the quadratic function of Joule heating. The proportionality constant in the former effect is the Peltier coefficient (π).

$$Q = \pi I \tag{7}$$

A third thermoelectric effect was observed by Thomson. He found that heat (Q) was generated or absorbed in addition to the Joule heat by passing current (I) through a conductor along a temperature gradient $\left(\frac{dT}{dX}\right)$:

$$Q = \tau I \frac{dT}{dX} \tag{8}$$

The proportionality constant (τ) is the Thomson coefficient.

The three thermoelectric effects are related through the Kelvin expressions:

$$\alpha T = \pi \tag{9}$$

$$\frac{d\alpha}{dT} T = \tau_1 - \tau_2 \tag{10}$$

The development of thermoelectric theory evolved from two parallel approaches: from thermodynamic derivations and from the electron theory of metals. More recent developments begin with these results and are concerned with the more complicated interaction terms such as those arising from phonon drag.

In 1928, Kammerer (102) initiated the thermodynamic approach by using a temperature-entropy diagram to describe thermoelectric phenomena. Three years later, Onsager (161) produced his often-quoted paper on the reciprocal thermal relations involving nonreversible processes. Onsager specifically

cited the Thomson, Hall, and Righi-Leduc effects. In 1932, Bruzs (18) added an explanation of the Seebeck and Peltier effects. Onsager's reciprocal relations were applied to thermoelectric, thermomagnetic, and galvanomagnetic effects by Callen (21) who was able to derive the Seebeck, Peltier, and Thomson effects as well as the two Kelvin relations. He also obtained the equations of the Hall, Ettinghausen, Nernst, and Righi-Leduc effects. A book by DeGroot (38) began with Onsager's reciprocal relations and outlined the thermoelectric derivations by several methods. By considering the entropy changes in a complete thermocouple, he derived the Seebeck, Peltier, and Thomson relations. DeGroot's book (38), an article by Callen (20), and an article by Domenicali (39) provided the best summaries of these derivations through 1954.

The second approach to thermoelectric theory started with the Lorentz-Sommerfield theory of conduction in metals about the same time the thermodynamic approach began. The free electron theory was first extended to nonmetals, then holes and electrons were considered together, and then interaction and scattering terms were added. Next, mean free path correlations and anisotropic variations were added, and finally, the concept of phonon drag was introduced by Gurevich (73) in 1945, to account for an unusual low temperature rise in the thermoelectric

power of metals. A similar contribution was found in semiconductors by Herring (81).

As can be seen by the above developments, any effect which serves to impede or divert the flow of heat or current will affect the thermoelectric properties. Irregularities frequently enhance the thermoelectric power as shown by Abeles (1)(2) first in a study of lattice defects in metals and second in a study of metallic grain boundary effects.

Domenicali's study (39) included the effects for anisotropic, inhomogeneous, and defect materials as well as the more perfect media. Greene (64) has proposed a theory of surface thermoelectricity based on a surface space charge region. The thermoelectric power of germanium powder which conducts through a surface layer was found by Kmetko (108) to be a function of the surface. A change of atmosphere from oxygen to water vapor also changed the sign of the thermoelectric power from plus to minus and altered its magnitude over several hundred microvolts per degree centigrade. Granville (60) studied the surface layers on germanium and lead sulfide by means of thermoelectric properties.

Thermoelectric measurements on single crystals of boron were made by Shaw (198). He found that hole conduction predominated at high temperatures, but at low temperatures, hole conduction predominated only in typically high-resistance crystals.

At low temperatures, electron conduction may predominate in low-resistance crystals. Thermoelectric power values ranged from -200 μv/°C to -600 μv/°C. Some samples increased in positive value with increasing temperature while others went through a maximum positive value between 200°C and 400°C.

Although the sign of the thermoelectrical potential is frequently used to determine the sign of the carriers, Henisch (78) pointed out that this test should be used with reservations. Distributed thermal potentials could alter the measured sign in samples with a heterogeneous distribution of impurity centers. Samples with contaminated surfaces could also exhibit thermoelectric potentials with misleading signs.

The Seebeck coefficient for a mixed conductor is:

$$\alpha = -\frac{k}{e}\,\frac{n_e\mu_e\left(2-\frac{E_F}{kT}\right) - n_h\mu_h\left(2-\frac{E_G - E_F}{kT}\right)}{n_e\mu_e + n_h\mu_h} \qquad (11)$$

where k is the Boltzman constant, e is the electronic charge, n_e is the number of electrons, n_h is the number of holes, μ is the mobility, E_G is the band gap, and E_F is the position of the Fermi level. A semiconductor with equal numbers of holes and electrons for the same mobility will have, then, a greatly decreased thermoelectric power because of an increased denominator in expression (11).

2. Thermal Conductivity. The basic equation for the conduction of thermal energy per unit time along a solid path is:

$$Q = -K\,A\,\frac{dT}{dX} \tag{12}$$

In a purely conductive system, the amount of heat carried per unit time is proportional to the area carrying heat and the temperature gradient causing the energy transfer. The proportionality constant is called the thermal conductivity.

The thermal conductivity is a more complex function in semiconductors than in metals and insulators. In metals, the transfer of thermal energy is by electron motion. In insulators, the movement of bundles of vibrational energy (phonons) throughout the lattice accounts for the transfer. In both metals and insulators, scatter and interference mechanisms which impede this transfer of thermal energy are present. Thermal energy is transported in semiconductors not only by electrons and phonons, but also by the motion of holes. With a limited number of charge carriers, the scattering of carriers is proportionately more important, and with more transfer mechanisms, interactions effects are more pronounced.

Because each mechanism of thermal conduction contributes to a different degree at each temperature, and because many absorption modes are present, the interpretation of thermal conductivity values for many semiconductors is semiempirical. This is particularly true for complex polycrystalline samples.

The subject of thermal conductivity in semiconductors and ceramics was reviewed by Drabble (40), Kingery (104), and Norton (157). Drabble's book, in particular, provided a comprehensive review of theories, methods of measurement, and a comparison of measurements with theory from which much of this survey was obtained.

All of the theories suggested to explain thermal conductivity must begin by approximating Eucken's law. This is an experimental law that states that as temperature is increased, the increased amplitude of vibration will decrease the passage of thermal energy. The thermal conductivity then is proportional to the reciprocal of temperature. This $\frac{1}{T}$ law is obeyed by many materials with low thermal conductivity. The high temperature end of the curve for better conductors is found to follow other functions dependent on the concentration of charge carriers.

The propagation of displacement waves through a material depends on the density of the particles and the elastic constants connecting them. The density determines the displacement of mass,

and the elastic moduli define the restoring forces. Propagation without loss occurs when the material density and its elastic moduli are both homogeneous. Irregularities caused by structural variations or interference effects cause scattering which reduces the thermal conductivity thus producing the $\frac{1}{T}$ law. The greater the displacement of atoms from their mean, the more the scattering effect. This is why a tightly-bonded solid of light atoms conducts more readily than a loosely-bonded material of heavy atoms in which large displacements are expected.

The thermal conductivity is made up of a lattice conductivity (K_L) and an electronic conductivity (K_e).

$$K = K_L + K_e \tag{13}$$

In a metal, Wiedmann and Franz showed experimentally that the ratio of thermal to electrical conductivity is the same for all metals at a given temperature. Lorenz showed that the ratio was proportional to absolute temperature. These observations for a degenerate metal are combined in the expression:

$$K = \frac{2\pi}{3}\left(\frac{k}{e}\right)^2 \sigma T \tag{14}$$

The Debye equation,

$$K_L = 1/4\ \rho C_v \lambda \tag{15}$$

applies to the conductivity of crystals where ρ is the density, C_v is the heat capacity per unit volume, and λ is the mean free path of the wave packet.

From these equations, the thermal conductivity of a semiconductor can be seen to be affected by the following:

1. The number of charge carriers which is determined by:
   the degree of purity, the nature of the impurities, the extent of mixed conduction;

2. The mobility of the charge carriers which is:
   a function of material and charge carrier effective masses;

3. The anharmonic elastic constants in the crystal which:
   redistribute phonon energy among the modes thus contributing to charge carrier-phonon interference and phonon-phonon interference, this is the source of isotopic effects;

4. The anharmonic elastic constants in the crystal which cause:
   unequal bonding or directional effects that contribute to scatter;

5. Crystal imperfections which:
   interact with phonons and act as sources and sinks of charge carriers;

6. Crystal boundaries which:
   being poor reflectors of phonons limit the mean free path to crystal size, the mean free path is therefore more limited in polycrystalline bodies than in single crystals and is still smaller in amorphous bodies and disordered systems;

7. The heat capacity which is:
   controlling only in a system where the mean free path is extremely limited.

In addition to the very low temperature maximum, the central position of a thermal conductivity vs. temperature curve has on several occasions exhibited a slight maximum instead of following the approximation to the $\frac{1}{T}$ curve. This effect was reported by Austin (9) and Kittel (107) for various compositions of glass and quartz crystal. While the thermal conductivity of quartz crystal climbed sharply at low temperature, the addition of a glass-phase produced increasing reduction at low temperatures. Fused quartz and boro-silicate glasses actually possessed slight maxima in the 100°C to 400°C region. Kittel proposed that the mean free path be limited to about the 4-15 angstrom range of the dimensions of the "unit cell" of the glass. With the mean free path limited by the disordered state of the glass, its thermal conductivity became a function of the volume heat capacity which decreased with temperature.

Wray (253) also obtained thermal conductivity curves that dropped at low temperatures for clear fused silica. Radiative effects were minimized in his experiment.

A study of alumina, magnesia, and beryllia by McQuarrie (137) produced two deviations from expected results. A plot of thermal conductivity vs. temperature indicated a maximum conductivity from about 500°C to 1000°C and a minimum for the region above 1000°C. McQuarrie stated that the low temperature rise in

conductivity for beryllia was to be expected because of its abnormally high conductivity. The higher temperature minimum in conductivity was explained on the basis of radiative transfer of energy through the body.

The concept of the transfer of energy by internal radiation has been proposed as a mechanism to account for a very marked maximum in the thermal conductivity of pure tellurium form 150°K to 500°K. A study was made by Devyatkova and reported by Drabble (40). Three samples of single crystal tellurium, each with a different impurity level, were measured. Only the least pure sample behaved as expected. The purest sample showed the most deviation from the thermal resistivity vs. temperature straight line function. In a sample transparent to infrared, Devyatkova expected energy transfer by photons to be considerable. The least pure sample then had sufficient free charge carriers to scatter the radiation and prevent the abnormal effect of the curve.

Beryllia was studied by Taylor (222) and found to follow exactly the $\frac{1}{T}$ relation to 1700°C. Above this temperature, complications such as grain growth affected the results. Taylor discounted the radiation mechanism in polycrystalline fine grain ceramics and suggested that deviations might result from an incomplete understanding of the theory.

Measurements of the thermal conductivity of refractory brick by Ruh (179) again produced many samples whose conductivity decreased with temperature. These were fireclay and silica compositions evidently with a high state of disorder. A clay-bonded silicon carbide sample not only had a high thermal conductivity, but its curve was almost horizontal and possibly even exhibited a slight maximum.

Deviations from expected behavior have been attributed to: (1) a high degree of disorder as in a glass or a bonded system, (2) an excessive number of charge carriers as in the low temperature effect for beryllia, and (3) a radiation contribution as in the high temperature effect for beryllia and in tellurium crystals at lower temperatures.

Thermal conductivities are measured by either static or dynamic methods. The static or steady-state method requires an exact determination of the heat input and pattern of heat flow. While measurements at thermal equilibrium are more accurate, they are also more time-consuming. If, instead, a dynamic method is used, the thermal gradients are observed as a function of time, and more rapid measurements are possible.

A comparative measurement is a variation of the steady-state method. In this case, the heat input is determined by

the thermal characteristics of a standard and not by an absolute electrical or calorimetric measurement.

Drabble (40) described a comparative apparatus constructed by Stuckes (215) which is of interest in this study. Since the procedure is described in the Experimental Procedure section of this investigation, it is sufficient to mention the chief problems associated with such a test unit. Good thermal standards and adherence to sound construction and operating techniques are certainly required. As in most steady state testing, the accuracy of the measurement depends on ones ability to get the heat to flow along the theoretical paths under the conditions in which a single mechanism of conduction prevails.

Very few measurements have been made of thermal conductivity of boron and the borostitials. The values that were reported have been assembled in Table IX. Briggs (16) has prepared a general bibliography on heat conduction in solids.

3. The Thermoelectric Figure of Merit. The thermoelectric figure of merit (Z) is:

$$Z = \frac{\alpha^2 \sigma}{K} \qquad (16)$$

Ioffe (93) pointed out that all three of the terms on the right are functions of the concentration of n, the concentration of charge carriers. The electrical conductivity (σ) and the

Table IX.

Thermal Conductivities of Boron and the Borostitials

Material	Thermal conductivity Kcal sec^{-1} cm^{-1} $°C^{-1}$	Temperature °C	Reference
B amorph.	0.0077	60	(219)
B px.	0.003	20-80	(217)
B_4C	0.05	1000	(104)
	0.07	100	(104)
B_4C	0.155	700	(183)
	0.180	500	(183)
	0.220	300	(183)
	0.290	100	(183)
B_4Si	0.023	70	(49)
B_6Si	0.023	70	(49)
$B_{13}P_2$	0.084	25	(165)

electronic thermal conductivity (K_e) are both proportional to n. The thermoelectric power (α) tends to approach zero with too high an increase in n. Ioffe showed that $\alpha^2\sigma$ reached a maximum at about $n = 10^{19}/cm^3$. He also pointed out (95) that $n = 2.5 \times 10^{19}/cm^3$ was the approximate dividing line between nondegenerate conduction and the beginning of degenerate conduction.

$$K_e = A\sigma \tag{17}$$

A nondegenerate $= 1.0 \times 10^{-6}$ (at 290°K).

A degenerate $= 1.65 \times 10^{-6}$.

It is clear that too high a degeneracy will reduce the Wiedmann-Franz ratio, but the introduction of a measured amount of impurity can be favorable. Ioffe stated that extensive doping can be used to increase $\alpha^2\sigma$ in spite of the attendant drop in mobility.

A review of the figure of merit by Drabble (40) led to the conclusions that:(1) the Fermi level of the best materials should be near the contributing band edge (i.e., the valence band for p-type and the conduction band for n-type materials). At this point, α is about 200 $\mu v/°C$. Higher values of α are not desirable because of a rapid decrease in n and thus also in σ. The second conclusion is that:(2) at optimum carrier concentration, Z depends on the carrier mobility (μ), the

the effective mass (m^*), the scattering parameter (p), and K_L as:

$$\frac{\mu}{K_L}\left(\frac{m^*}{m}\right)^{3/2} \tag{18}$$

Both the numerator and the denominator of the first term $\left(\frac{\mu}{K_L}\right)$ are usually large in covalently bound materials and small in ionically bound materials.

Ioffe (93) called boron a crystal with pure valence bonds with an energy gap of 1.1 ev and an impurity gap of 0.5 ev. From its properties, Ioffe conclude that $\frac{m^*}{m} = 0.7$.

Many thermoelectric materials depend on high temperature for efficient operation. Too high a temperature, even though the material can withstand it, leads to other complications some of which Ioffe (94) summarized. He stated that additional conductivity was caused by diffusional flow of electron-hole pairs, exciton flow, the drag of phonons by pair flow, the drag of phonons by exciton flow, and heat transfer caused by radiation.

Chasmar (26) has considered the effect of energy gap upon a choice of material for thermoelectric application. He point out that the gap should be sufficient to prevent degradation of the figure of merit by the buildup of minority carriers, i.e., intrinsic conductivity. To the contrary, large band gap materials usually have low carrier mobilities and high thermal

conductivities. It is best, then, to have a material in which the band gap is just large enough for operation.

III. EXPERIMENTAL PROCEDURE

A. Materials

For all of the hot-pressed compacts, the starting materials were either finely powdered boron monophosphide, BP, or a suitable mixture of amorphous boron and amorphous red phosphorous. The materials were used in one of the seven patterns shown in Table X. Most of the 83 hot-pressed compacts were prepared by the first scheme, i.e., the rapid decomposition of BP in the hot-press as pressing conditions were reached. By pressing BP below 1550°C, a soft compact of BP with little or no decomposition was produced.

The slow decomposition of ten samples of BP to $B_{13}P_2$ was carried out in vacuum as shown in the third scheme. One other was slowly decomposed in hydrogen while three others were rapidly heated to $B_{13}P_2$ in the induction furnace as shown in scheme four.

Since, as shown in the next two methods, amorphous boron and amorphous phosphorous could be reacted rapidly, BP and $B_{13}P_2$ could be produced at will by controlling the boron-to-phosphorous ratio and the temperature of reaction. By placing the boron-phosphorous mixture into a furnace preheated to between 1600°C and 1800°C, the subphosphide was produced. An excess of 10 to 20% phosphorous was added to ensure a phosphorous atmosphere

Table X.

Preparation Procedures

	Starting material	Fast reaction furnace	Slow decomposition vacuum furnace	Product of hot-pressing
1.	BP →			→ $B_{13}P_2$
2.	BP →			→ BP
3.	BP →		→ $B_{13}P_2$	→ $B_{13}P_2$
4.	BP →	→ $B_{13}P_2$ →		→ $B_{13}P_2$
5.	B + P →	→ $B_{13}P_2$ →		→ $B_{13}P_2$
6.	B + P →	→ BP →		→ $B_{13}P_2$
7.	B + P →			→ $B_{13}P_2$

long enough for reaction to take place. At lower temperatures and with a slight excess of phosphorous over the one-to-one atomic ratio, pure monophosphide was produced. Twenty-one such reactions were carried out, each under slightly different conditions. The products were analyzed and the best ones used for hot-pressing.

The final method is that of reaction hot-pressing which was quite successful. The technique here was to preheat the induction furnace, place the cold mold in a massive hot susceptor, and press as soon as the optical pyrometer indicated that reaction temperature was attained. This material compared favorably with that of the hot-pressed compounds.

Although some of the BP was made by direct reaction, most of the BP used in methods one through four was supplied by The Monsanto Company. This material was prepared originally by combining ferroboron and phosphorous or ferrophosphorous. Boron monophosphide formed and the iron was removed by acid leaching. This process is now covered by Stone's patent (207) assigned to The Monsanto Company.

The Fisher Chemical Company and The U.S. Borax Company supplied pure amorphous boron. Ultrapure amorphous boron was obtained from The Leytess Metal and Chemical Corporation.

Technical grade red phosphorous from The Fisher Chemical Company was used for preliminary trials, but ultrapure phosphorous was obtained from The American Agricultural Chemical Company and used for the final preparations.

A product of The Allis-Chalmers Company, Cerac 3, was obtained as a sample of $B_{13}P_2$. Several pure samples of $B_{13}P_2$ were obtained through the courtesy of Dr. Matkovich of The Carborundum Company.

B. Hot-pressing

A hot-press was constructed for the pressing of the boron phosphide samples. It is described in the 1961 Annual Report of the ONR project (62). It was designed to press molds up to eight inches in length. For most of the samples prepared in this study, an inner graphite-tube susceptor was added to take two and a half inch outside diameter molds, three inches long. By drilling an off-center hole up through the base and through the mold-support carbon blocks, a sight path for an optical pyrometer was provided. This measured the temperature on the bottom of the mold immediately adjacent to the ram. This sight path was flushed with helium while pressing to remove phosphorous vapor. The phosphorous pentoxide which formed at the top of the hot-press was condensed in a water-cooled steel suction cap fitted over the outside silica cylinder.

The silica cylinder was surround by a 7-1/2 inch ID induction coil with forty turns which was connected to a 20 kw output spark-gap converter high frequency power supply. Between the silica tube and the machined graphite susceptor tube was a packing of carbon black insulation. Carbon blocks were machined to fit above and below the mold to reduce vertical heat loss.

The graphite molds were 2-1/2 inches in diameter by 3 inches in height. The ram diameters were either 19/32 or 3/4 inch. All molds were cooked out at 2000°C before use to remove volatiles. The first mold used, see Figure 5, had quarter-inch thick tips of boron nitride (BN) on the cylindrical rams. The insides of the mold were painted with a suspension of BN powder in a 50% water - 50% alcohol solution. In one series of runs, two samples were prepared one above the other each with BN tips above and below.

It is interesting to note that the use of boron nitride as a high temperature liner was introduced by Weintraub (234) in 1913. He used it to protect the "purity" of boron parts being pressure sintered.

As boron or boron phosphide was heated from 1800°C to 2000°C, the rate of carbide formation increased markedly. This carbon came from impurities, pick-up from contact with the

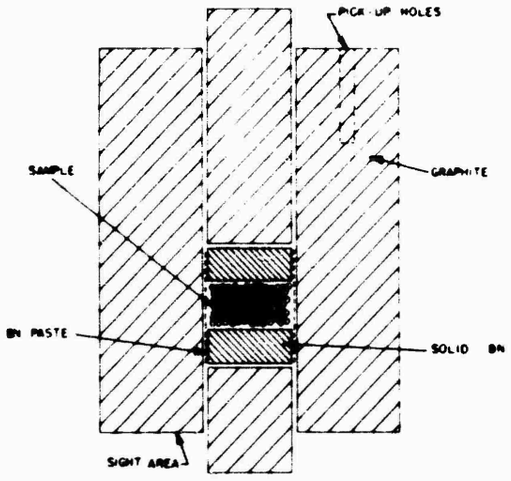

Figure 5. Coated Mold for Hot-pressing

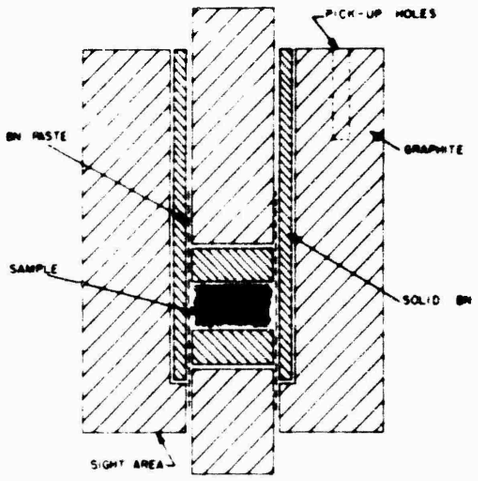

Figure 6. Completely-lined Hot-press Mold

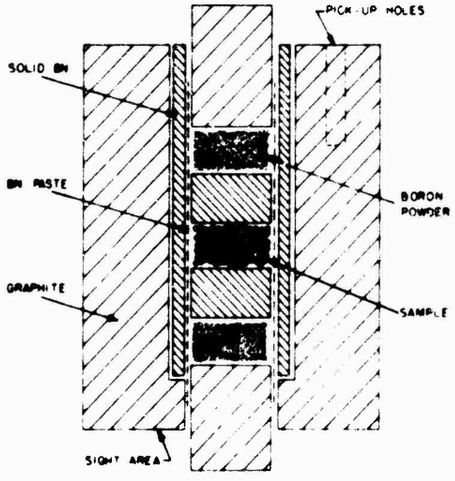

Figure 7. Lined and Sealed Hot-press Mold

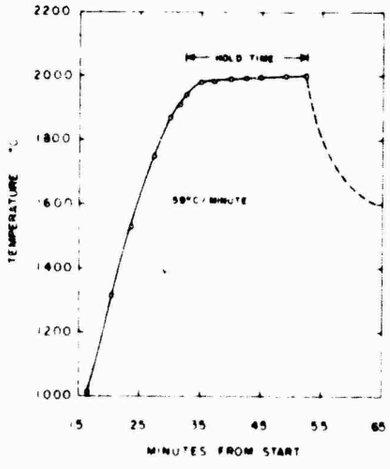

Figure 8. Typical Hot-pressing Time-Temperature Curve

graphite mold, volatile carbon compounds, or any combination of these factors. Carbon monoxide and dioxide were particularly suspected of being the cause of sample contamination. After obtaining pure starting materials and isolating the sample, the next requirement was to seal the sample and reduce the effect of volatiles.

The second mold design was fully lined with solid boron nitride as shown in Figure 6. The machined boron nitride sleeve was forcibly pressed into the center of the graphite mold prepared for it. The boron nitride paste was still used to coat the inside of the mold to increase the seal. A variation in the use of the fully lined mold is shown in Figure 7. Boron powder was placed above and below the sample as shown. As the temperature increased, the boron changed to boron carbide thus sealing the sample in and keeping out volatile forms of carbon. The outside plugs pressed first, thus making possible sufficient pressure on the sample for high density. Helium flow was increased inside the susceptor and nitrogen flow was added between the silica tube and the graphite susceptor. The gases acted to reduce oxygen which could form carbon monoxide and dioxide.

An optical pyrometer was aimed at the sight area shown in Figures 5, 6, and 7. This was calibrated against a standard light bulb and the temperature distributions inside the mold

determined by a high-temperature thermocouple. As a further check, a hole was drilled up into a mold thus putting the optical sight area right next to the sample.

A tungsten 3% rhenium vs. tungsten 25% rhenium thermocouple with a thoria sleeve was used for calibration. This thermocouple is available from Engelhard Industries, Inc. Each type of mold and each sample position was measured and the results related to the optical measurements used in operation. Consequently, all pressing temperatures have been corrected and pressing temperature tolerances estimated.

The temperature vs. time curve for each pressing was plotted, and the pressing rate and hold-time tabulated. A sample heating curve is included in Figure 8 since the heating rate is a function of furnace heat capacity, heat loss, power output, and coupling. This sample was heated at 59°C per minute and held between 1950°C and 2000°C for twenty minutes. Other pressings were made at heating rates from 7°C to 86°C per minute with most of them at 60°C per minute. Hold-times varied from 0-78 minutes with most of them 0, 10, or 20 minutes.

Pressing temperatures range from 1360°C to 2180°C. Most of the samples were pressed between 1930°C and 2030°C with best tolerances estimated at 20°C and poorest at 50°C. All pressings were made between 5000 psi and 6000 psi. The 6000 psi figure

was the maximum dictated by the strength of the rams and the strength of the carbon block below the bottom ram. Since the sight hole angled up from beneath the bottom ram, exact placement of the mold was required each time both to prevent failure in the blocks and to ensure an exact sight area.

As an alternate method to the solid boron nitride linings, a sleeve of tungsten was inserted for two hot-pressings. Solid boron nitride ram tips were used within the tungsten sleeves. The first sample of BP pressed at 1850°C produced a poorly-bonded compact and a mild reaction between sample and sleeve. The second attempt at 2000°C produced a very hard compact which melted where the edges touched the sleeve. The compact was highly crystalline and exhibited mixed X-ray diffraction patterns of tungsten borides.

C. Reactions

Reactions were carried out in the induction-powered hot-press. The graphite mold and its carbon spacers were removed from the graphite susceptor tube. An alumina combustion tube was inserted vertically and a heavy graphite ring placed in the susceptor tube and around the alumina tube but not touching it.

Many samples were prepared in alumina crucibles shaped from bubble alumina refractory bricks supplied by The Norton

Company. Covers, plugs, and spacers were also made from this material because it has excellent thermal shock resistance.

Since reactions were carried out between 1600°C and 1800°C, the carbon alumina reaction must be considered. To reduce this reaction which proceeds rapidly above 1725°C, contact was minimized. Since alumina tubing becomes porous in the higher reaction temperatures, helium was continuously flushed through the inner alumina tube containing the sample in a 10-inch alumina crucible. Nitrogen was flushed through the area between the central alumina combustion tube and the outer silica tube. The helium and nitrogen were needed to eliminate an influx of volatile carbon compounds which reacted readily with the boron or the decomposing boron phosphide. Twenty-one samples were prepared in this manner with reaction times from 5-35 minutes. By simply interchanging the helium and nitrogen, a simple test was made in two reactions to see what nitrides formed. Boron powder in the sample crucible was subjected to nitrogen in the 1600°C to 1800°C range with markedly different results.

Two methods were used for the reactions. In the first, sample crucibles were raised on alumina rods into a preheated reaction zone, held for a suitable combination period, and removed before combined phosphorous could be further reduced.

In the second, cold sample crucibles were heated in a furnace which could be rapidly heated and cooled by reducing the mass to be heated.

D. Decompositions

The ten vacuum decompositions were carried out in the temperature range 1140°C to 1360°C for between 13 hours and 69 hours. The BP powder supplied by The Monsanto Company was used for all of the decompositions. For the vacuum decompositions, it was placed in an alumina boat. This boat was placed in an evacuated silica tube which was connected to a mechanical vacuum pump through a liquid nitrogen trap.

One sample was decomposed at 1000°C for 24 hours in a continuous stream of pure hydrogen.

Three samples were rapidly decomposed in a helium atmosphere in the reaction furnace at 1600°C to 1800°C. Decomposition time ranged from 15-30 minutes.

E. X-ray Studies

X-ray diffraction patterns were obtained for all powders prepared by decomposition and reaction. Because of the extreme hardness of the hot-pressed compacts, their sufaces were ground and patterns determined for the solids by flush mounting them in micarta holders machined for the purpose. The major peaks were tabulated for over 170 compacts and for portions taken from the preparations.

In addition, a precision study was made of the spacing between the 104 and 021 peaks of the $B_{13}P_2$ X-ray diffraction patterns. This information was needed to distinguish between $B_{13}P_2$ and $B_{12}P_2$ since they were expected to have different values if they were present as distinct compounds. About 130 "doublet" spacings were measured.

Since indications pointed to the presence in the compact of two distinct X-ray patterns, knowledge of the extent of possible solid-solutions between them was desirable. By using Cohen's method (32) as outlined by Henry (80), three major X-ray diffraction peaks from a pattern were selected and the rhombohedral unit cell parameters determined. Peaks were selected from three mutually perpendicular sets of planes which best defined the change in shape of the unit cell as the interstitial atoms were changed. Parameters were determined using different groups of planes and two references. Since no fiduciary point had been determined for the patterns, the parameters were referred primarily to the 100 intensity peak of $B_{13}C_2$ which was given a recognized angle from the literature. Because in some samples the carbide content was sufficient to make the phosphide 100 peak indistinct, the $B_{13}P_2$ 100 peak was used as a seondary reference point.

With two references and many composition variables from the boron-phosphorous-carbon system, about 280 sets of parameters were determined. Since each set required several hours of calculation to solve the three simultaneous equations involved, the IBM 1620 Computer was used.

The X-ray diffraction work was done on a General Electric (XRD-5) Diffraction Unit with copper radiation. Additional X-ray measurements were made using the General Electric (XRD-6) Fluorescent X-ray Unit. Over 100 samples were analyzed using chromium radiation and an E.D.T. crystal in an atmosphere of helium.

F. Analyses

The compositions of the compacts, reaction products, and decomposition products fall in the ternary diagram of boron, phosphorous, and carbon. For this reason, analysis of two of these, carbon and phosphorous, suffices to fix the composition of the materials. The carbon analyses were carried out with a Leco Carbon Analysis Unit. The phosphorous in the samples was estimated by X-ray flourescent technique. Chemically analyzed samples and compounds of known compositions were used for calibration. The chemical analyses for phosphorous were carried out by the ammonium phosphomolybdate technique.

The second phase of analysis consisted of spectrographic estimation of impurities in the starting materials and the finished products. Samples were subjected to a dc arc analysis. Impurity levels were determined by the use of comparison standards. A Bausch and Lomb Large Quartz Littrow Spectrograph was used. The emission spectroscopy results were tabulated so that relative impurity levels could be compared to electrical properties. Spectroscopic analyses of the mold and mold-liner materials were included.

G. Hardness Measurements

Hardness measurements were made on five polished samples of various phosphide-carbide compositions. The hot-pressed compacts were surface ground with a 100 mesh diamond wheel, then diamond ground on an embedded wheel to 30 microns. A diamond paste of 30 microns followed by one of 15 microns was used next on a brass lap for fine grinding. This was followed by 6 micron and then 1 micron diamond polishing paste on photographic paper. Olive oil was an effective lubricant.

Twenty-seven samples of hot-pressed compacts and several of the prepared powders were cast in polyester resin to provide a firm mount for polishing. In addition to the polishing procedure just cited, many variations were tried such as glass laps and alumina, silicon carbide, and boron carbide abrasive powders.

The use of silicon carbide paper and heavy pressure on the surface to be polished is also effective. It is most important to use sufficient diamond abrasive well embedded for grinding and to be certain to have the proper sizes. A high polish should be rapidly attained with the right selection of powder sizes.

Many of the samples mounted would not polish. Those prepared at lower (below 2000°C) temperatures tended to have hard particles loosely bonded. Particles pulled out of the surface of these, ruining any polish already obtained. The samples which polished well were prepared at high temperatures and were the better cemented specimens. These were used for hardness measurement.

The hardness testing was done with a Wilson MO Tukon Microhardness Tester using a Knoop pyramidal diamond indenter. This is a microindentation hardness tester using shallow small area indentations. It is used with loads from 10-1000 grams. Knoop hardness number values (kg/mm^2) were plotted against load (grams). For each point graphed, 20 to 100 indentations were averaged. Histograms were drawn to evaluate the precision of the average. The instrument was aligned by a factory representative immediately before use and checked on a standard sample of known hardness. The Knoop diamond indenter had angles

of 130° and 172°30' with a long to short diagonal ratio of 7/1. This indenter lasted for five load curves but fractured on the sixth.

H. Density Measurements

The density of solid samples was determined both by volume measurement and weight and by mercury displacement with similar results.

The density of reacted and decomposed powders and of small solid chips was determined by the High Density Liquid Method. Krumbein (122) pointed out that acetylene tetrabromide (tetrabromethane) with a density of 2.96 gm/cm^3 at 20°C is miscible in all proportions with carbon tetrachloride with a density of 1.58 gm/cm^3 at 20°C. This is a linear miscibility so a series of high density liquids was prepared and powder densities determined by a flotation test with a centrifuge.

I. Microscopy

Both optical and electron microscopes were used for the study. A reflecting optical microscope was used from 100 to 400 magnifications. Samples polished as for the hardness tests were etched and inspected. The best etching agent was fused sodium hydroxide although some samples were etched with concentrated nitric acid and sulfuric acid. Fused alkalis attacked the surface, but aqueous alkalis and other acids had no effect. Fused sodium peroxide reacted too rapidly. Electroetching in fused sodium hydroxide accelerated the etching.

The optical microscope was used on polished and etched samples from hot-pressing, on fractured surfaces, and on powders. The same types of samples were examined with the RCA Electron Microscope.

With the latter instrument, magnifications from 1400 to 8000 power were used. The etched and fractured surfaces were impressed into a softened cellulose acetate film (Fax Film, Ladd Research Industries) which was shadowed with platinum and coated with a film of carbon. The acetate was removed and the replica placed on a grid for examination.

Eighteen representative photographs were selected from the several hundred taken and are reproduced in this study. Information on particle, grain, and crystal size, grouping, and shape was obtained. Etch patterns, porosity, fractures, and grain details were also found. The intergranular paths along which phosphorous escaped were obvious.

J. Electrical Conductivity

Two electrical conductivity units were constructed for measurement of electrical conductivity versus temperature by the standard Four-Point Probe Method. The units were inserted in evacuated copper tubes which could be heated to 400°C or cooled by liquid nitrogen to 130°C below zero. The tube tops were water-cooled and sealed with replaceable Parker Seals.

The inserted unit consisted of U-shaped mounting blocks of fired wonderstone which held the sample between current-carrying contacts. Tension was applied by forcing mica sheets between the contacts and the frame. This material supplied pressure at both high and low temperatures. Several layers of mica were put under the sample to maintain a pressure against the two steel needles pushing down from the top. The potential across the needles when divided by the current gave the sample resistance. The product of resistance and cross sectional area divided by the length between the needles gave the resistivity of the sample. The needle mount and the U-shaped sample mount could be raised and lowered on brass thread stock which attached them to the tops. The application of a gold chloride ($HAuCl_4$) solution to the points and current contacts greatly reduced contact resistance.

The current was accurately determined by measuring the potential across a standard resistor. Potentials were measured with a Leeds and Northrup Precision Potentiometer and a Leeds and Northrup K-2 Potentiometer. A Hewlett Packard Microvoltmeter was used when sample contact resistance was high. Accurate measurements free of rectification effects were obtained by reversing current direction. Care had to be taken to eliminate the thermoelectric potentials which occurred upon occasion.

K. Thermal Conductivity and Thermoelectric Power Measurements

These measurements were made in the thermal conductivity apparatus described in the 1959 Annual Report of the ONR project (63). This test unit is similar to that discussed by Stuckes (215). It is a comparative device in which a linear heat flow is set up through an unknown sample. The same heat flows through two samples of known thermal conductivity, one above and one below the unknown. Thermal gradients are measured across all three samples by thermocouples placed in silver blocks adjacent to the samples. The quantity of heat is determined from the standards and then the thermal conductivity of the unknown is calculated from the heat, the unit gradient, and the area. By measuring the potential across the gradient-measuring silver blocks on either side of the sample, the thermoelectric power is obtained.

All surfaces were polished before each run. Considerable pressure was applied to the stack by a spring mounted ouside the hot zone and by spacers forced in between the ceramic frame and the heat sink at the bottom of the stack. The thermal gradient was supplied by a heater at the top of the stack. The entire stack, consisting of heater, silver block, standard, silver block, unknown, silver block, standard, silver block, and heat sink, was supported on three legs of 3/16-inch ceramic thermocouple

tubing. This tubing also carried the thermocouple and contact wires into the stack in the furnace. Tests were made in a vacuum from room temperature to 600°C. The same measuring potentiometers and meter were used as for the electrical conductivity tests.

Anomalous values from the phosphide compacts were avoided by measuring at the highest temperatures first. Several tests were run to confirm the need for this procedure.

L. Hall Effect and Magnetoresistance Measurements

Measurements of dc Hall effect were made with a magnet producing a field of approximately 7000 gauss. The sample was mounted in a unit inserted into a brass tube centered in the magnetic field. An "O" ring was used for a vacuum seal since all measurements were made under vacuum. A noninductive heater wound on a heavy copper tube was interchangeable with a liquid nitrogen Dewar vessel. Either of these could be moved up over the sample tube and within the pole pieces of the magnet. The magnet current, the sample current, and the potentiometers were all supplied by heavy-duty batteries for stability.

Since the Hall potential was in the 0-30 microvolt region the biggest problem was that of making noise-free contacts both to the sample and in the circuit. The Five-Contact Method was

used with a potentiometer across the two upper Hall probes. This potentiometer consisted of several resistance boxes and a slidewire. These same two upper probes were used for magneto-resistance measurements as in a Four-Point Probe system. Tapered-plug contacts and screw-terminal contacts were used. Sliding contacts were avoided except for a linear wire type. The Leeds and Northrup K-2 Potentiometer was used for the Hall potential and the Leeds and Northrup Precision Potentiometer was used for temperatures. The Hewlett Packard Microvoltmeter was used for preliminary balance and to trace noise in the circuit.

The most difficult problem was that of maintaining five noise-free contacts on the sample at both high and low temperatures. After much experimentation with cemented contacts, pressure contacts, and with resistance-reducing films and chemicals, a simple technique was developed. A rectangular frame was machined from wonderstone. When fired, this became a good electrical ceramic mount. Before firing, a number of small holes were drilled through the frame for positioning and tying wires, two on the side 1/16-inch apart for the top contacts and one on the bottom corner for the end contact. All five contacts were improved by the application of a small amount of gold chloride ($HAuCl_4$) solution. Little square pieces of copper were placed

over the ends of the sample. The second current contact was a flattened copper contact wedged between the copper square at the end of the sample and the upper side of the frame. Once again, pressure was maintained by forcing three or four pieces of mica into the gap. The fifth contact, on the bottom, was attached to a floating block which was positioned at the center of the bottom and forced against the sample by inserting several pieces of mica between the floating block and the frame.

Samples had a length to width ratio at at least 4/1. After mounting and before measuring, the samples were cleaned by sandblasting.

Measurements were made from 170°K to 680°K. For the two Hall measurements, a field of 7050 gauss and a current of 0.2 amps were used. This current was reduced to 0.09 amps for the magnetoresistance measurement.

An attempt was made to measure all points in both current directions and with both magnetic fields of orientation. For some of the steep areas of the curve, as temperature slowly changed, this was not possible. These areas were run and re-run until the curve shape was firmly established.

With a high thermoelectric power, these samples produced sizeable thermal currents by Peltier cooling if the current were allowed to flow continuously in one direction. For this reason, the current was cycled for stability before each reading. It was found that if the magnetic field, current value, and potentiometer balance could be obtained within five seconds after starting the current in the desired direction, thermoelectric effects did not interfere. The potential increased exponentially beyond five seconds. The balance point was approached each time the current was in the desired direction until a stable reading was obtained.

IV. RESULTS

A. Compound Preparations

1. Preparation by Decomposition. Boron monophosphide (BP) was decomposed by either a long low heat (1000°C to 1400°C) in vacuum or a rapid high heat (1600°C to 1800°C) in helium. The product in both cases was boron subphosphide powder ($B_{13}P_2$) of nominal composition. The vacuum preparation is the preferred method because it is easier to control and is more likely to produce the desired 13/2 boron to phosphorous ratio. Typical results are given in Table XI. Even though analyses indicate a composition approaching a 13/2 boron to phosphorous ratio, densities for the powders are usually lower than the calculated 2.74 g/cm^3 of rhombohedral $B_{13}P_2$. Densities frequently approximate 2.53 g/cm^3 which is the calculated value for rhombohedral $B_{12}P_2$.

Samples for vacuum decompositions were placed in alumina boats in heavy silica tubes. After each decomposition, a dark amorphous layer rich in boron covered the sample. The $B_{13}P_2$ was slightly volatile from 1200°C to 1400°C and usually formed a condensation ring on the cooler end of the boat. The phosphorous that evolved upon decomposition condensed in the cooler area beyond the ring and in a liquid-nitrogen-cooled cold trap. The condensate usually contained about 80% silica and 20% phosphorous.

Table XI

Results of Decomposition of Boron Monophosphide

Sample	Atmosphere	temperature °C	Hours	Density	% C start	% C finish	% P	Δd 104-021
D-4C	vacuum	1212-1227	48	2.50	5.2	12	34	0.034
D-5B	vacuum	1230-1265	69	2.44	5.2	13	24	0.039
D-7A	vacuum	1222-1254	68	2.56	5.2	10.8	30.5	0.039
D-7C	vacuum	1222-1254	68	2.59	5.2	-	-	-
D-8G	vacuum	1300-1360	61	2.48	5.2	11	28	0.036
D-10A	hydrogen	1000	24	2.7-2.96	5.2	6	65	-
D-11C	helium	1600-1800	1/4	2.8-2.96	5.2	-	-	0.038, 0.059
D-12B	helium	1600-1800	1/2	2.53	5.2	7.9	21.6	0.050

Sample D-10A is the product of heating BP in dry hydrogen for 24 hours at 1000°C. This is the preparation cited by Mellor (143) for making B_6P_3. Diffraction patterns were found in the product for BP and $B_{13}P_2$, but no other lines occurred.

2. Preparation by Reaction. Boron subphosphide was also prepared by reacting rapidly the amorphous elements from 1600°C to 1900°C in a helium atmosphere. By increasing the B/P ratio and working at 1600°C, good samples of BP were prepared. For samples prepared this way, the temperature range as shown in Table XII is slightly misleading. This is the furnace temperature range. The variation within this range is determined by the sample position within the furnace. Since each sample was split into four to six fractions for analysis, a letter (A, B, C, or D) in the sample number is indicative of position and thus of temperature. The three R-15 samples (Table XII) show the effect of furnace temperature variation.

The values under BP and $B_{13}P_2$ represent the intensity of the major X-ray diffraction peaks for these compounds. The high BP value for R-15B is a function, not only of temperature, but also of phosphorous atmosphere since the sample was above the other two and received their phosphorous output.

All samples in Table XII had less than 1% carbon. Most contained 0.3% carbon. The column Δd (10h-021) is the spacing

Table XII.

Preparation of Boron Phosphides by Reaction from the Elements

Sample	Temperature °C	Time min.	B:P ratio	Density g/cm³	Δd 104-021	BP	$B_{13}P_2$	% P
R-2B	1600-1800	2	2/1	2.38	0.039	0	270	27
R-4B	1600-1800	15	2.2/1	2.51	0.039	240	140	-
R-5C	1600-1800	21	2.2/1	2.54	0.041	0	240	31
R-6C	1600-1900	15	2.5/1	2.45	0.041	0	280	41
R-10B	1600-1800	5	1/1	2.52	0.040	165	160	-
R-11A	1600-1800	20	1/2	2.53-2.70	0.042	600	45	-
R-14B	1600-1750	33	1/2	2.52	0.039	27	140	21
R-15B	1600-1750	27	1/2	2.89	0.059	630	22	-
R-15C	1600-1750	27	1/2	2.52	0.038	36	165	22
R-15D	1600-1750	27	2/1	2.54	0.050	16	240	28
R-18A	1600-1750	35	2/1	2.52	0.040	33	190	26
R-19A	1600-1800	37	1/1	2.92	0.041	660	43	-
R-19B	1600-1800	37	1/1	2.54	0.040	73	150	-

in angstrom units between the 104 and 021 X-ray diffraction peaks of $B_{13}P_2$. High values in Table XII may be attributed to interference in the measurement by the major BP peak.

Boron and phosphorous in the proper ratio were placed in an alumina crucible which in turn was placed in a vertical alumina tube. This tube was inserted longitudinally within the graphite susceptor of the hot-press. Since such alumina tubes become porous in the region of the reaction temperatures, a slight positive helium pressure was maintained in this tube. To reduce further the influx of volatile carbon compounds, particularly carbon monoxide, nitrogen was passed through the area between the inner alumina tube and the outer silica tube of the hot-press-reactor construction during reaction.

This experimental operation is described to explain a variation introduced into the compound preparation procedure. Among the borostitials prepared so far, a boron subnitride is notably absent. An attempt was made to synthesize what might be the missing compound. Boron nitride (BN, hexagonal) is extremely stable and is the expected product of nitriding boron. Nevertheless, if boron and phosphorous react from 1600°C to 1800°C, identical conditions might produce a subnitride. By switching the helium and nitrogen lines and by filling the inner crucible with amorphous boron rather than boron and phosphorous, these conditions were produced.

The X-ray diffraction (Cu$K\alpha$ radiation) patterns for samples R-20C and R-21B are compared in Table XIII with the pattern for BN (hexagonal). Most of the remaining lines can be accounted for by comparison with α-rhombohedral boron. The 021 peak of the boron is notably missing, although a strong unaccounted-for line appears at 39.4°. The α-rhombohedral boron pattern does not appear in any of the reactions or hot-pressings that did not have nitrogen surrounding the sample.

B. Results of Hot-pressing

1. Effect of Maximum Temperature. A double series of hot-pressed samples was prepared at the temperatures indicated in Table XIV. An attempt was made to keep as the only variable, the maximum pressing temperature. Two samples (A and B) were pressed each time. The A sample is the bottom one. The flow of helium about the mold is from bottom to top. Temperatures for the A series are slightly more exact than those of the B series.

The effect of pressing temperature on density is shown in Figure 9. A large slump occurred while pressing at temperatures from 1600°C to 1800°C. Above this latter temperature, density increased to 2.70 g/cm^3 for sample P-42. All samples were made by hot-pressing BP which is decomposed in the mold.

Table XIII.

X-ray Diffraction of the B-N System

R-20C		R-21B		BN		α-rhomb. B.	
2θ Cu	I	2θ Cu	I	2θ Cu	I/Io	2θ Cu	I/Io
20.7	8	20.5	7			20.9	45
21.8	27	22.0	24			21.9	100
26.7	145	26.7	93	26.7	100		
						25.1	2
34.9	52	35.0	39			35.3	70
36.0b	8	36.4b	11			36.2	40
37.3b	10	37.3b	12				
39.4	33	39.4	25				
41.7	39	41.8	30	41.5	15	41.4	4
42.8	14	42.6	11			42.4	4
						42.8	55
44.0	23	44.0	16	43.9	6		
						44.6	< 2
50.2	22	50.3	14	50.2	13		
51.4b	10	51.8b	9				
54.4b	9	54.4b	8				
55.0	16	55.2b	9	55.1	6	55.1	4
						56.3	8
						57.5	8
						57.8	13
59.4	5						

Table XIV.

Conditions of Preparation for the Series P-21 to P-42

Sample	Source	Pressing temp. °C	Mold type	Hold time minutes	% C	Measured
P-21A	1	1380	Fig. 5	6	5.5	
P-22A	1	1450	5	6	5.5	
P-23A	1	1525	5	0	6.1	
P-24A	1	1600	5	0	6.4	
P-25A	1	1725	5	0	12.0	
P-26A	1	1800	5	0	13.3	
P-27A	1	1900	5	0	14.5	σ
P-28A	1	2000	5	0	18.2	K, α
P-29A	1	2080	5	0	24.9	
P-30A	1	2100	5	0	18.2	
P-21B	1	1420	5	0	6.7	
P-22B	1	1485	5	0	8.5	K,α,σ
P-23B	1	1560	5	0	5.0	
P-24B	1	1640	5	0	14.8	
P-25B	1	1760	5	0	11.2	
P-26B	1	1830	5	0	11.8	
P-27B	1	1940	5	0	12.0	
P-28B	1	2030	5	0	13.8	
P-29B	1	2120	5	0	12.9	
P-30B	1	2135	5	0	9.7	HM
P-41	1	2060	5	0	16.2	
P-42	1	2180	5	0	13.6	

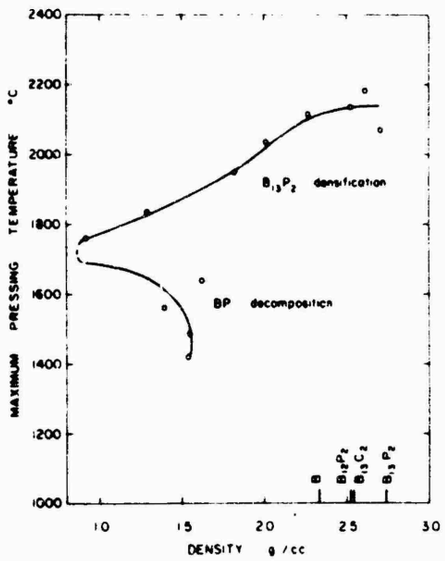

Figure 9. Density and Preparation Temperature (P-21 to P-42)

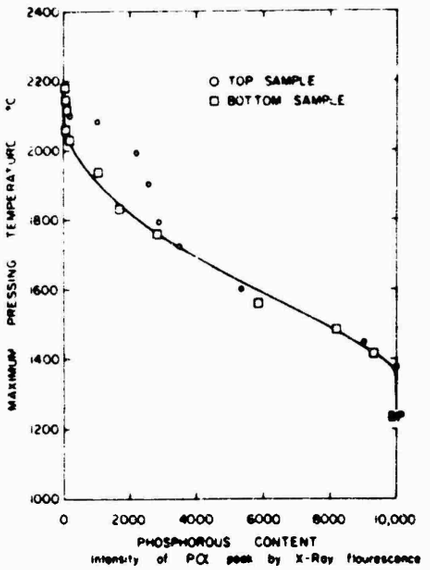

Figure 10. Phosphorous Content by Fluorescent Analysis at Various Preparation Temperatures (P-21 to P-42)

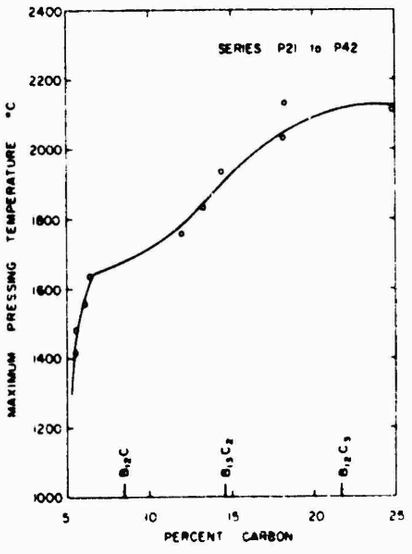

Figure 11. Carbon Content (Leco) at Various Preparation Temperatures (P-21 to P-42)

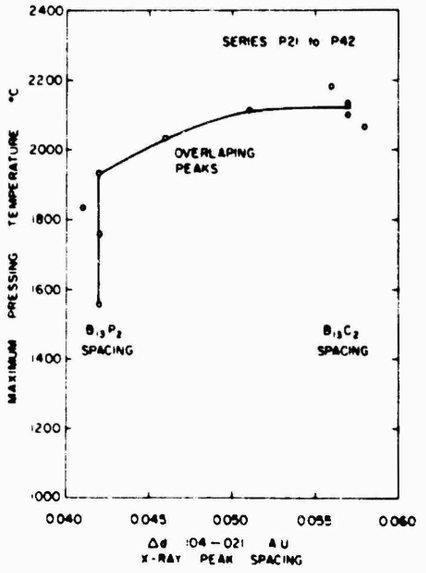

Figure 12. Preparation Temperature Effect on Spacing Between 104 and 021 X-ray Diffraction Peaks (P-21 to P-42)

The starting material contained 5.2% carbon which, at higher temperatures, was converted to boron carbides. As decomposition progressed, the 5.2% carbon increased because of the loss of so much phosphorous.

This decrease in phosphorous content is shown in Figure 10. The abscissa represents, by the intensity of the X-ray fluorescent P-α line for phosphorous, the amount of phosphorous present. The curve is regular for the bottom samples, but the top sample values deviate from the expected at high temperatures. This may be due to their being in the phosphorous vapor coming from the bottom samples either at pressing temperature or while cooling. The deviation at Pα = 2800 occurs at about the intensity that one could obtain for $B_{13}P_2$ (2700) with this carbon content (12%).

The effect of maximum temperature on the carbon content of the sample is shown in Figure 11. The BP starting material which contained 5.2% carbon decomposed rapidly at 1600°C. Above the temperature, the relative carbon content increased as phosphorous was expelled.

As the maximum pressing temperature increases, $B_{13}P_2$ changes to $B_{13}C_2$. Changing the size of the interstitial atoms would also change the unit cell dimensions. This latter change can be followed by measuring the spacing between the 104 and 021

X-ray diffraction peaks of $B_{13}P_2$. The 021 peak has an intensity of 100, and the 104 peak has an intensity of 80 at d = 2.569 A. This 80 peak almost coincides with the 80 peak at d = 2.57 A for $B_{13}C_2$.

Any sudden increase in carbide content then increases the peak separation for the phosphide pair. Thus, in Figure 12, a reference to $B_{13}P_2$ or $B_{13}C_2$ spacing is a measure of the distance between the $B_{13}P_2$ 021 (100) peak and the double peak which may be either or both $B_{13}P_2$ 104 (80) and $B_{13}C_2$ 104 (80). The curve of Figure 12 breaks sharply just above 1900°C.

The results of hot-pressing at different maximum temperatures are seen clearly in Figure 13. The abscissa represents the intensity of X-ray diffraction patterns. The maximum intensity as determined for the strongest line for each of the three compounds is assigned a value of 100. In this way, the formation and decomposition of each compound can be followed at various temperatures. The intensity scale does not represent percent composition but is related to it. Since the development of good crystal structure takes time, this plot probably has an inherent lag built into it. This might mean that the temperatures of change, indicated in Figure 13, may be slightly high.

Sample colors, sample hardness, and degree of sample bonding, all closely follow the temperatures of change seen in Figure 13. Brown samples occur up to about 1550°C. Most of the phosphorous evolution upon pressing takes place between

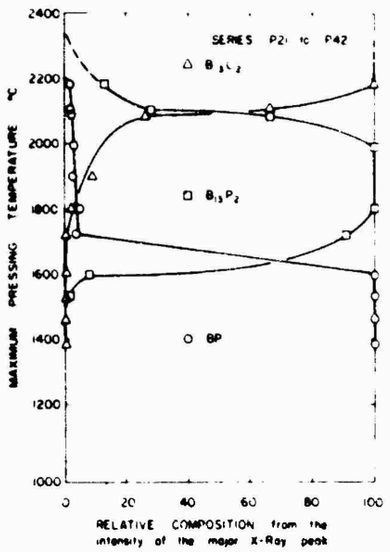

Figure 13. X-ray Composition at Various Temperatures of Preparation (P-21 to P-42)

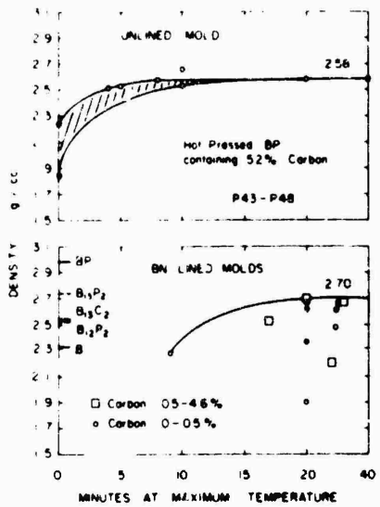

Figure 14. Densities as a Function of Time-at-Temperature

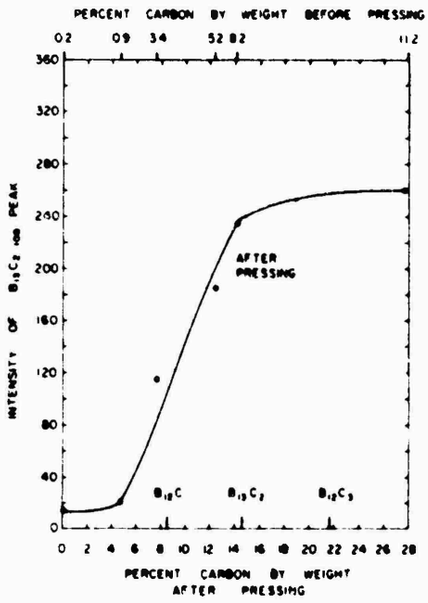

Figure 15. Carbide Formation Related to Variation in Carbon Content (P-49 to P-54)

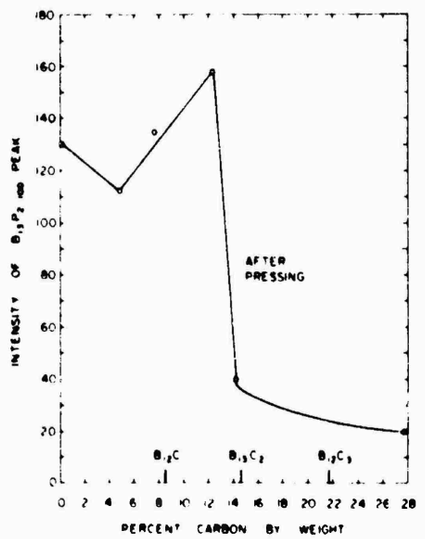

Figure 16. Phosphide Decomposition Related to Variation in Carbon Content (P-49 to P-54)

1450°C and 1550°C. Above 1600°C, samples are light gray if pure and darker gray with increased carbon content. If carbon-free, the color gray predominates to 2050°C. At this point, samples become very dark gray to black and have a somewhat metallic luster. Samples with higher carbon content darken from 1850°C to 2050°C.

A distinction should be made between particle hardness and strength of particle-to-particle bonds resulting from hot-pressing. All three compounds have exceedingly hard crystallites, but boron monophosphide sinters very little even immediately below its decomposition temperature. The best compacts of BP were obtained after partial decomposition. These compacts were still soft-bonded.

Boron subphosphide does sinter into hard-bonded compacts. The carbon-free subphosphide compacts sinter best above 2000°C. Those with moderate carbon sinter strongly even at lower temperatures (to 1800°C). As expected, the high carbide samples are very strongly bonded. As a rule, the higher the phosphorous content at the beginning and ending of pressing, the more difficult it is to obtain strong bonds between particles. The results of the rule are particularly evident in samples selected for polishing. Of twenty samples, only nine polished well. The

other eleven were damaged easily when loosely-bonded particles pulled out of the matrix and ground into the surface.

2. Effect of Time-at-pressing Temperature. A number of identical samples were hot-pressed, each with a slightly different hold-time at the pressing temperature (1950°C to 2000°C . Increasing the time increased the decomposition and thus increased the relative carbon content above the 5.2% carbon at the start of the hot-pressing. This carbon increase and the phosphorous decrease are shown in Table XV. The density-time curve for these samples is shown in the upper curve of Figure 14. After ten minutes hold-time, the phosphorous content drops sharply and a constant density is reached.

The lower curve in Figure 14 was an attempt to show the time-at-temperature effect when the carbon was eliminated. These samples, taken from Table XVII, were made with low carbon material in BN lined molds. The densities did not approach an expected curved line as indicated. The absence of correlation in the lower curve of Figure 14 is significant. It indicates that better sintering and densification in the more pure samples could be obtained at a higher temperature. It may also be indicative of a decreased rate of heat transfer caused by the lower thermal conductivity of the mold lining.

Table XV.

Composition as a Function of Time at Temperature

Sample	Source	Pressing temp. °C	Mold type	Hold time min.	% C	% P	Measured
P-43	1	1950	Fig. 5	0	9.9	11	K,α
P-33	1	1970	5	0	12.8	38	
P-9	1	1990	5	4	(8.9)	(36)	
P-44A	1	2000	5	5	15.6	(31)	
P-45A	1	2000	5	8	15.1	7	
P-52	1	1990	5	10	12.4	(32)	
P-45B	1	1990	5	10	16.9	5	
P-46A	1	1990	5	20	17.6	5	
P-47	1	1950	5	40	19.1	3	
P-48	1	1950	5	80	v.high	partly melted	

3. Effect of Carbon Content. A number of samples listed in Table XVI were pressed at 2000°C to 2050°C with identical heat cycles. The variable in this series was the amount of carbon in the sample before pressing. All six samples were BP to start. Sample P-49 was prepared from the reaction of the elements in a separate furnace. The remaining five samples were prepared from the BP with 5.2% carbon. The first attempt to change the carbon content was by froth flotation. The samples with 3%, 8%, and 11% carbon were prepared this way. To reduce the carbon to 1%, a dense liquid (acetylene tetrabromide, density = 2.98 g/cm^3) separation was used with centrifuging.

In Figure 15, the intensity of the major peak in the $B_{13}C_2$ X-ray diffraction pattern for the compacts is compared with the carbon content before and after pressing. The intensity of the $B_{13}P_2$ major peak is compared with the per cent carbon by weight after pressing in Figure 16. The carbide formed depends, of course, on the carbon present. When sufficient carbon is present to fill all of the interstitial sites (the $B_{13}C_2$ point) two things happen: the carbide X-ray intensity effectively stops increasing, and the phosphorous content drops sharply as the carbon replaces phosphorous.

Table XVI.

Ultimate Composition as a Function of Initial Carbon Content

Sample	Source	Pressing temp. °C	Mold type	% C start	% C finish	% P finish	Measured
P-49	3,6	1990	Fig. 6	0	0.2	24	
P-50	1	2025	5	0.9	4.8	18	
P-51	1	2025	5	3.4	7.6	-	
P-52	1	2025	5	5.2	12.4	0.6	
P-53	1	2030	5	8.2	14.2	0.4	σ
P-54	1	2025	5	11.2	27.7	0.3	K,α

all held 10 minutes at temperature.

4. Hot-pressing Pure Samples. In every attempt to obtain a correlation between properties and composition, pure materials must be obtained. In this investigation, one objective was to determine the properties of polycrystalline boron subphosphide. This pressing procedure required the excluding of other elements, primarily carbon, and the obtaining of a reasonably stoichiometric ratio around $B_{13}P_2$, and the producing of a series of compacts with a phosphorous content above and below this ratio.

Hot-pressed samples prepared in BN lined molds are listed in Table XVII. The first three samples had a high carbon content at the start of pressing and were used merely to work out the technique. The remaining samples were given the additional protection of a boron seal above and below the sample as shown in Figure 7.

With ultrapure amorphous boron, ultrapure amorphous phosphorous, and a fully protected mold, samples P-67B and P-70B had a carbon content below 0.1% which was the lower limit of detection.

Occasionally, a sealed sample such as P-68B or P-64B, had a high carbon content. This indicates that the seal was incomplete or that the mold lining cracked.

In Table XVII, the starred samples were made by decomposing BP. The samples marked with a single cross were pressed from

Table XVII.

Samples Hot-pressed in Lined Molds

Sample	Source	Pressing temp. °C	Mold type	Hold time min.	% C	% P	Measured
P-36	1*	1885	Fig. 6	10	12.0	45	
P-37	1*	2000	6	11	7.8	-	M
P-40B	3,6‡	1960	7	17	4.6	7.0	
P-49B	3,6*	1960	7	9	0.21	24.0	
P-55	3,6*	1960	7	20	0.44	22.0	K,α
P-56	3,6*	1960	7	20	0.33	27.5	σ,R
P-57B	3,6+	1960	7	20	2.2	21.0	H,M
P-58B	3,6+	1960	7	20	1.2	20.5	
P-59B	3,6+	1960	7	0	1.4	16.0	
P-60B	3,6+	1960	7	0	1.9	20.0	
P-62B	3,6+	1960	7	20	0.5	19.5	σ
P-64B	2,5‡	1985	7	28	3.3	31.0	σ,R
P-66B	2,5+	2000	7	29	0.25	16.0	σ
P-67B	2,5+	1980	7	29	0.04	14.0	K,α,σ
P-68B	2,5‡	1970	7	32	2.1	25.2	
P-70B	2,5‡	1970	7	30	0.03	31.0	H,K,α,σ

*as BP
+as $B_{13}P_2$
‡B + P react in hot-press

prepared $B_{13}P_2$. The compacts marked with a double cross were the product of reaction hot-pressing. Boron and phosphorous were reacted at the same time as they were hot-pressed.

In samples prepared in unlined molds, if $B_{13}P_2$ were the starting material, a lower phosphorous content resulted. Starting with BP or B + P (ratio about 1/1), a product with a higher phosphorous content was obtained under identical conditions of pressing. This is more evident in unlined molds because of their shorter hold-times at temperature.

Several other samples, as shown in Table XVIII were prepared for comparative use. Sample P-72 is approximately $B_{12}C_3$ and P-71B is approximately $B_{13}C_2$. The others were used in various test procedures.

At the end of the listing of each sample in Tables XIV to XVIII is a key to the ultimate use of the samples:

Symbol	Used for:
H	Hardness measurement.
M	Subject of microscope study.
σ	Electrical conductivity measurement.
K	Thermal conductivity measurement.
α	Thermoelectric power measurement.
R	Hall effect measurement.

Some of the transition temperatures of importance in hot-pressing are summarized in Table XIX. The most important concept to keep in mind while interpreting these effects is the position

Table XVIII.

Hot-pressed Samples

Sample	Source	Pressing temp. °C	Mold type	Hold time min.	% C	% P	Measured
P-72	9	2190	Fig. 5	0	24.8	0	H,σ,M
P-71B	3	2120	5	10	14.8	0	σ,M
P-15	1	1970	5	0	11.1	(18)	H,M
P-32	1	1870	5	0	7.2	(10)	M
P-39B	1	1980	5	0	10.9	-	M
P-69	1	2000	5	10	11.3	0.2	σ

Table XIX .

Transition Temperatures in Degrees Centigrade

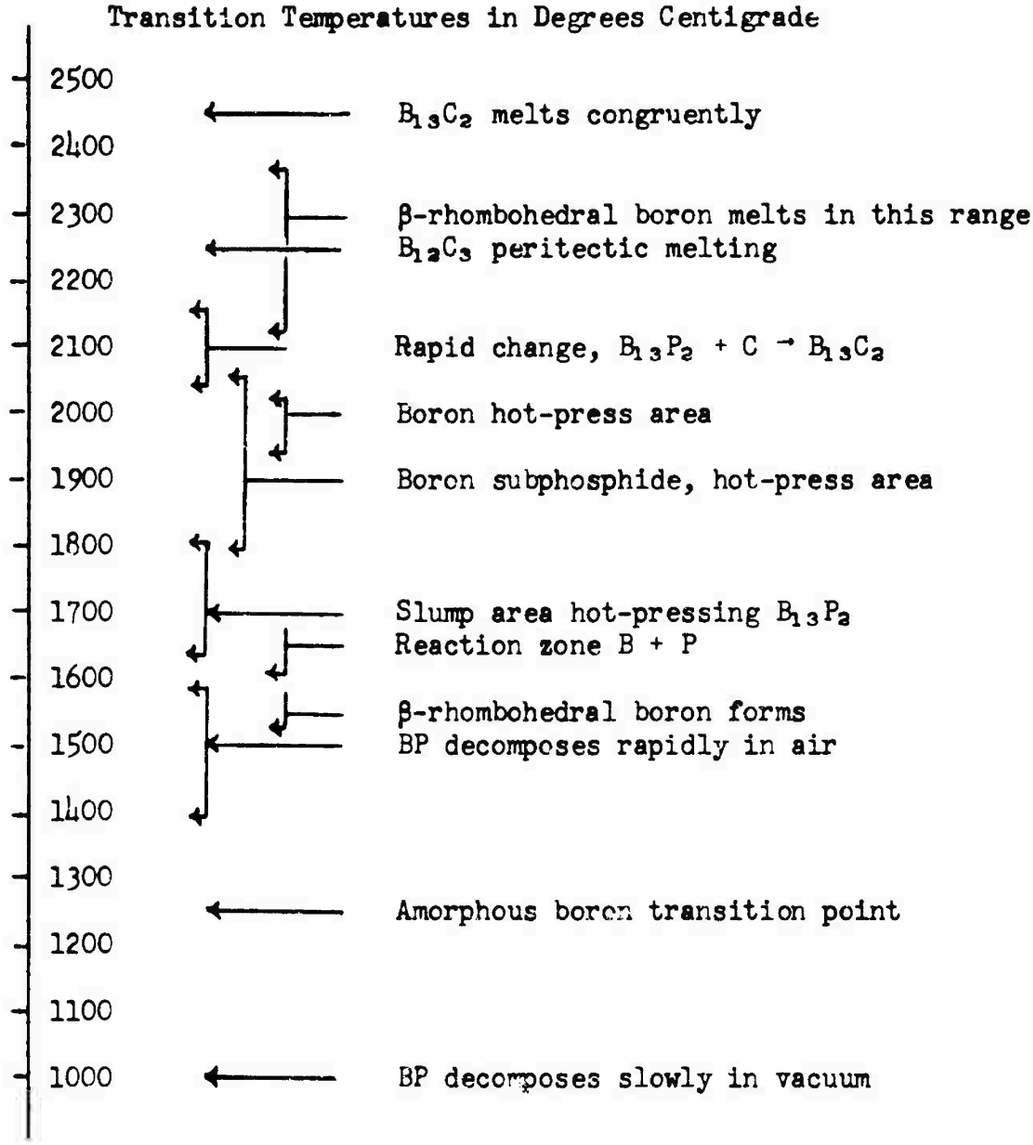

of the sample in its phase diagram. This position determines the pressing characteristic, the sintering temperature, and the extent of crystallization of the sample.

C. Results of Microscopic Examination

Samples with varying phosphide and carbide content were examined with a reflecting microscope and an electron microscope. Eighteen representative photographs from this examination are reproduced in Figures 17 through 34. These photographs are captioned in Table XX, and sample properties and composition are summarized in Table XXI.

The descriptions of photographs given in the three pages of Table XX include the sample number, its composition, its particular preparation, and a pair of magnification numbers. The second number is the approximate magnification as printed.

Figures 17 through 19 are powders photographed with the electron microscope. Amorphous boron and amorphous phosphorous were reacted to produce the $B_{13}P_2$ powder of Figure 17. Reacted material usually had a particle size range from 0.05 - 0.2 microns. Sample R-10C had particles approximately 0.16 microns in size. Many of the particles seen in Figure 17 are agglomerates.

Particles of the boron phosphide (BP) supplied by The Monsanto Company are shown in the electron microscope photograph, Figure 18. Most particles are in the range of three to seven

Table XX.

Descriptions of Photographs

Figure 17	Figure 18
Particles of Boron Subphosphide ($B_{13}P_2$) Prepared by Reaction of the Elements (Electron Microscope 2000X, Printed 2500X) (R-10C)	Particles of Starting Material (BP) (Electron Microscope 1400X, Printed 1750X) (1)
Figure 19	**Figure 20**
Particles of $B_{13}P_2$ Prepared by Decomposition of BP (Electron Microscope 1400X, Printed 1750X) (D-8E)	Lightly-etched Areas between Large Grains, Phosphide Removed (Optical Microscope 50X, Printed 250X) (P-15)
Figure 21	**Figure 22**
Fracture Areas around Lightly-etched Indentation from Microhardness Testing (Optical Microscope 100X, Printed 1000X) (P-15)	Fracture Areas around Lightly-etched Indentation from Microhardness Testing (Optical Microscope 100X, Printed 500X) (P-15)

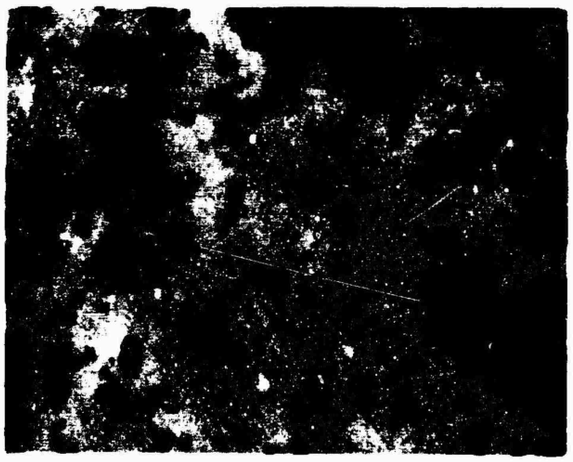

Figure 17

Figure 18

Figure 19

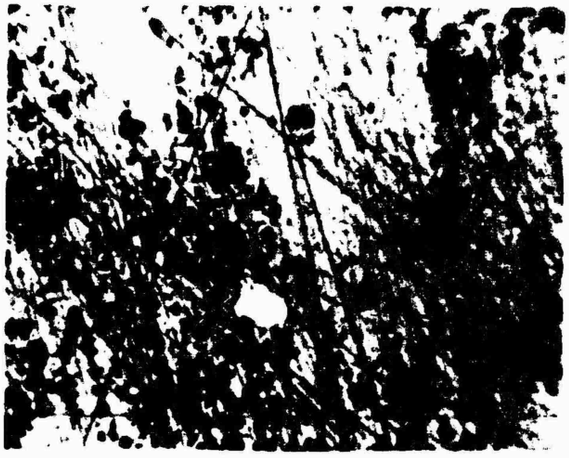

Figure 20

Figure 21

Figure 22

Table XX. (cont'd).

Descriptions of Photographs

Figure 23

Heavily-etched Area, Focused down in the Grain Boundary, P-15 (Optical Microscope 250X, Printed 1250X)

Figure 24

Heavily-etched Area, Focused on Grain Surface, P-15 (Optical Microscope 250X, Printed 1250X)

Figure 25

Replica of Surface Etched until Crystals Were Removed (Electron Microscope 5600X, Printed 10,000X) (P-15)

Figure 26

Lightly-etched Carbide Diffusion Band around Crack (Optical Microscope 50X, Printed 250X) (P-15)

Figure 27

Medium Grains at Start of Sintering, P-32, Replica of Fracture Surface (Electron Microscope 1400X), Printed 1750X)

Figure 28

Escape Path of Phosphorous Vapor between Partly-sintered Grains, P-57B, Replica of Fractured Surface (Electron Microscope 1400X, Printed 1750X)

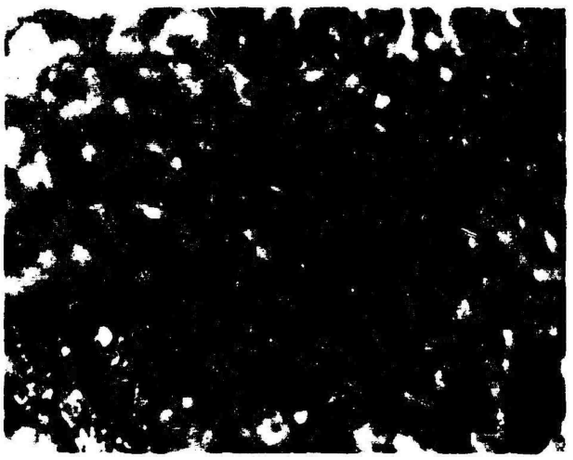

Figure 23

Figure 24

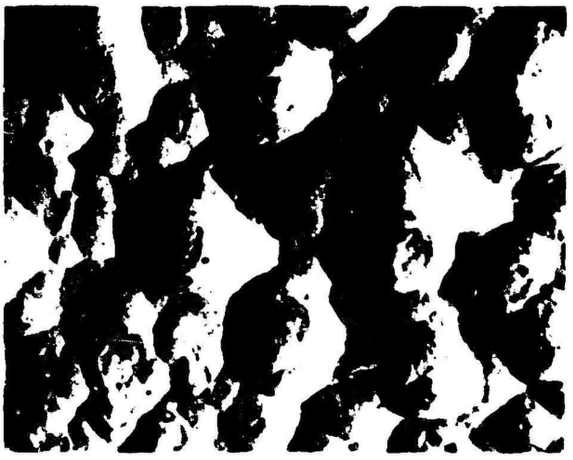

Figure 25

Figure 26

Figure 27

Figure 28

Table XX (cont'd.).

Descriptions of Photographs

Figure 29

Large Grain Growth from Small Particles, P-32, Replica of Fractured Surface (Electron Microscope 1400X, Printed 1750X)

Figure 30

Carbide Grain Growth from Fine Particles, P-72, Replica of Fractured Surface (Electron Microscope 1400X, Printed 1750X), $B_{13}C_3$

Figure 31

Grain Detail on Well-sintered P-39B, Replica of Fractured Surface (Electron Microscope 1400X, Printed 1750X), Partly Crystalline

Figure 32

Grain Detail of P-71B, Moderately Crystalline $B_{13}C_3$, Replica of a Fractured Surface (Electron Microscope 1400X, Printed 1750X)

Figure 33

Portion of a Large Grain with Crystal Faces Forming, P-37, Replica of a Fractured Surface (Electron Microscope 4000X, Printed 5000X)

Figure 34

Extensive Crystallization, P-37, Replica of a Fractured Surface (Electron Microscope 2000X, Printed 5000X)

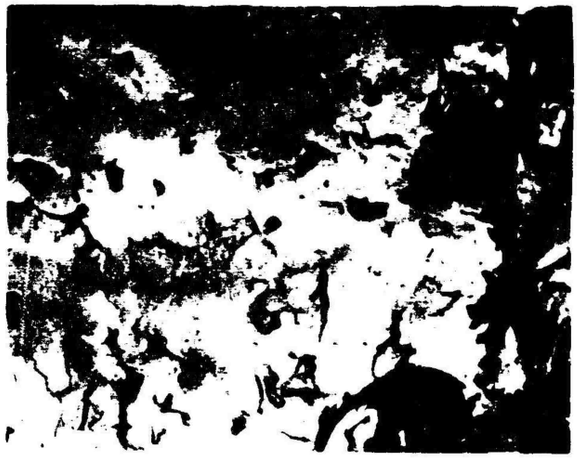

Figure 29

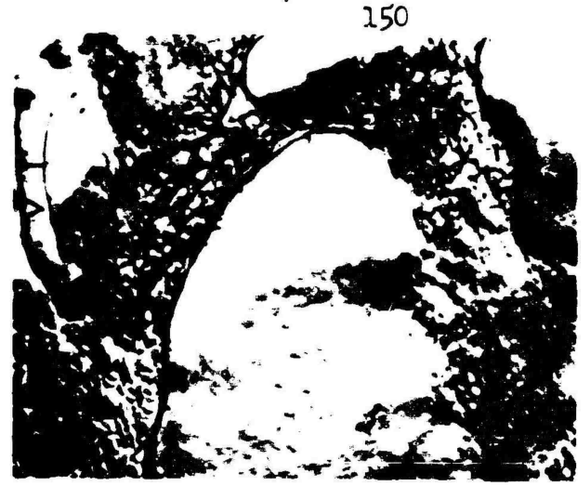

Figure 30

Figure 31

Figure 32

Figure 33

Figure 34

Table XXI.

Results of Microscopy

Sample	% C	% P	Density g/cm³	Porosity	Crystallinity	Grain size (microns)
B-2 up.	-	-	2.33	-	amorphous	0.01-0.1
R-15C	($B_{13}P_2$)	-	2.54	-	slight	0.09
R-10C	($B_{13}P_2$)	-	2.53	-	slight	0.16
D-8E	($B_{13}P_2$)	-	2.54	-	crystalline	1-10
BP	5.2	-	2.97	-	crystalline	1-14
P-70B	0.03	31.0	2.66	2-4	none	3-40 well sintered
P-57B	2.2	21.0	2.69	1-2	none	3-14 lightly sintered
P-32	7.2	(10)	1.65	-	none	22-27 well sintered
P-37	7.8	high	2.0	-	high	3-12 well sintered
P-30B	9.7	low	2.53	-	slight	1-13 lightly sintered
P-39B	10.9	low	1.5	-	slight	1-12 lightly sintered
P-15	11.1	(18)	2.3	below 1/2	none	1-15 well sintered
P-71B ($B_{13}C_2$)	14.8	0	-	-	moderate	5-7 well sintered
P-72 ($B_{12}C_3$)	24.8	0	2.54	4	none	13-30 well sintered

microns. The larger ones are as large as 14 microns. Almost all particles show evidence of crystallinity and many are hexagonal in form, Figure 18.

A similar photograph, Figure 19 (sample D-8E), is of the $B_{13}P_2$ formed when the BP was decomposed slowly in vacuum. Particles are of one to ten microns in size and are crystalline but slightly less crystalline than the BP starting material. In addition, all particles have fuzzy edges. Many more fine particles were also evident.

Figures 20 through 26 are of hot-pressed sample P-15 which contains 11% carbon, about 18% phosphorous, and is well sintered and polished. An etch for three minutes in fused sodium hydroxide produced the pattern shown in Figure 20. The lines are scratches that were accented by the etching. The scratches do not continue through the dark areas which are the etch holes produced by removal of the more soluble phase. These holes are usually two to five microns in size with the larger ones 10-15 microns, i.e., about the same as the starting material BP. The large light areas are between 80 microns and 210 microns in diameter. It is possible that these large areas were produced by reaction with the free graphite grains in the starting material. A black hole (20-30 microns in diameter) was found in the center of a number of large areas.

High load hardness indentations produced cracks where the high stress points at the indent corresponded to weak areas in the surface indented. Light etching in fused sodium hydroxide caused chips to lift out at the cracks. Such glass-like fracture areas are shown in Figures 21 and 22. At least six large fracture areas can be seen in the portion of the indent (Figure 21), but the detail is difficult to reproduce because of the low depth of field. Fractures occur in the regions where the dark etch holes are most numerous. This can be seen clearly in Figure 21. The two "butterfly-like" fractures of Figure 22 are at the center angles of the diamond indenter.

Photographs of the same area were taken through the reflecting microscope, Figures 23 and 24. The surface was etched for 18 minutes in fused sodium hydroxide. The diagonal band which separates the light areas corresponds to the band of dark etch holes shown in Figure 20. The photograph in Figure 23 is focused down into this etched-out band. The Figure 24 photograph is focused on the light, possibly carbide rich surface on either side of the band.

A number of small rhombohedra can be seen both in the band and on the surfaces. These are usually one to four microns in size. Light reflects strongly from different surfaces as the angle of the reflected light is changed.

The surfaces are of random orientation and at various heights. Each rhombohedra extends above its immediate surroundings. The smallest angles for the rhombohedra measure between 65 and 67 degrees.

In addition to the rhombohedra, a number of needles or plate-like chips can be seen in both the band and surface areas. These particles are 7-13 microns long by two microns thick. More chips or needles extending above the background exist in the large surface grain than in the band.

A short additional etch with fused sodium hydroxide removed all rhombohedra and chips from the surface. Attempts to obtain the crystals by etching other samples produced only isolated areas with crystals. This same sample, P-15, after a total etch of 25 minutes, was examined with the electron microscope. The "blister-like" pattern of Figure 25 is a photograph of a replica of this surface. The little round "blisters" are the cavities left after a grain has been removed by etching.

The crystals (rhombohedra and chips) were the center portions of the particles at the start. As these particles were pressure sintered together, phosphorous escaped leaving areas of high and low phosphorous content. Light etching attacked the grain boundaries first, Figure 20. Further etching removed more and more of the boundary between particles until the crystalline center of the particles was

uncovered. Continued etching then freed the crystal and left the blistered bottom seen in Figure 25. Each cavity is one to five microns in size.

With both the reflecting microscope and the electron microscope, a few etch pits were evident. Attempts to etch with boiling concentrated sulfuric acid probably produced them.

The dark area at the bottom of Figure 26 is a crack that formed during preparation. The dark band across the middle is either a surface region which has lost more phosphorous than the bulk or a diffusion band indicating the ingress of carbon to form carbide. The sample was given a brief fused alkali etch which was followed by extreme boiling in concentrated sulfuric acid. Sulfuric acid etching emphasizes the scratches. The pattern across the top one third of the photograph matches in size and number the holes of Figure 20. Continued etching left a single horizontal band dividing the top two thirds of the photograph. The sharpness of this boundary indicates that the effect is caused by the diffusion of carbon which is known to be quite rapid in a boron matrix.

Figures 27 through 34 are photographs taken with the electron microscope of replicas of the fractured surfaces.

Figures 27 and 29 are of sample P-32 which sintered to form grains of 10-27 microns. In Figure 27, small particles have formed into chain-like larger grains. In Figure 29, a massive grain has been formed from particles which are one to five microns in size. Voids have not been completely absorbed.

Sample P-57B, Figure 28, has a high phosphorous content and a low carbon content. It is lightly sintered and is permeated with a number of paths such as the one to five micron wide horizontal band across the middle of the photograph. This is emphasized by some of the plastic from the replica which was incompletely stripped from the platinum-carbon shadow and backing material. The plastic is black (absorbing) and can be seen in the cracks between the grains. Many such plastic-outlined regions resemble a river and its tributaries. These paths are evidently the escape paths for phosphorous vapor. They are particularly evident in this sample because, with a low carbon content, sintering was light. Particles in this sample were 3-14 microns in size.

Sample P-72 (Figure 30) had a composition which was essentially $B_{12}C_3$. It was prepared at a higher temperature (2190°C) than were most of the other samples (2000°C) inspected with microscopes and has a totally different appearance from the others. It seems to have two phases. Large (20-25 micron)

well-rounded grains such as those seen in Figure 30 are common. Between these is a very fine grain material. No evidence of crystals was seen.

Sample P-39B (Figure 31) is slightly crystalline and has small grains, 1-13 microns. Its low density and low phosphorous content may account for its appearance. The sample has been sufficiently hot for the large light particles in the top left portion of the photograph to sinter lightly. On the other hand, much of it looks highly porous as if phosphorous had escaped but pressure was not applied or maintained sufficiently late in the heating cycle to cause complete densification.

The composition of sample P-71B (Figure 32) is approximately $B_{13}C_2$. It was prepared at 2120°C and was moderately crystalline as seen in the photograph. Some of the black between grains is caused by remnants of replicating plastic. Most of the crystals are from five to seven microns in width. The samples were prepared from amorphous boron and graphite.

Figures 33 and 34 show the crystal faces developing in sample P-37. These crystals have grown from the surface of grains about 12 microns in diameter. This sample probably has more crystallization than the comparable P-15 because P-37 was held at temperature (2000°C) for 11 minutes.

D. Results of Analyses

1. Emission Spectroscopy. Emission spectroscopy was used to determine the approximate amount and probable source of the impurities in the compacts. In order to identify the source of an impurity, analyses of the starting materials as well as the mold and mold liner materials are included in Table XXII. The composition of representative compacts is given in Table XXIII.

Sample 1 in Table XXII is the BP used for many of the decompositions and high carbon hot-pressings. A chemical analysis indicated 0.02% iron. After decomposition, the iron content of sample D-7A was 0.8%. In like manner, the iron was found to increase when BP was hot-pressed. This was followed by X-ray fluorescent analysis for the series P-21 to P-30. The iron content was inversely proportional to the phosphorous content.

Boron samples 3 and 4 were combined with phosphorous sample 6 for many of the low carbon samples. In this case, magnesium and calcium would be expected in the product. For best results, boron (B-2) and phosphorous (P-5) were combined in molds fully lined with boron nitride. The product of this preparation should contain aluminum from the mold liner. If the

Table XXII.

Spectrographic Analyses of Starting Materials

Sample	Source	% C	1-10%	0.1-1%	0.01-0.1%	0.001-0.01%	Under 0.001%
1.BP	Monsanto	5.2	-	Fe,Si	Ca,Cr,Cu, Mg,Ni,Pb	Al,Mn,Ti	Be
2.B up.	Leytess	0	-	-	-	Cu	Ca,Fe,Mg
3.B	Fisher	0.2	-	Mg	Al,Cu,Fe, Mn,Pb,Si	Ca	-
4.B	U.S.Borax	0.3	-	Mg	Al,Cu,Fe, Mn,Pb,Si	Ca,Ni	-
5.P up.	A.A.C.	0	-	-	-	Mg	-
6.P	Fisher	0	-	Ca	Al,B,Fe, Mg,Si	Sn	-
7.graphite	Speer	100	-	-	B	Ti,Fe	Cu,Mg,Ni, Si
8.BN	Carborundum	-	-	Al	Ca,Fe,Mg, Pb,Si	Cu	Mn
9.$B_{12}C_3$	Norton	24.08	-	Al,Ca,Cu, Mg,Mn,Si	-	-	-

Table XXIII.

Spectrographic Analyses of Compacts

Sample	Source	% C	% P	1-10%	0.1-1%	0.01-0.1%	0.001-0.01%	Under 0.001%
P-70B	2,5	.03	31.0	-	-	Ca,Mg,Si	Al	Mn,Pb
P-66B	2,5	0.25	16.0	-	Al,Fe, Mg,Si	Ca,Mn,Pb	Cu	Cr,Ni
P-64B	2,5	3.27	31.0	-	Si(0.1) Fe(0.1)	Al,Ca,Cu, Mg,Pb	-	Mn
P-56	3,6	0.33	27.5	-	Mn,Si	Al,Cu,Ca, Pb,Mg	Cr,Ti	-
P-27A	1	14.5	12.0	-	Fe,Mg, Si	Al,Cr,Cu,Ca, Ni,Pb,V	Mn,Ti	Be
P-53	1	14.2	0.4	-	Fe,Mg, Si	Ca,Cr,Cu, V	Al,Mn,Ni, Pb,Ti	Be
P-71B	3(7)	14.8	0	-	-	Ca,Mg,Mn, Si	Cu,Pb	Al
P-22B	1	8.49	67	-	Fe,Si	Ca,Cr,Cu, Mg,Ni,V	Al,Mn,Pb, Ti	Be

lining or seal were cracked, then impurities from the graphite and carbon should increase. Emission spectroscopy, therefore, provides an excellent test for the quality of protection.

The first three samples listed in Table XXIII were prepared from the purest materials with the best protection. The preparation of P-70B was excellent. Sample P-66B acquired impurities from the mold liner. The high carbon content of sample P-64B probably indicates an incomplete seal or a damaged liner. Since the best samples were cut from the lined molds to prevent cracking, it was difficult to tell if the liner cracked.

Sample P-56, prepared from amorphous boron and phosphorous, has a concentration of manganese and silicon. It would be expected to have more manganese and calcium unless they are somewhat volatile. Samples P-27A and P-53 have the expected concentration of iron, magnesium, and silicon. The hot-pressing of boron (B-3) in an unlined mold (sample P-71B) produced essentially $B_{13}C_2$ with a collection of impurities from the boron and the graphite mold. Sample P-22B has approximately the same composition as the BP starting material.

A comparison of Tables XXII and XXIII indicates the following about the preparation of boron subphosphide hot-pressed compacts:

(1) Samples prepared from BP-1 will be very high in carbon and will contain appreciable quantities of iron, silicon, and magnesium.

(2) Samples prepared from boron (B-3 or B-4) and phosphorous (P-6) may be low in carbon and will probably contain appreciable quantities of manganese and silicon.

(3) The most carefully prepared samples of boron subphosphide will probably contain less than a total of 0.1% impurity. This figure includes carbon.

2. Chemical Analyses. The major peak for the X-ray diffraction pattern of graphite was not reliable for determining carbon content. Too many other patterns interfered. The major peak of the B_4C pattern was used for relative determinations (e.g., Figure 13) but the carbon in most samples was determined by the Leco gas analysis technique. The results of this determination are used in twelve tables and eight figures in this study. The technique is effective down to 0.1% carbon. Several samples with values reported below this may be anything from zero to 0.1% carbon.

Chemical analyses were combined with X-ray fluorescent analysis to determine the amount of phosphorous in the hot-pressed compacts. All samples, powders and solids, were analyzed by X-ray fluorescence. A series of powders and a

series of hot-pressed compacts were analyzed chemically and the results used to calibrate the X-ray fluorescent intensities. The results are used in nine tables and three figures in this study.

The carbon analyses had considerably more precision of measurement than the phosphorous samples. Many factors such as density of packing, carbon content, and inhomogeneity had to be considered in making the phosphorous determinations. Because of this, the phosphorous content listed is good to within 10% of the percentage given. From test measurements that were made, most measurements are well within 5% of the figure cited. When the figure is in parenthesis, it is an estimate made from the best sample available, and an error as high as 20% is possible.

3. X-ray Analyses. Identification of the phases present was made by X-ray diffraction. Only three patterns (BP, $B_{13}P_2$, and $B_{13}C_2$) were obtained for the hot-pressed compacts. Two other products (BN and possibley α-rhombohedral boron) were identified in the nitrogen-boron reaction (Table XIII).

In addition to using X-ray diffraction for identification of phases, two X-ray techniques were used to follow the change in the unit cell dimensions. The first of these was

described under the Results of Hot-pressing in the section on the Effect of Maximum Temperature. The change in the spacing between the 104 peak and the 021 peak of the $B_{13}P_2$ pattern is plotted against the maximum pressing temperature in Figure 12.

Unit cell parameters were determined by applying Cohen's method (32) to the diffraction patterns. Solutions to Cohen's equations were obtained by using an IBM 1620 Computer which made a large number of determinations feasible. Use of this technique requires the selection of three diffraction peaks representing planes which bound the unit cell. If different groups of peaks are used, slight variations in the a and c values can be expected. When relating a and c values to composition, a consistent set of three peaks should be used as well as a single fiduciary point. In using Cohen's method, one must either know the angle exactly or refer to one peak whose angle is well established. In Table XXIV, the calculated cell dimensions are related to carbon content. The D group is made up of the 021, 015, and 211 planes. The S group is made up of the 021, 110, and 211 planes. Unfortunately, as the composition changes from $B_{13}P_2$ to $B_{13}C_2$, the fiduciary peak $B_{13}P_2$ (021) is lost. Table XXIV does show a gradual change through a narrow solid solution range caused by the change in phosphorous content. This is followed at about 12 to 14% carbon by a complete shift in pattern.

Table XXIV.

Dimensional Changes in X-ray Parameters
Related to Carbon Content

Sample	Percent carbon	$B_{13}P_2$ 100 reference D group a	D group c	S group a	S group c	$B_{13}C_2$ 100 reference S group a	S group c	Δd $B_{13}P_2$ 104-021 spacing
P-49	0.21	6.031	11.95	6.031	11.95			0.041
P-50	4.75	6.099	12.13	6.103	12.18			0.044
P-51	7.63	6.464	12.95	-	-			-
P-52	12.40	5.895	11.93	6.146	-	5.744	12.831	0.046
P-53	14.2	-	-	-	-			0.050
P-54	27.7	-	-	-	-			0.046
P-72(B_4C)	24.8					5.646	13.03	-
C-2($B_{13}P_2$)	0.31	5.973	11.83	5.985	11.96			-
P-62	0.53	6.014	11.92	6.016	11.94			0.039

D group	021	015	211
S group	021	110	211
Δd	021	104	

An attempt was made to relate cell dimensions and phosphorous content for the boron subphosphide samples prepared in this study. The a and c values for 27 samples of known phosphorous content were calculated with the D group of planes. Plots of a against phosphorous content and c against phosphorous content gave identical results as seen in Figure 35. At 30.6% phosphorous, a large minimum was obtained in cell dimensions. This corresponds to a composition $B_{13}P_2$. No evidence of a minimum or a maximum at 32.3% phosphorous exists so $B_{12}P_2$ is unlikely. A second minimum does exist at 22% phosphorous. This might correspond to a ratio $B_{10}P$. The peaks for $B_{13}P_2$ and $B_{10}P$ are sharp and well formed.

The data may be questioned on the basis of the tolerance in the phosphorous determinations. The estimated tolerance of 10% has been found by test analyses to be bettered considerably in practice. Most such tests were well within 5% of the value expected. A favorable factor is that these fluorescent analyses for phosphorous content were all made on one test date with identical conditions. Therefore, even if the accuracy is questionable, the precision is good.

Because these data could still be questioned, the results will be given with qualifications. Similar figures were obtained with the S group of planes. This still does not ensure that

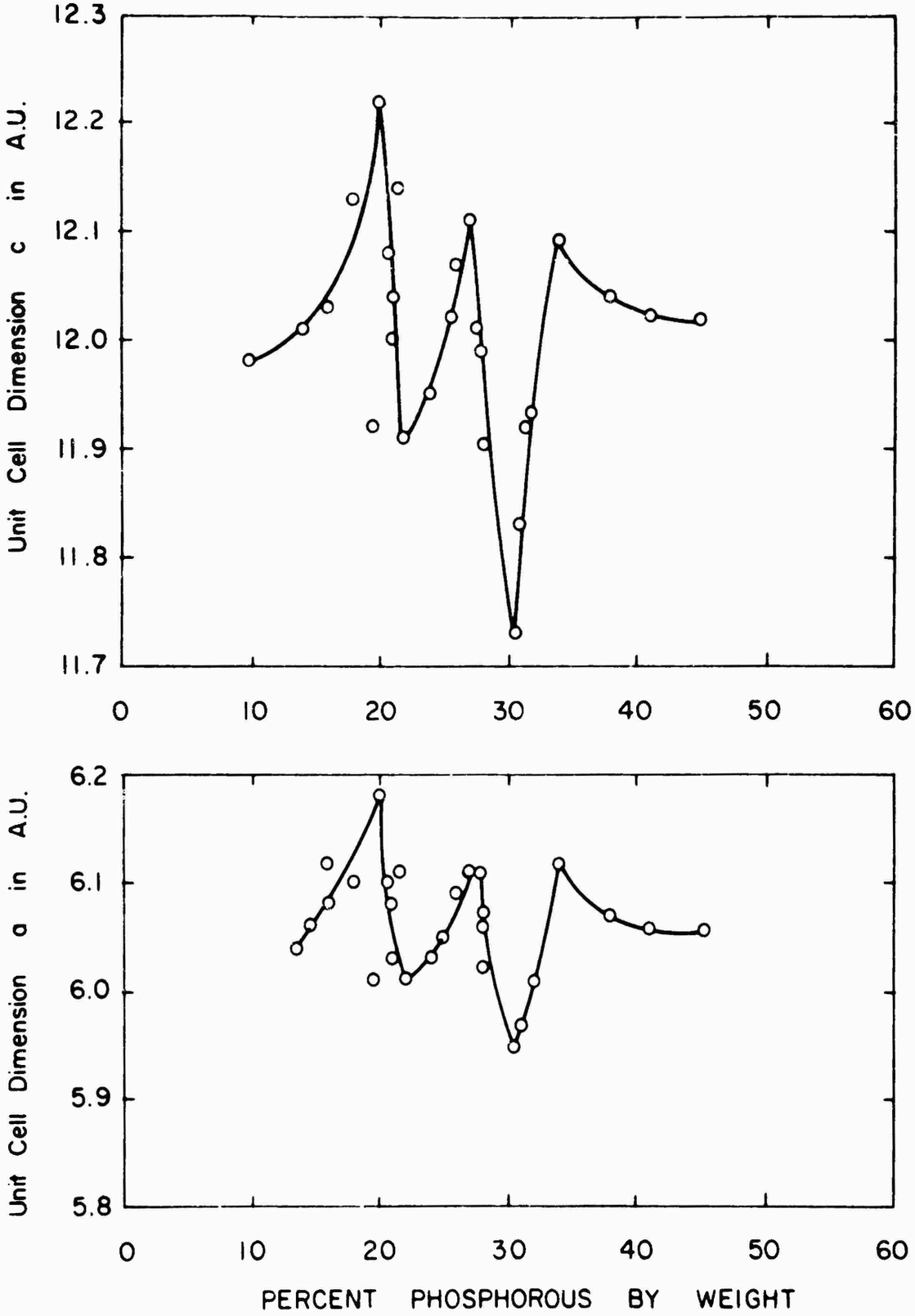

Figure 35. Unit Cell Dimensions as a Function of Phosphorous Content.

these data are real because they still depend on the same phosphorous analyses.

The solid solution range about the $B_{13}P_2$ peak is from 26.5 to 34%. The solid solution range about the $B_{10}P$ peak is from 20 to 26.5%. Eutectics or equivalent points then might occur at 20%, 26.5%, and 34% phosphorous.

E. Results of Property Measurements

1. Hardness. Five curves of Knoop microhardness at loads from zero to 1000 grams were prepared. These are shown in Figures 6 through 40. In each figure, the detail around the peak hardness has been expanded in an insert.

Figure 36 presents the hardness spectrum for sample P-70B which is an ultrapure specimen with 31% phosphorous. The peak hardness, 100 gram hardness, and 1000 gram hardness values taken from the five curves are represented in Figure 41 as a function of carbon and phosphorous content. A further attempt is made in Figure 42 to relate the peak hardness values obtained at various carbon contents with values reported by Samsonov (187). The 100 gram hardness values and 1000 gram hardness values are compared to the percent carbon and percent phosphorous in Figure 43.

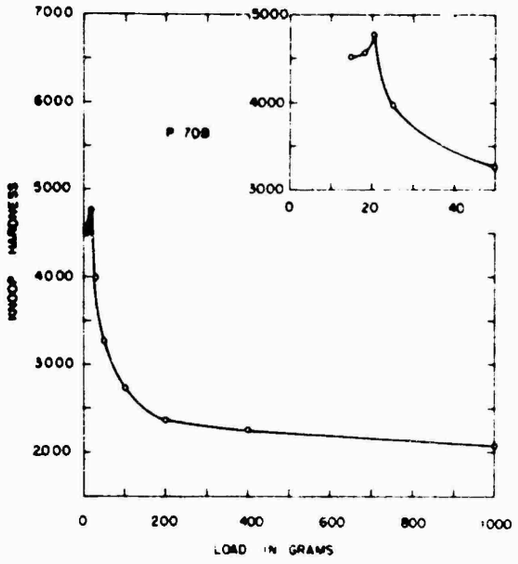

Figure 36. Knoop Hardness at Various Loads for P-70B, All Boron Phosphide

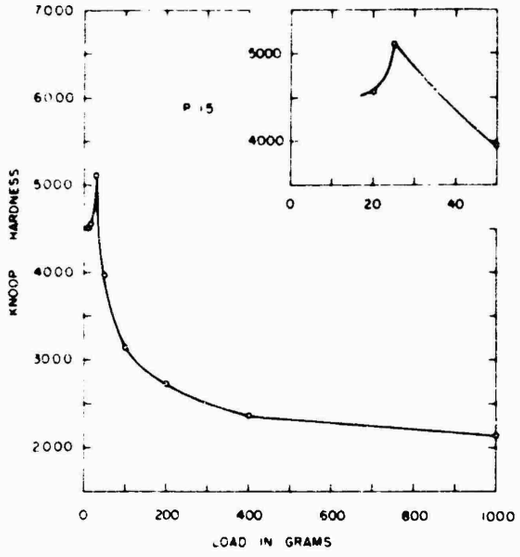

Figure 37. Knoop Hardness at Various Loads for P-15, Rich in Boron Phosphide, Medium Carbon Content

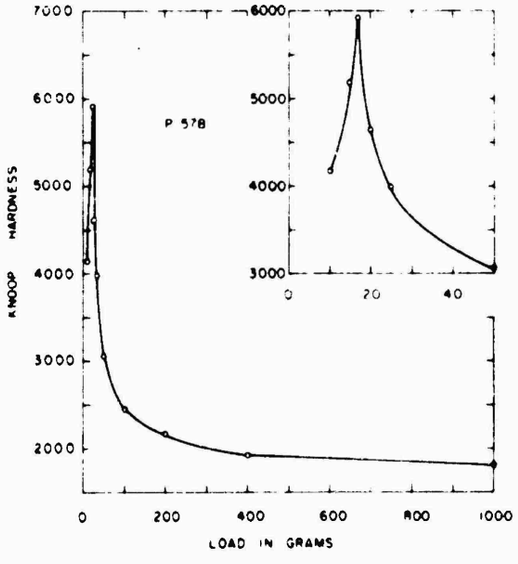

Figure 38. Knoop Hardness at Various Loads for P-57B, Low Carbide Content, Medium Phosphide Content

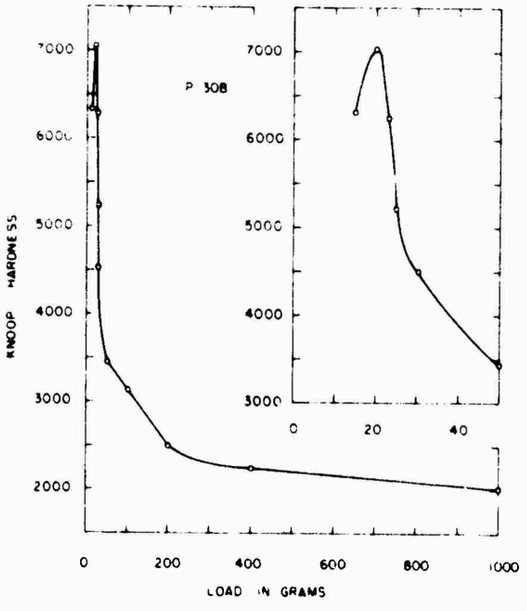

Figure 39. Knoop Hardness at Various Loads for P-30B, Low Phosphide Content, Medium Carbide Content

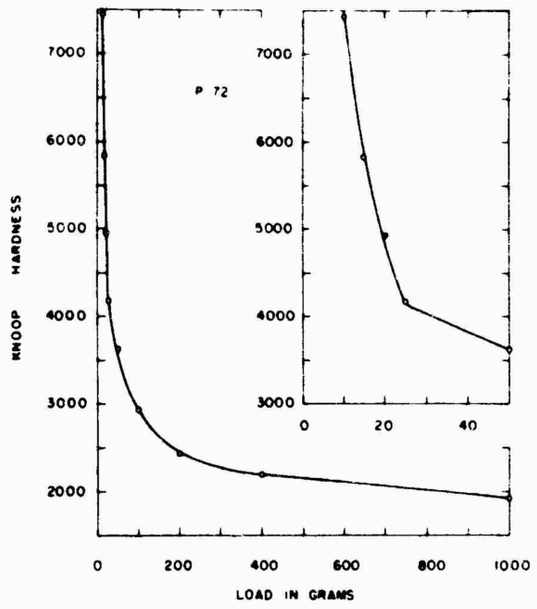

Figure 40. Knoop Hardness at Various Loads for P-72, All $B_{12}C_3$

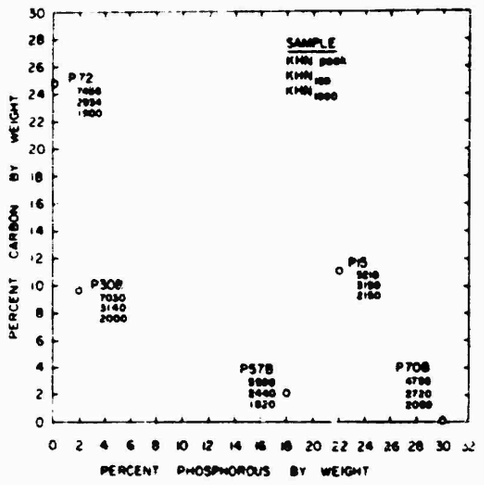

Figure 41. Correlation of Knoop Hardness and Percent Phosphorous and Carbon

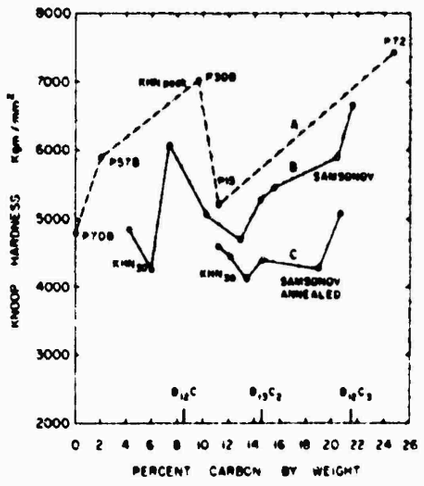

Figure 42. Measured Knoop Hardness Compared with Data Obtained by Samsonov (187)

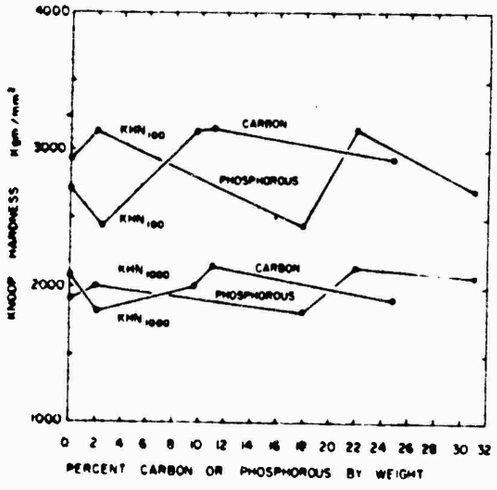

Figure 43. Effect on Knoop Hardness of Composition and Load in the Fracture Region

2. Thermal Conductivity. Seven samples were tested for thermal conductivity from 400°K to 850°K. The samples were selected to provide a range of carbon and phosphorous compositions. Values for sample P-28A with 7% phosphorous and 18.2% carbon are shown in Figure 44.

Early experience with boron subphosphide compacts produced obviously erroneous values for thermoelectric power. In conversation, Chaberski of The Carborundum Company suggested that the values could be stabilized by making the measurements at elevated temperatures first. This was thought to remove moisture which combined with surface phosphorous to produce phosphoric acids which in turn enhanced thermoelectric potentials with electrochemical potentials.

For this reason, thermal conductivity values were also checked as indicated by the arrows showing the sequence of measurements in Figure 44. After heating in a vacuum, as shown in this figure, the upper curve but not the lower curve was reproducible. All subsequent thermal conductivity measurements were made after heating in vacuum at 850°K.

Figures 45 and 46 present the results for samples P-67B and P-70B which contain 14% and 31% phosphorous respectively. Both contain less than 0.1% carbon. These measurements are followed by measurements on samples with higher carbon content. In Figures 47, 48,

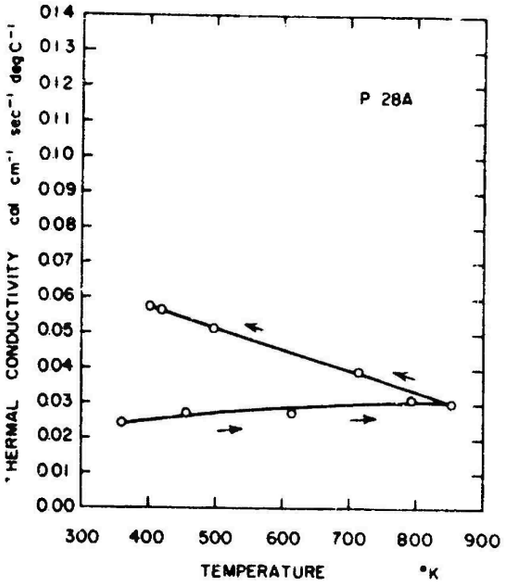

Figure 44. Thermal Conductivity of P-28A (7% Phosphorous, 18.2% Carbon)

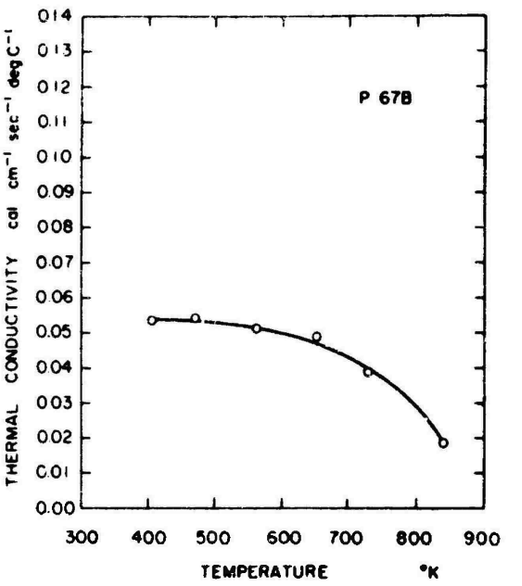

Figure 45. Thermal Conductivity of P-67B (14% Phosphorous, Less than 0.1% Carbon)

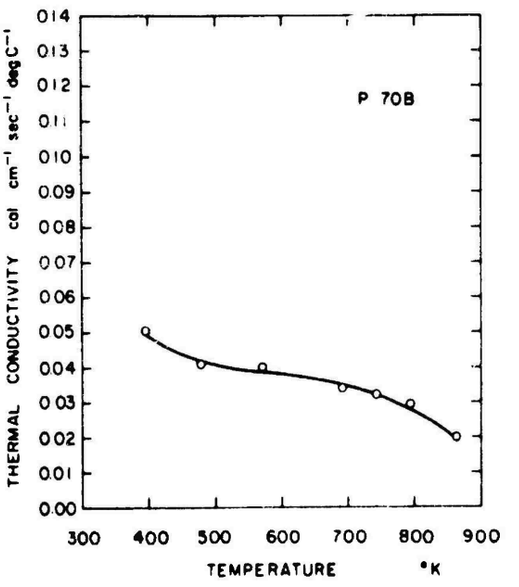

Figure 46. Thermal Conductivity of P-70B (31% Phosphorous, Less than 0.1% Carbon)

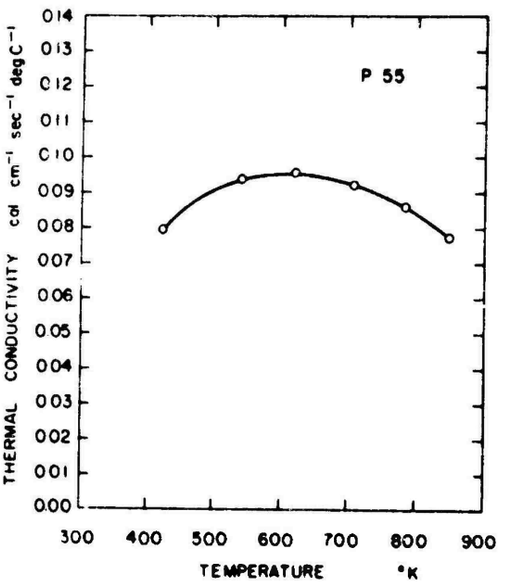

Figure 47. Thermal Conductivity of P-55 (18% Phosphorous, 0.44% Carbon)

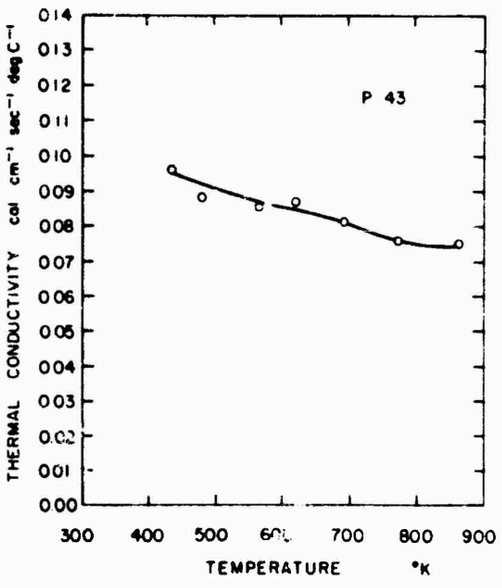

Figure 48. Thermal Conductivity of P-43 (11% Phosphorous, 9.9% Carbon)

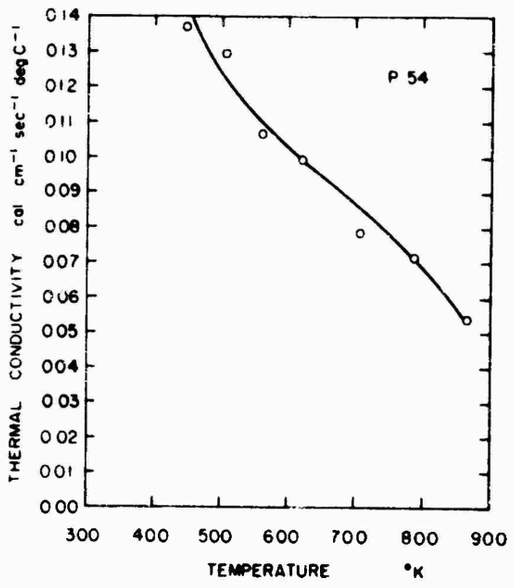

Figure 49. Thermal Conductivity of P-54 (5% Phosphorous, 27.7% Carbon)

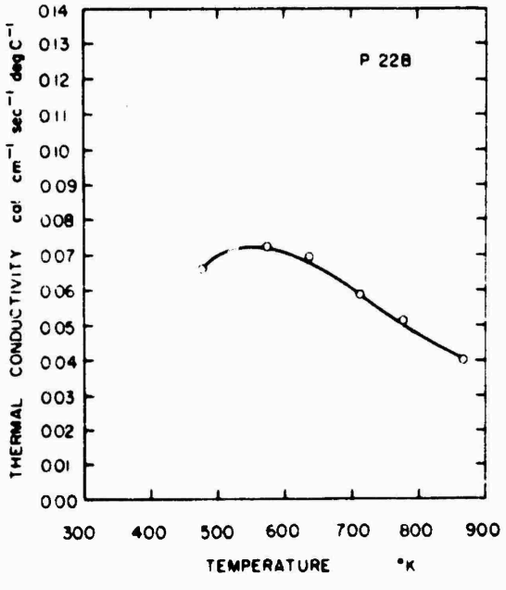

Figure 50. Thermal Conductivity of P-22B, Essentially BP

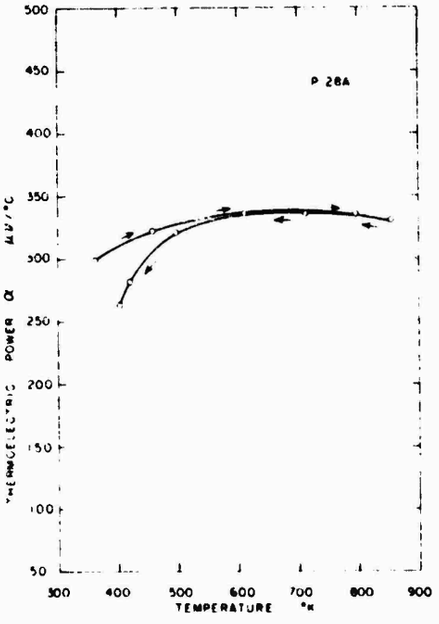

Figure 51. Thermoelectric Power of P-28A (7% Phosphorous, 18.2% Carbon)

and 49, the carbon content of samples P-55, P-43, and P-54 measures 0.44%, 9.9%, and 27.7%, respectively. The corresponding phosphorous content for these samples is 18%, 11%, and 5%.

The final thermal conductivity curve (Figure 50) reports the values obtained from sample P-22B which is essentially boron monophosphide. The BP from which this sample was hot-pressed was decomposed slightly to increase the bonding of the particles.

3. Thermoelectric Power. The measurement of thermal conductivity was accompanied by a measurement of thermoelectric power. The same seven samples were measured over the temperature range from 400°K to 850°K. The seven curves are reproduced in Figures 51 to 57. A check similar to that made in the thermal conductivity measurements was also made to determine the effect of adsorbed moisture on the thermoelectric potential. The double curve of Figure 51 resulted. When the sample was first heated in vacuum above 650°K, reproducible results were obtained. Several additional checks were made, and the results were all similar to those reported in Figure 51.

The effect of carbon content on thermoelectric power was measured by Samsonov (187). His results are presented in Figure 58 for comparison with similar measurements reported in Figure 59. The numbers next to the points in Figure 59 refer to the percent phosphorous by weight.

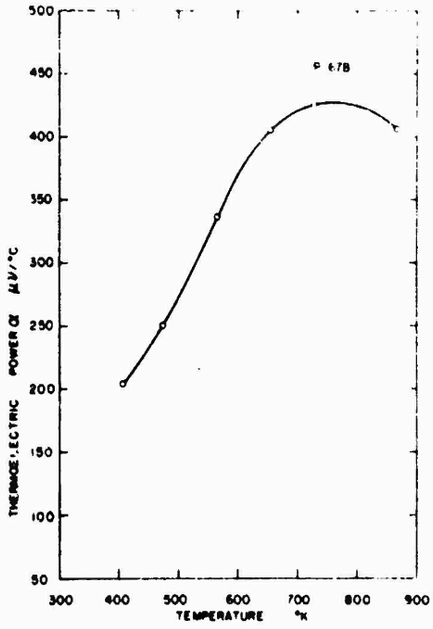

Figure 52. Thermoelectric Power of P-67B (14% Phosphorous, Less than 0.1% Carbon)

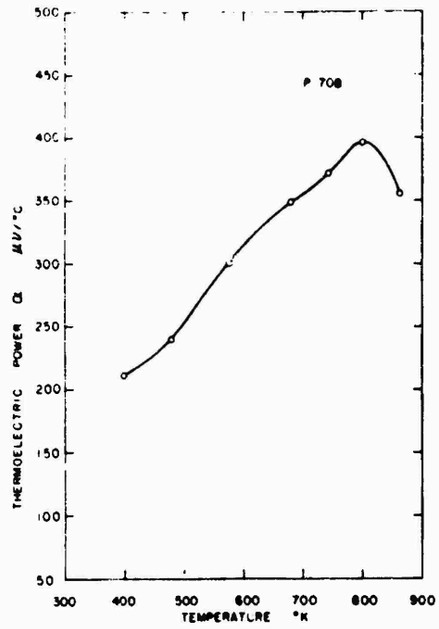

Figure 53. Thermoelectric Power of P-70B (31% Phosphorous, Less than 0.1% Carbon)

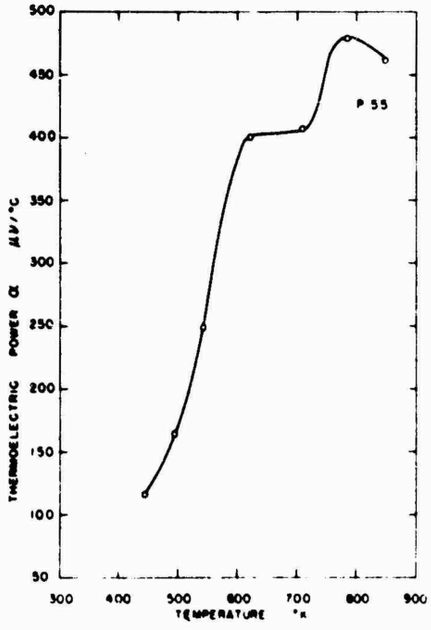

Figure 54. Thermoelectric Power of P-55 (18% Phosphorous, 0.44% Carbon)

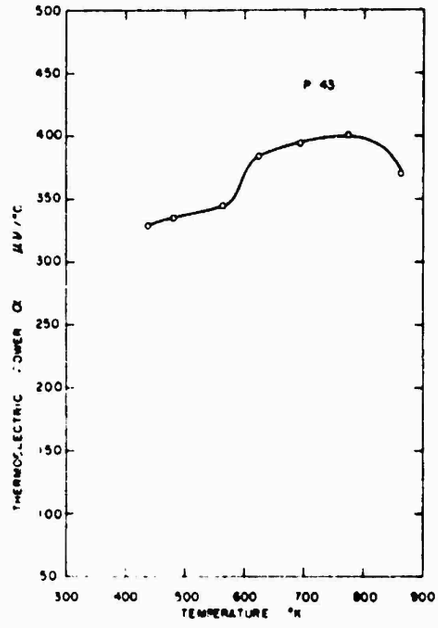

Figure 55. Thermoelectric Power of P-43 (11% Phosphorous, 9.9% Carbon)

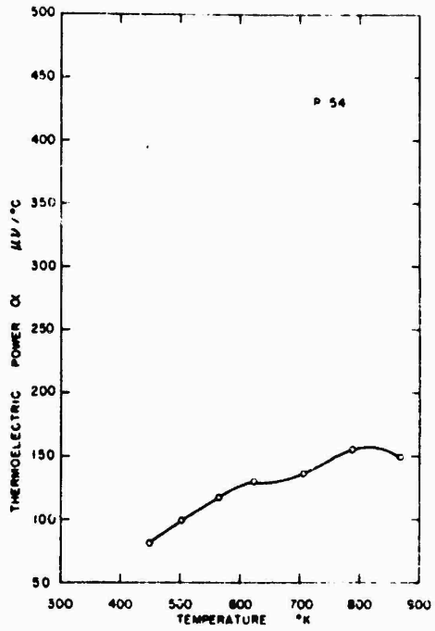

Figure 56. Thermoelectric Power of P-54 (5% Phosphorous, 27.7% Carbon)

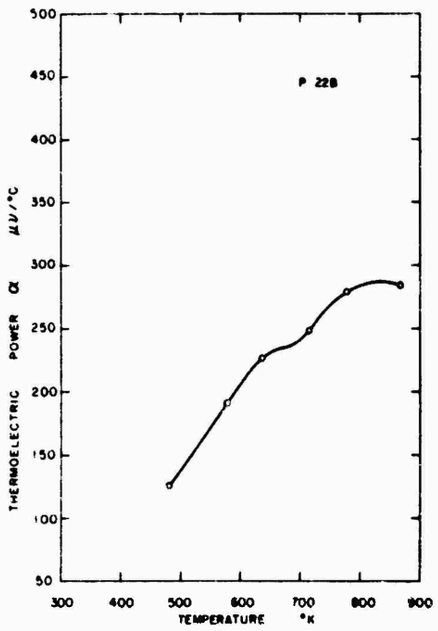

Figure 57. Thermoelectric Power of P-22B, Essentially BP

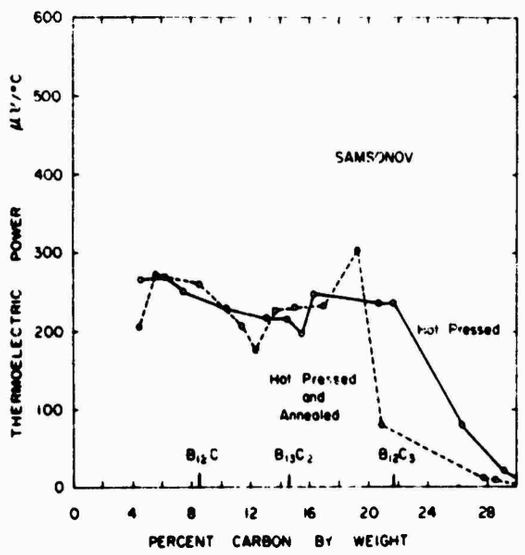

Figure 58. Thermoelectric Power of the Boron Carbides as Obtained by Samsonov (187)

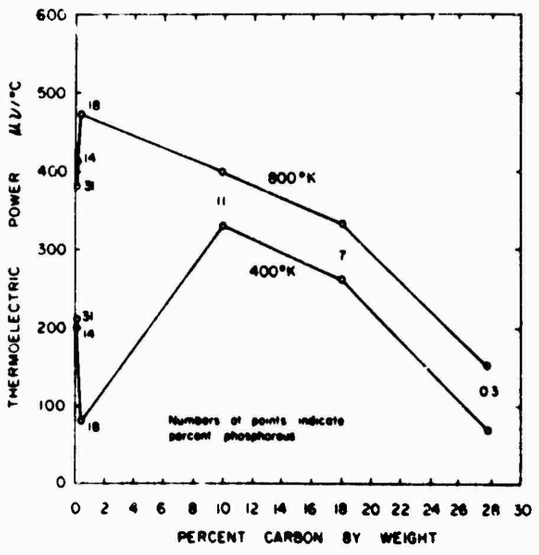

Figure 59. Thermoelectric Power as a Function of Temperature and Composition

4. Electrical Conductivity and Activation Energies. The logarithm (base 10) of electrical conductivity is shown as a function of the reciprocal of absolute temperature ($°K^{-1}$) for twelve samples in Figures 60 to 71. The composition and sample number are reported for each figure in Table XXV. Intrinsic and extrinsic activation energies have been determined where possible, and these results are presented in Table XXV. Only two of the samples, P-64B and P-22B, had distinct extrinsic slopes. The other ten samples had conductivities which changed gradually along the gentle curve which is characteristic of boron and the borostitials.

Different scales have been used for the ordinates in these twelve curves. The high temperature end of each curve approaches a steep intrinsic line between 500°K and 1000°K. A common intrinsic line does not appear to exist.

The low temperature ends of the curves fall into three groups. The four samples with the lowest low-temperature conductivity values are P-62, P-66B, P-67B, and P-70B. These were prepared in lined and sealed molds. Except for P-62, they were prepared from ultrapure boron and phosphorous. Sample P-62 does have a distinctly higher value of low-temperature conductivity than the other three samples in this group.

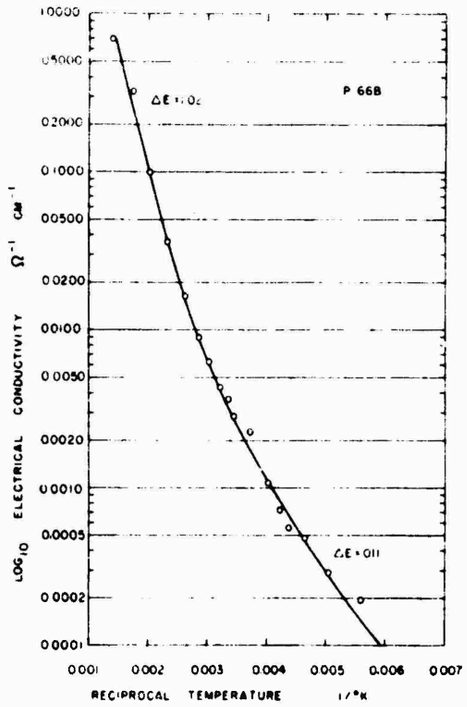

Figure 60. Electrical Conductivity at Reciprocal Temperatures for P-66B (0.25% C, 16.0% P)

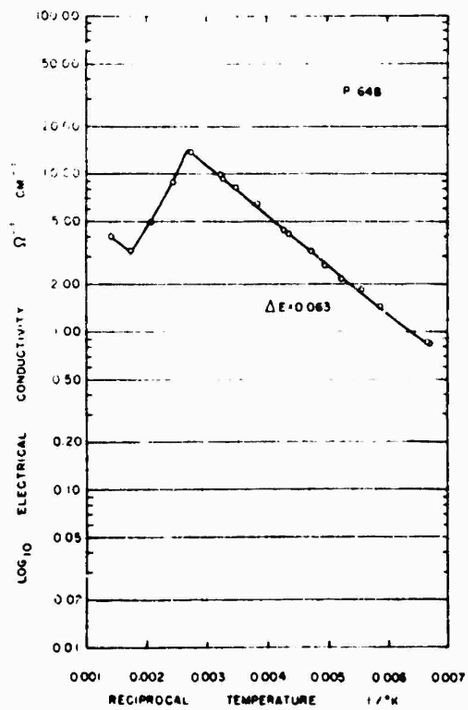

Figure 61. Electrical Conductivity at Reciprocal Temperatures for P-64B (3.3% C, 31.0% O)

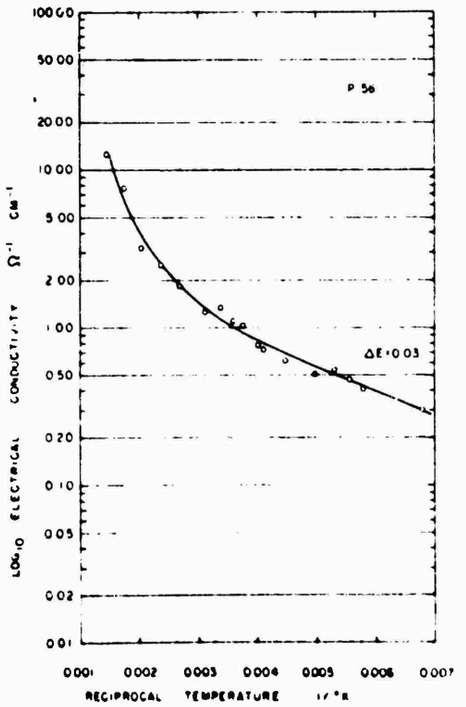

Figure 62. Electrical Conductivity at Reciprocal Temperatures for P-56 (0.33% C, 27.5% P)

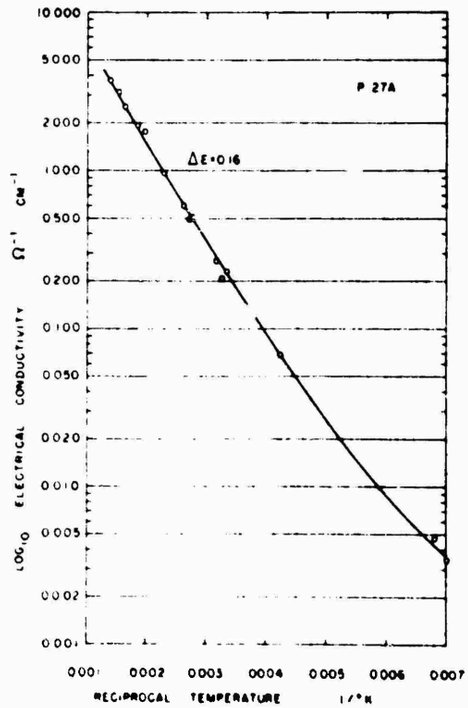

Figure 63. Electrical Conductivity at Reciprocal Temperatures for P-27A (14.5% C, 12.0% P)

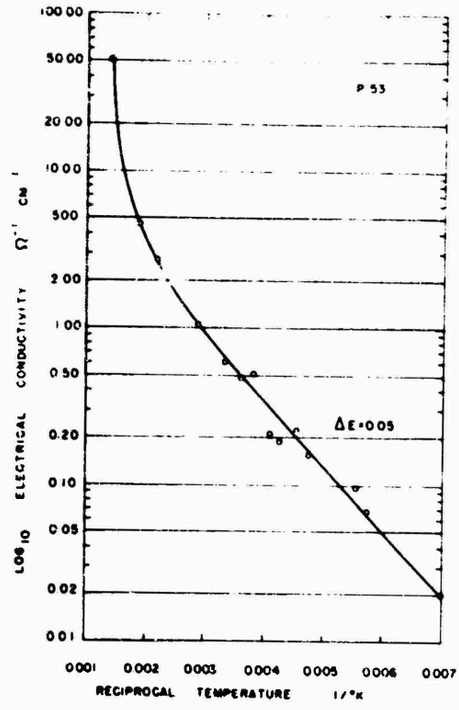

Figure 64. Electrical Conductivity at Reciprocal Temperatures for P-53 (14.2% C, 0.4% O)

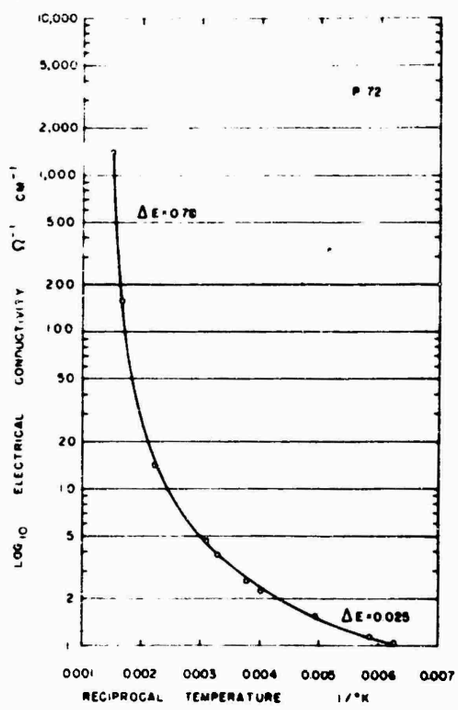

Figure 65. Electrical Conductivity at Reciprocal Temperatures for P-72 (Composed of $B_{12}C_3$)

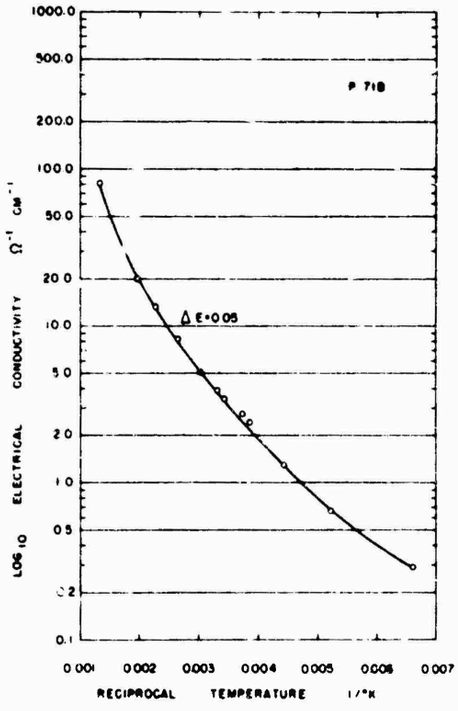

Figure 66. Electrical Conductivity at Reciprocal Temperatures for P-71B (Essentially $B_{13}C_2$)

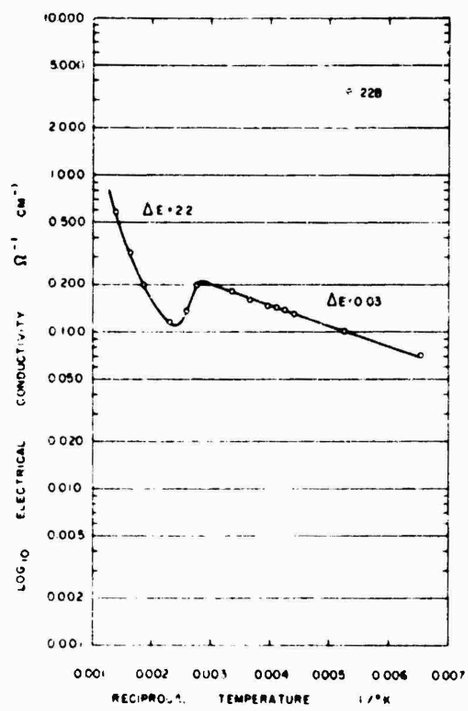

Figure 67. Electrical Conductivity at Reciprocal Temperatures for P-22B (Essentially BP)

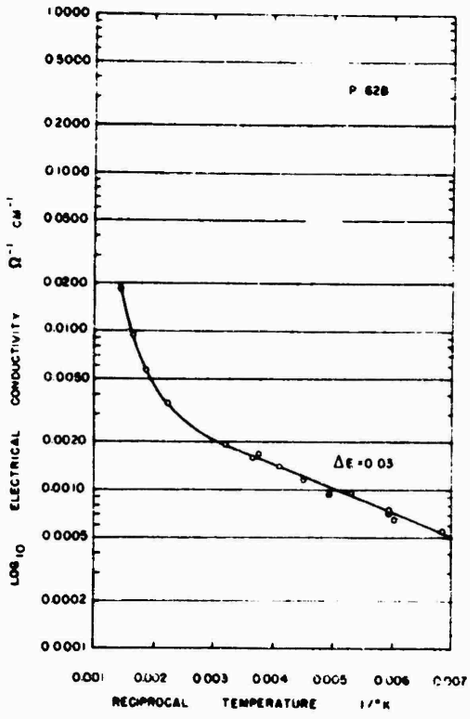

Figure 68. Electrical Conductivity at Reciprocal Temperatures for P-62B (0.53% C, 19.6% P)

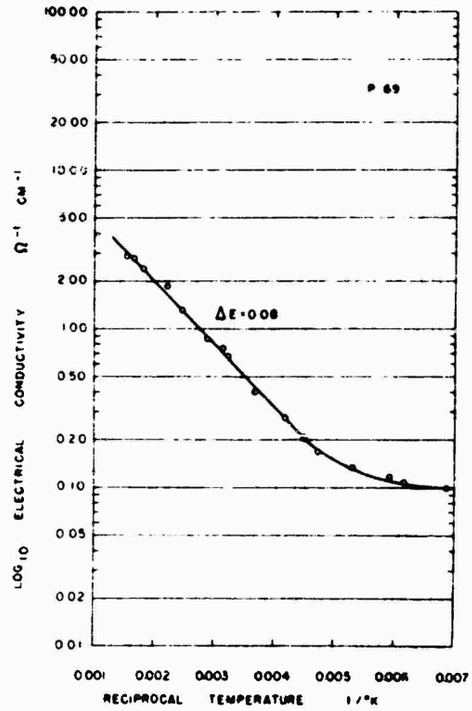

Figure 69. Electrical Conductivity at Reciprocal Temperatures for P-69 (11.3% C, 0.2% P)

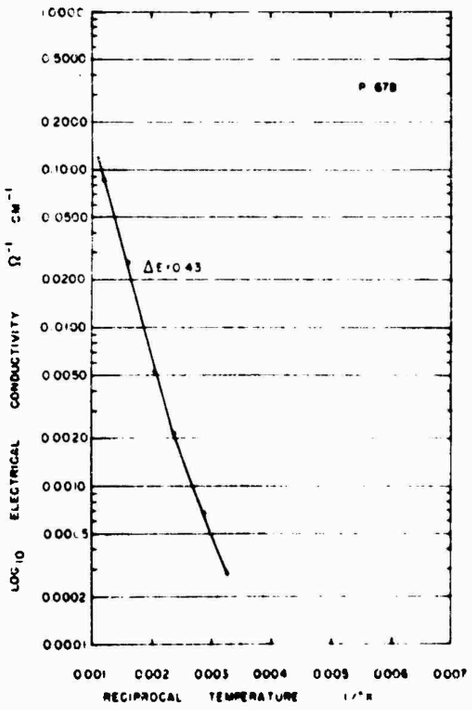

Figure 70. Electrical Conductivity at Reciprocal Temperatures for P-67B (Less than 0.1% C, 30.8% P)

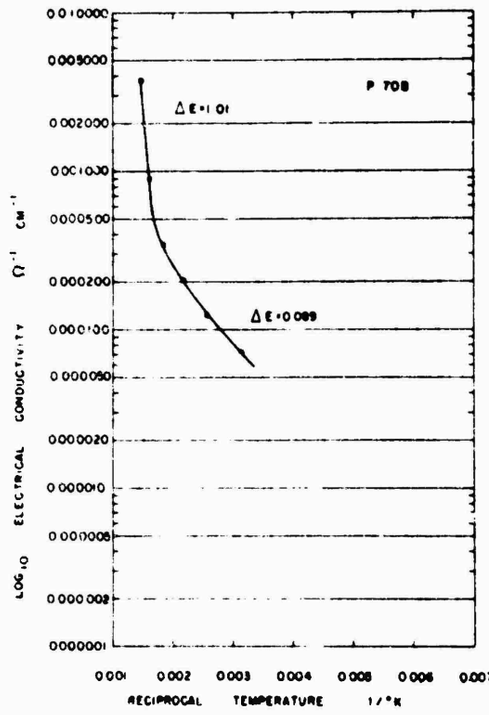

Figure 71. Electrical Conductivity at Reciprocal Temperatures for P-70B (Less than 0.1% C, 30.8% P)

Table XXV.

Activation Energies

Figure	Sample	% C	% P	Resistivities RT Ωcm	Activation energies ev intrinsic	extrinsic
60.	P-66B	0.25	16	278	1.02	0.11
61.	P-64B $B_{13}P_2$	3.3	31	0.1	-	0.06
62.	P-56 $B_{13}P_2$	0.33	27.5	0.9	-	0.03
63.	P-27A	14.5	12.0	4.0	-	0.16
64.	P-53	14.2	0.4	1.5	-	0.05
65.	P-72 $B_{12}C_3$	24.8	0	0.3	0.78	0.025
66.	P-71B $B_{13}C_2$	14.8	0	0.3	-	0.05
67.	P-22B BP	8.5	67.9	570	2.2	0.03
68.	P-62	0.53	19.6	540	-	0.03
69.	P-69	11.3	.2	1.7	-	0.08
70.	P-67B below	0.1	16.5	4,160	0.43	-
71.	P-70B below	0.1	31	16,700	1.01	0.089

The second group of samples arranged by their low-temperature conductivity values are P-27A, P-53, P-22B, and P-69 in order of increasing conductivity. Sample P-22B was prepared at low temperature and had a composition approximately that of BP.

The remaining four samples all had a low-temperature (150°K) conductivity of just below 1 $ohm^{-1}cm^{-1}$. This group of four included the two carbide sample, P-72 ($B_{12}C_3$) and P-71B ($B_{13}C_2$) and samples P-56 and P-64B. The latter two samples had phosphorous contents close to that of $B_{13}P_2$ (30.6%).

5. The Thermoelectric Figure of Merit. The thermoelectric figure of merit is directly proportional to the electrical conductivity and the square of the thermoelectric power. It is inversely proportional to the thermal conductivity. All three of these measurements were made as functions of temperature for samples P-22B, P-67B, and P-70B. Figures of merit values for the three samples are presented in Figure 72. The maximum value was about $10^{-5}°K^{-1}$. Even though all three factors were not measured on the same sample, it was possible to match samples and produce figure of merit curves for composite data. Samples P-43 and P-27A had similar carbon and phosphorous contents (10 to 15%), and samples P-54 and P-72 were essentially $B_{12}C_3$. The composite figure of merit curves are shown in Figure 72.

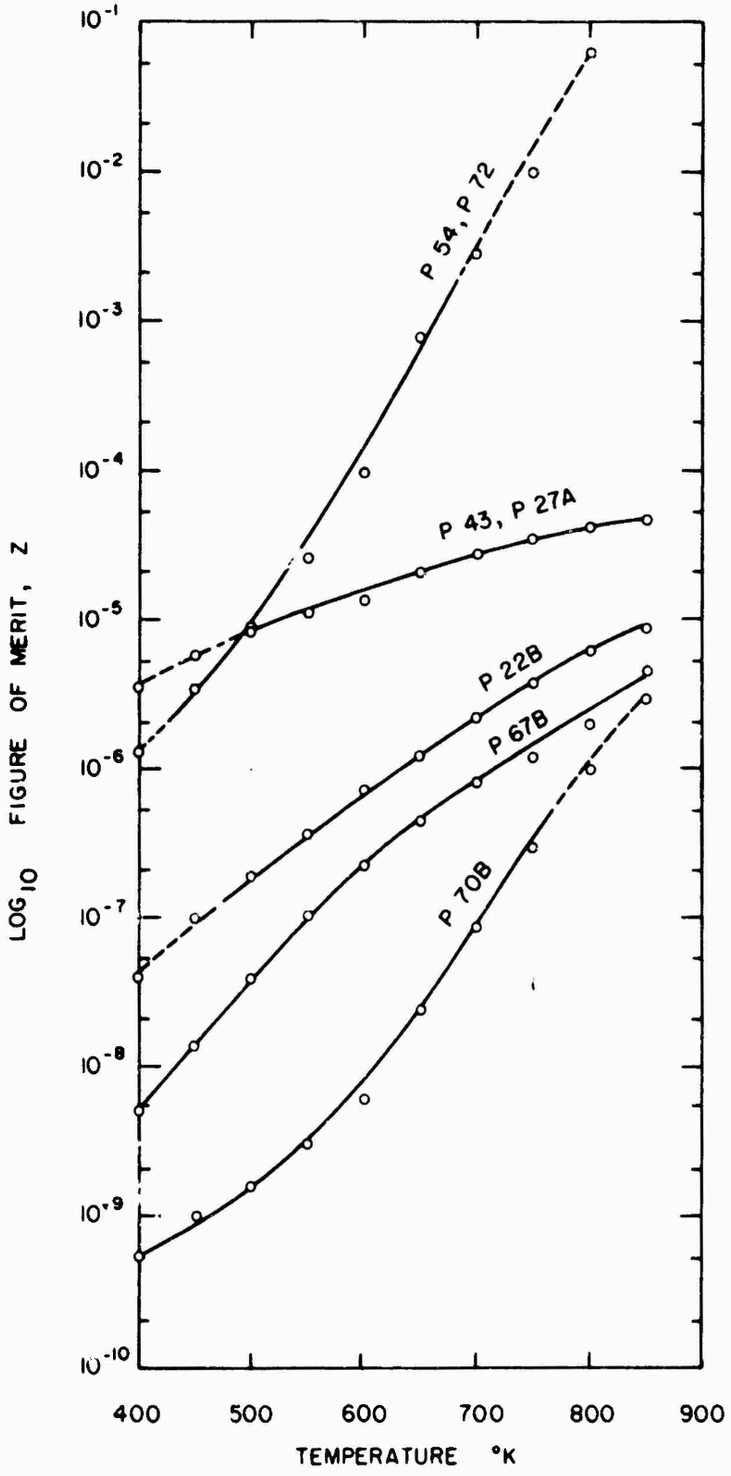

Figure 72. Thermoelectric Figure of Merit of Representative Samples at Various Temperatures

6. Results of Measurement of Hall Effect. The Hall coefficient was measured as a function of temperature for two samples. The logarithm (base 10) of the Hall coefficient for sample P-64B is plotted against the reciprocal of absolute temperature ($°K^{-1}$) in Figure 73. A similar curve for sample P-56 is presented in Figure 74. Figure 75 is a comparison of the two sets of measurements. The Hall coefficients are presented as functions of temperature (°K).

The Hall potentials are unusually low. They are so low that they were difficult to measure. The sign of the Hall potential, like the sign of the thermoelectric power, indicated that these samples are p-type above 375°K. The other unusual feature of these Hall potentials is the change of sign which occurred three times below 375°K for both samples.

Both samples measured had low carbon content and a phosphorous concentration close to that of $B_{13}P_2$.

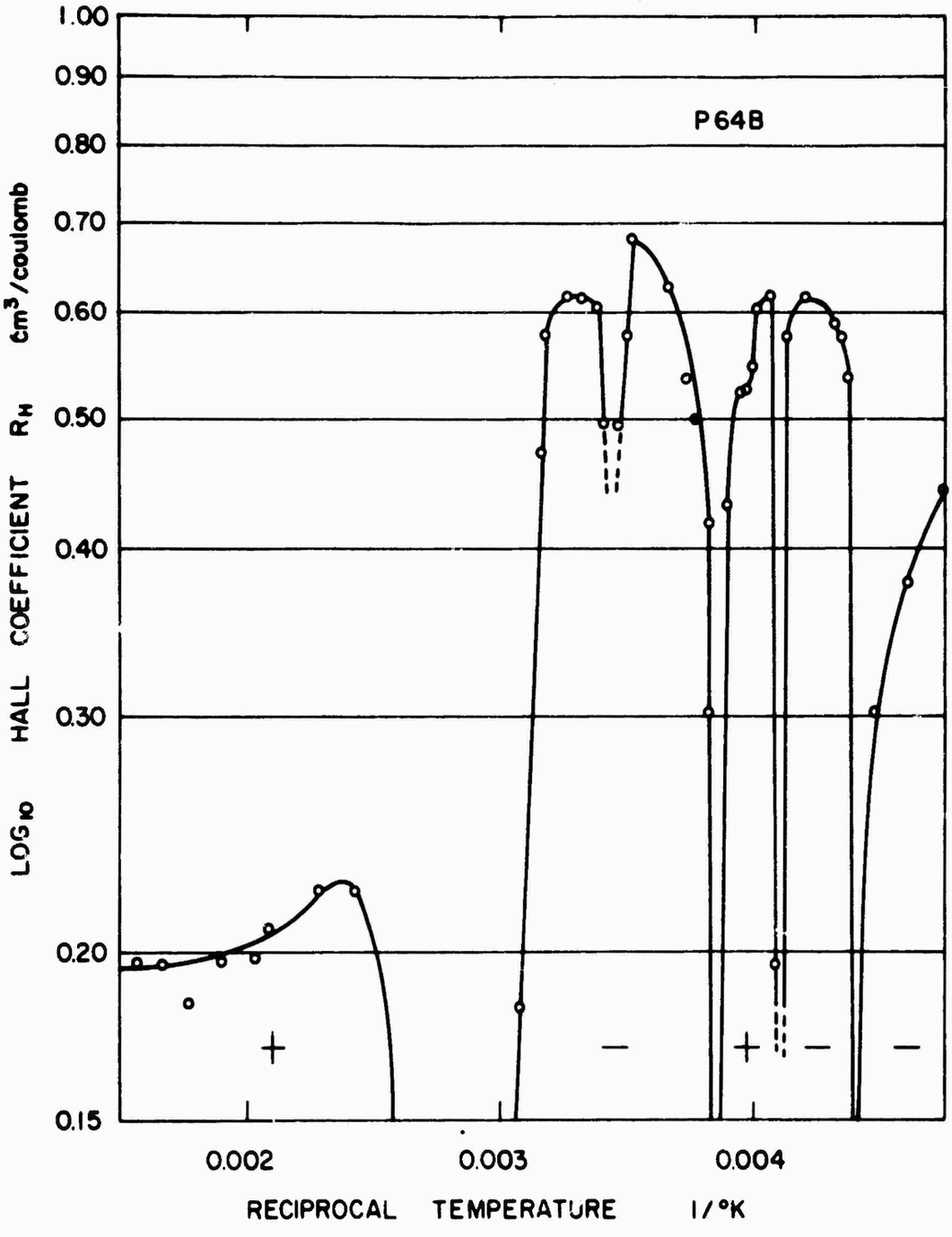

Figure 73. Logarithm of the Hall Coefficient of P-64B at Reciprocal Temperatures

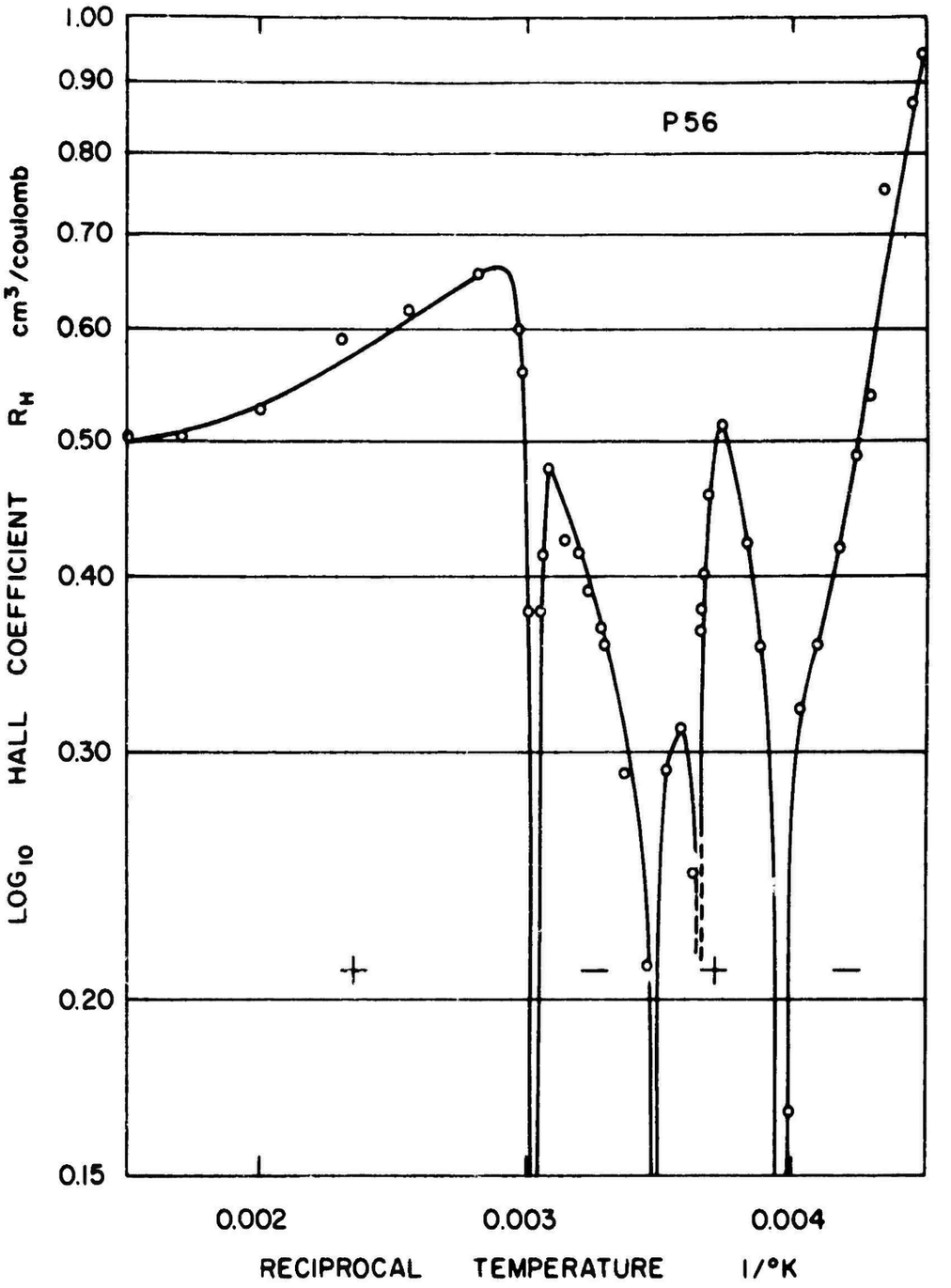

Figure 74. Logarithm of the Hall Coefficient of P-56 at Reciprocal Temperatures

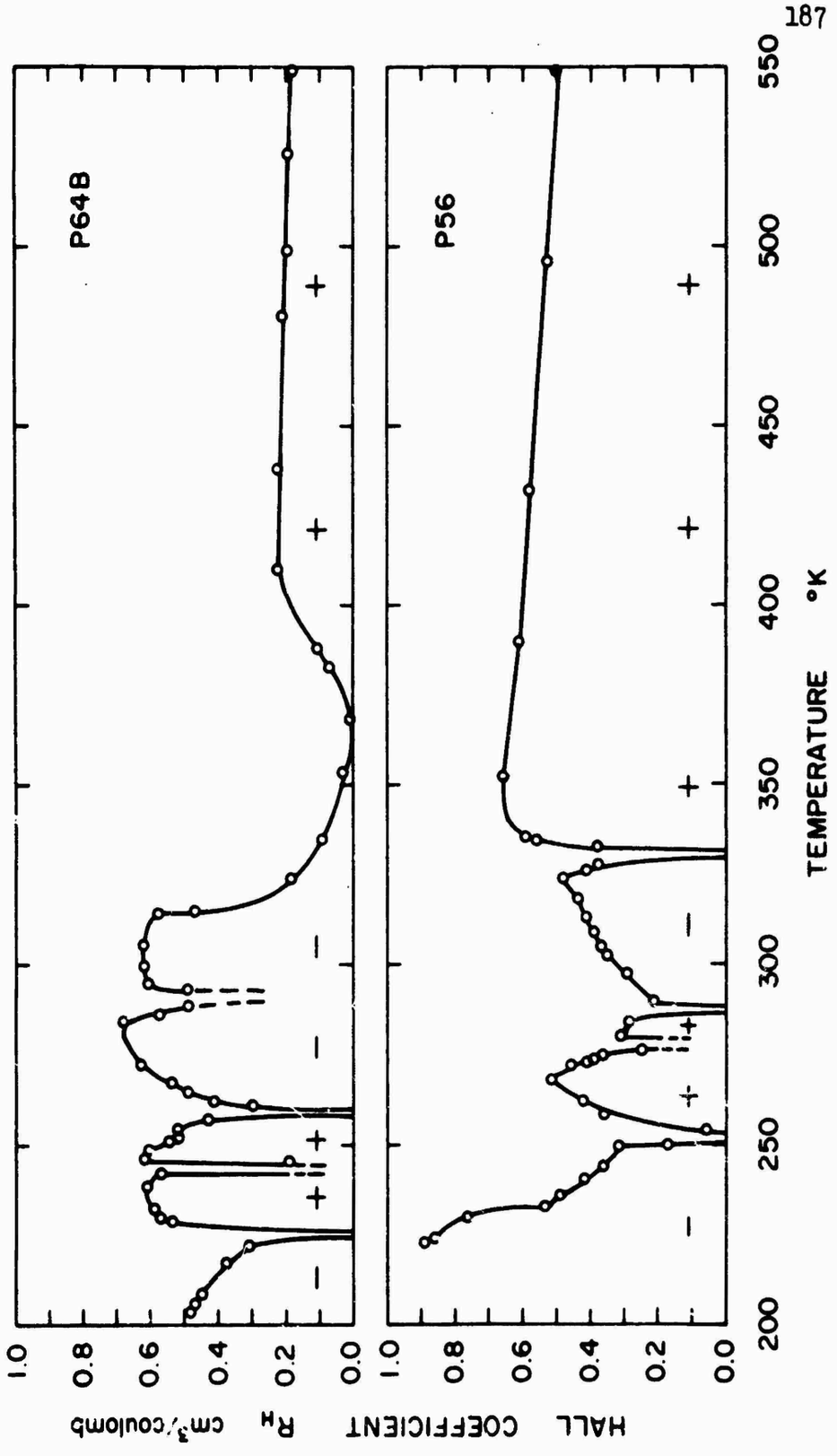

Figure 75. Comparison of the Hall Coefficient at Various Temperatures for Samples P-64B and P-56

V. DISCUSSION OF RESULTS

A. General Background

A review of the literature reveals that boron subphosphide is a most interesting subject of study and an example of an equally interesting system of compounds of similar structure. The discovery of the rhombohedral structure of $B_{13}C_2$ started the series. Next, the confirmation of α-rhombohedral boron provided the parent member of the group. Since then, rhombohedral $B_{12}Si_3$, $B_{13}P_2$, and $B_{13}As_2$ have been confirmed. These compounds together with other classified and unclassified ones are listed in Table XXVI. Much can be learned about the boron-phosphorous system from a study of the family.

The boron-phosphorous system is difficult to study because the compositions of interest require very high temperature preparations. At such high temperatures, control of potential impurities from containers and from the atmosphere is particularly difficult as is control of the temperature itself. The high strength of the bonds in the B_{12} structure which is reinforced by extra bonds from the interstitial elements is another source of a problem (hardness) one encounters in working with the borcstitials. The third factor which contributes to

Table XXVI.

Borostitial and Related Compounds

Number of interstitial atoms per B_{12} group	Rhombohedral	Tetragonal	Orthorhombic
0	α-rh.B		
1	$B_{12}S$	α-$B_{12}Al$ $B_{12}Ga$	β-$B_{12}Al$
1.2			$B_{10}Al$
2	($B_{12}P_2$) ($B_{12}O_2$)		
3	$B_{13}As_2$ $B_{13}C_2$ $B_{13}P_2$ $B_{12}Si_3$ $B_{13}O_2$		
unclassified			
$B_{12}C$ $B_{12}Si$		$B_{12}Ge_x$ $B_{12}Sn_y$	

the difficulty of working with the boron-phosphorous system is the ease with which the composition changes. As seen in the B-C system (phase diagram, Figure 3), preferred compositions which are called compounds exist with solid solution ranges on either side of them. Similar preferred compositions and solid solution ranges would be expected in the boron-phosphorous system and might explain the large variations in composition with a single phase identified by X-ray diffraction.

Many of the hot-pressed compacts contained appreciable quantities of carbon. Such a system (B-C-P) can be approached in several ways. It can be studied as a boron-phosphorous system with impurities or a boron-phosphorous-carbon ternary system. The system may be considered as a combination of derivatives of a basic B_{12} structure with simple variations on the properties of α-rhombohedral boron.

Since many of the compositions prepared by hot-pressing approached either boron subphosphide or boron subcarbide, the compositions may be considered as located in the phase diagram defined by a double salt system (e.g., $B_{13}P_2$-α and $B_{13}C_2$-β). Here α and β can be small positive or negative numbers.

The selection of any one of these methods of expression will depend upon the purpose assigned. For instance, to explain conduction mechanisms, it may be best to see how the conduction

of boron has been modified by interstitial additions, or conversely, how boron added to fixed compounds may have modified their properties. On the other hand, to interpret X-ray parameters, one system (e.g., boron-phosphorous) might be considered with other elements (e.g., carbon, silicon) viewed as unwanted impurities.

In any case, the preparations usually involve dynamic changes controlled by reaction rates, diffusion, crystallization, and phase changes. Thus, any phase diagram can only express what could be if sufficient time were available for equilibrium. A large difference, therefore, is possible between what could be and the highly disordered often composite structure produced at high speed in a hot-press at 2000°C. Properties, then, are frequently closely related to the method selected for manufacture. A structure-sensitive variation is superimposed on the variation of properties associated with materials and amounts.

B. Composition and Distribution

X-ray analysis was used to determine the compositions in the product. A look at the phase diagram for the boron-carbon system (Figure 1) indicates that the major compound is $B_{13}C_2$. Its X-ray diffraction pattern was quite common in some of the hot-pressed compacts such as those made from BP with 5.2% carbon

or those made in unlined graphite molds. The major line of the graphite pattern was frequently found in such samples.

In the several samples with low phosphorous content and 8.5% carbon content, the length of scan made with the X-ray diffraction machine was too short to permit recognition of any separate pattern attributable to $B_{12}C$.

The boron-phosphorous system was known to have two X-ray diffraction patterns, one BP and the other $B_{12}P_2$ or $B_{13}P_2$. Matkovich (139), during the course of this study, established, on the basis of its rhombohedral X-ray pattern and a comparison of its calculated and experimental densities (both 2.74 g/cm^3), that the compound was $B_{13}P_2$. This has been clearly demonstrated and verified in this study as well.

If $B_{12}P_2$ with its rhombohedral pattern existed, the center three sites shown in Figure 2 would be occupied as phosphorous-blank-phosphorous, and the calculated density would be 2.53 g/cm^3. If, on the other hand, the compound were $B_{13}P_2$, the center sites in Figure 2 would be occupied by phosphorous-boron-phosphorous, and the calculated density would be 2.74 g/cm^3. Boron carbide, $B_{13}C_2$, has a density of 2.54 g/cm^3, and the highest density reported for any form of boron is 2.46 g/cm^3 for the α-rhombohedral form.

Compacts with 5.2% carbon have been shown (at 2100°C) to approach a density of 2.70 g/cm^3 (Figure 9) and 2.58 g/cm^3 after being held for 10 minutes at 2000°C (Figure 14, upper part). Low carbon samples prepared in lined and protected molds approached a density of 2.70 g/cm^3 at only 2000°C.

Reactions between the elements frequently produced samples with densities above 2.6 g/cm^3 with the pattern of BP absent. Slow decompositions of BP in vacuum produced some of the best specimens approaching the composition of $B_{13}P_2$. Analyses of the boron to phosphorous ratio could not be used as support because samples containing more or less phosphorous could be found for every sample which analyzed 13/2. The stopping point in the decomposition was not sharp when the decomposition was carried out in this manner. Many of the densities of samples prepared by reaction did seen to be low. This could be the result of unreacted free amorphous boron (density, 2.35 g/cm^3).

The measurement of the spacing between 104 and 021 X-ray diffraction peaks of the boron subphosphide pattern would indicate two definite groupings if two subphosphides existed. Only one was found. In addition, this was found to be sensitive to the build-up of the carbide 80 intensity peak and was used to follow that shift.

A final bit of evidence supporting the presence of $B_{13}P_2$ over that of $B_{12}P_2$ is the measurement of X-ray unit cell parameters in the phosphide pattern as a function of phosphorous content. The distinct minimum at 30.6% phosphorous corresponds exactly to the percentage phosphorous present in $B_{13}P_2$.

Perhaps as interesting as what was found is an examination of what was not found. No pattern was found in the phosphide compacts for any crystal form of boron or for B_6P_3. An attempt to synthesize this B_6P_3 produced only a mixture of $B_{13}P_2$ and BP.

A number of measurements of the rhombohedral unit cell parameters by Cohen's method indicates that a narrow solid solution range exists in the B-P system around $B_{13}P_2$, and a similar one exists in the B-C system around $B_{13}C_2$. No extensive solid solution between the two compounds was found, although smaller regions of solid solutions may exist near the compounds.

A problem which closely parallels the problem of the composition of boron subphosphide exists in the boron-oxygen system. The problem is outlined by Rizzo (175) and is mentioned in the Related Materials portion of the Review of the Literature. Rizzo claimed a formula of B_6O (density, 2.59 g/cm^3) for the suboxide because the best powder densities were 2.62 g/cm^3, and hot-pressed densities were 2.588 g/cm^3. (The theoretical density for $B_{13}O_2$ is 2.80 g/cm^3.) The unjustified assumption that

a definite B to O ratio will be attained may account for such a conflict. It might also require the consideration of carbon content as did the phosphide problem. No mention was made of the extent of carbon contamination or of any precautions taken to eliminate it. Even a small amount of carbon makes a great deal of $B_{13}C_2$ with a low density.

Grain growth in the boron subphosphide system is low at 2000°C. The starting particle size of 1-13 microns is still found in most of these samples. One sample, P-32, held at 2000°C for eleven minutes had grains which had grown to 22-27 microns. Another, P-70B, held at 1970°C for 30 minutes had grains as large as 40 microns.

Crystallization took place in a sample, P-71B, with a composition of $B_{13}C_2$ which was heated to 2120°C for 10 minutes. Sample P-37, heated to 2000°C for 11 minutes, crystallized strongly. This sample contains 7.8% carbon and has a very strong pattern of $B_{13}P_2$. Its phosphorous content is high (25 to 30%) but cannot be precisely established.

A better understanding of the crystallization and grain growth of these samples will be possible when more complete phase diagrams exist for the two systems.

One other size effect was noted and this is the formation of large (80-210 microns) areas apparently of carbide. These

seem to be a product of the carbon flakes in the starting material. In many of these, a large very dark void can be seen in the center. Not only is this a source of inhomogeneity in the samples, but it helped to disclose differences in reactivity of the crystallite cores and their surfaces or grain boundaries. The boundaries were attacked first in a fused alkali etch. This boundary attack continued until the central crystal was freed. From etching polycrystalline high purity semiconductors, one learns that the disordered state or region with impurity concentration etches more rapidly than more perfect or pure crystals. This would indicate that a deep surface was modified by partial decomposition, absorption, or some other mechanism.

A study of rhombohedral unit cell parameters as a function of phosphorous content (Figure 35) indicates not only the presence of $B_{13}P_2$ at 30.6% phosphorous, but also the possible presence of another compound at 22.2% phosphorous. As pointed out in the Results section, the phosphorous measurements are precise but may be slightly inaccurate. A content of 22.2% phosphorous, however, corresponds exactly to the content of $B_{10}P$ which might easily be analogous to $B_{10}Al$.

A number of samples had decomposed to low phosphorous content. One such, D-12B, was one of the few with extra diffraction lines of unexplained origin. The pattern of D-12B is

compared to that of $B_{13}P_2$ in Table XXVII. Sample D-12B contained 7.9% carbon and 21.6% phosphorous and had no diffraction lines of $B_{13}C_2$. The unexplained lines might then be assigned to $B_{10}P$. They might also be attributed to $B_{12}C$ although a complete absence of any $B_{13}C_2$ lines makes this doubtful. One might also speculate as to whether a low figure for the density of $B_{10}P$ might account for some of the apparently low densities obtained in reactions. The existence, then, of $B_{10}P$ is unresolved, but sufficient evidence exists that further study is recommended.

The other unresolved problem of composition is that of the X-ray pattern obtained from the B-N system and presented in Table XIII. Both amorphous boron samples were heated to between 1600°C and 1800°C in a nitrogen atmosphere. The total time to maximum heat was 35 minutes, and the estimated time above 1600°C was seven minutes. In other reactions with phosphorous present, BP and $B_{13}P_2$ X-ray patterns were obtained, but no pattern resembling α-rhombohedral boron was ever found.

Hoard (84) points out that β-rhombohedral boron should be produced whenever boron is heated above 1500°C regardless of whether or not fusion occurs.

The density of BN is 2.25 g/cm^3, and α-rhombohedral boron is 2.46 g/cm^3. The densities of eight samples prepared from

Table XXVII.

X-ray Diffraction Patterns for D-12B and $B_{13}P_2$

D-12B			$B_{13}P_2$				
2θ Cu	d	I	I/I_o	d	New	Low	High
22.9	3.720	72	60	3.88			
30.0	2.976	65	60	2.978			
35.0	2.562	124	80	2.569			x
35.7	2.513	390	100	2.522			x
39.9	2.257	5			x		
41.6	2.169	35			x		
42.0	2.149	43	40	2.149			
45.0	2.013	6			x		
46.0	1.971	12	5	1.971			x
46.7	1.943	22	5	1.946			x
47.2	1.924	54	50	1.927			
53.2	1.720	4	5	1.722			
55.9	1.643	52	70	1.645		x	
56.3	1.633	25	20	1.632			
57.5	1.601	16	10	1.607			
58.5	1.576	12	10	1.582			
60.2	1.536	96			x		
61.6	1.5043	78	90	1.509		x	
62.2	1.491	48	50	1.495			
65.7	1.420	48	50	1.426			
66.1	1.412	32	30	1.417			
67.2	1.392	40	50	1.397		x	
68.6	1.374	5			x		
72.0	1.310	73			x		
72.9	1.300	35	60	1.300		x	
73.3	1.290	24	20	1.293			
73.7	1.284	23	30	1.287		x	
75.8	1.254	15	1	1.265			x
77.9	1.225	25	60	1.229		x	
79.8	1.201	6	20	1.205		x	
80.7	1.190	6	20	1.193		x	

amorphous boron (density, 2.35 g/cm^3) and nitrogen gas were all between 2.25 g/cm^3 and 2.35 g/cm^3. No heavier fraction existed. The powders were a dark blue-gray with scattered small white patches.

The possible explanations then are either that the pattern remaining after that of BN is subtracted is either α-rhombohedral boron or a subnitride. If it represents the boron, the third most intense peak has shifted 3.4° (copper radiation), and it is possible that α-rhombohedral boron formed while cooling. If, as the density indicates, it could be a subnitride, the subject should be investigated further to fill in a vacancy in the borostitial family.

C. Preparations and Hot-pressing

The direct reaction of the elements is a suitable technique for the preparation of BP or $B_{13}P_2$. Proper ratios (B to P), times, and temperatures can be determined empirically. The control of phosphorous pressure is essential for high quality products for research or for commercia production where, for instance, selected or maximum hardness values are desired.

Samples of $B_{13}P_2$ composition can be prepared by hot-pressing BP in a mold fully lined with BN and sealed with boron plugs. All hot-pressing information is based on 6000 psi

pressing pressure. Hot-pressing between 2000°C and 2100°C will produce a high density product which can have a total impurity below 0.1%.

One of the limitations in this study was the small size of the samples. A larger sample would have made control over the phosphorous content much easier although thermal lag would have increased.

In pressing samples in unlined molds at 2000°C, a 10 minute hold-time is desirable. Pressing at 2000°C in molds with a one-eighth-inch thick BN sleeve requires at least 30 minutes for densification. This time can be reduced at higher temperatures.

Strong compacts of BP cannot be prepared by hot-pressing unless either partial decomposition takes place or a binding agent is added.

Reaction hot-pressing is a very useful technique for the preparation of $B_{13}P_2$ compacts. Excellent samples were prepared with properties identical to those obtained from hot-pressing BP.

For maximum strength in $B_{13}P_2$ compacts, the percentage of boron carbide should be appreciable. From the data in Figure 42, the carbide binding agent should have the compositions representing compounds in the B-C system.

For control of impurities while hot-pressing boron phosphides, the use of a mold lining of boron nitride (BN) seems best. The suggested maximum working temperature of solid BN in an inert atmosphere is 1650°C. If it is well contained, it is suitable for lining molds to 2100°C. It is essential to bake out graphite and BN parts before using them for hot-pressing. Graphite pieces contribute many volatile carbon and sulfur containing compounds to the sample if these volatiles are not removed first. Pieces of BN can only be hot-pressed if considerable B_2O_3 is added. Samsonov (187) pointed out that the boron anhydride becomes quite volatile from 1100°C to 1300°C and so can also be baked out.

An attempt to use tungsten liners was successful to 1850°C but not above this temperature. Tungsten borides formed readily above 1850°C.

While it would be best to eliminate completely graphite parts from the hot-pressing equipment to prevent contamination, the next best procedure is to isolate them. Carbon can enter a sample by contact or as a gaseous product. Hot-pressing furnaces usually have highly reducing atmospheres. Under these conditions, carbon monoxide is thought to be the source of much of the contamination.

The deviation from the curve as drawn in Figure 10 is for the top sample only. This is probably the combined result of the presence of more phosphorous vapor about a slightly cooler sample. The top samples were usually 35°C cooler than the bottom samples in the same mold. The break from the curve may be indicative of the slight tendency in favor of the formation of the composition $B_{13}P_2$.

Some of the temperatures of preparation and hot-pressing are summarized in Table XIX. These ranges are all approximate and depend on the conditions used in this study. It is also true that the temperature zones shown in Table XIX are functions of composition or of position in a phase diagram.

D. Hardness

The Knoop microhardness measurements shown in Figures 36 through 40 represent thousands of indentations. Each point is the average of 20 to 100 indentations. Every indent was at least five times the narrow diameter from the nearest visible void or other indent. Later etching revealed that a certain percentage of the indents crossed grain boundaries or were within five narrow diameters of grain boundaries particularly at high load. A histogram was constructed for each point and measurement was continued until a regular shape developed.

The microhardness values related to composition, Figure 41, are the peak value, the 100 gram load value, and the 1000 gram load value, respectively. In Figure 42, the peak values are compared to 30 gram load hardness values reported by Samsonov (187) for the boron-carbide system. The measured curve and Samsonov's curve are roughly comparable. It appears that carbon content is a major factor in determining the hardness values in mixed samples.

Sample P-72 is $B_{12}C_3$ and has a much higher peak hardness than sample P-70B which is $B_{13}P_2$. Samples P-30B and P-15B have almost the same carbon content, and again the sample with the higher phosphorous (P-15) content has a lower peak hardness. This difference in hardness, however, may just as logically be assigned to sample P-30B falling on the extra hard composition of $B_{12}C$, with sample P-15B having just enough more carbon to miss that composition.

By coincidence, graphing peak hardness as a function of phosphorous content produces a very straight line between the values of P-72 and P-70B. This can only be coincidence, however, and does not reflect the effect of phosphorous except at the compounds at the ends of the line.

In the first four hardness curves, Figures 36 through 39, there is a decrease or fall-off in hardness at loads below the load value associated with the peak hardness. This decrease has

has been attributed by Grodzinki (69) to the elastic recovery of the indentation at low loads. He has shown that by changing the definition of hardness from load needed to produce an area of indent to that load needed to produce a constant indent, this low load fall-off is eliminated. Since this region of the curve depends on elastic behavior, $B_{13}P_2$ is more elastic than $B_{12}C_3$. The curve for $B_{12}C_3$ showed no fall-off at all.

Grodzinski's theory called for a linear fall-off from peak hardness to zero load as a result of the elastic effect. In P-70B (Figure 36) and P-15 (Figure 37), the low load fall-off flattens out. These are the two samples with highest phosphorous content. The flattening out at low loads indicates that pure elastic behavior is being supplemented by plastic flow. A possible cause of this effect might be the collection of free phosphorous in the grain boundaries. Such a build-up would act as a lubricant and enhance plastic flow by movement of particles at very low loads.

The hardness seems to approach a constant value at the other end of these curves. These high load values of hardness for such brittle materials must be examined carefully.

In samples P-15 and P-30B, some cracks were noted about indents made with a 1000 gram load. At the same load, many more cracks were seen for sample P-70B. The fourth sample, P-57B,

even had a large number of cracks around indents made with a 400 gram load. The remaining sample, P-72, had extensive cracking around indents made with 200 gram loads, 400 gram loads, and 1000 gram loads.

The more cracking seen in a sample, the lower the hardness for that sample at 1000 gram load. The 100 gram load values also were a function of the extent of cracking except for the value of P-72. An examination of Figure 43 shows how closely the 100 gram values follow the 1000 gram values. This may indicate that the extent of cracking is greater than seen in the microscope.

Griffith cracks were thought to exist naturally in materials, but Stroh (213)(214) has shown how a pile-up of dislocations caused by plastic flow can initiate a crack. This would probably happen at loads just above the peak load. Fracture should, therefore, be considered as part of every property measurement for these brittle materials when plastic flow is extensive.

E. Thermoelectric Evaluation

Measurements of the thermoelectric value of boron subphosphide have indicated (19)(45) that it might have exceptional properties as a thermoelectric material. To evaluate compositions, the thermal conductivity, thermoelectric power, and

electrical conductivity must be considered separately. Then they must be combined in the figure of merit in which a low thermal conductivity and high values of thermoelectric power and electrical conductivity are desired.

A comparison of the thermal conductivity curves shows that a sample of $B_{12}C_3$ (P-54, Figure 49) has the highest set of values. The lowest curve is of $B_{13}P_2$ (P-70B, Figure 46). The values for P-22B, Figure 50, are midway between these.

Sample P-67B (Figure 45) is very low in carbon. It has a very low thermal conductivity, but it has half the phosphorous content of the $B_{13}P_2$ sample.

The remaining three samples have curves that lie in the middle. The two highest (P-55 and P-43) have lower carbon and higher phosphorous content than the third (P-28A) which has relatively low thermal conductivity. Based on the pure samples, carbide content rather than phosphide content seems to indicate higher thermal conductivity. In these three mixed samples, this is not necessarily true. This change is not unexpected if one considers the many structural factors that can be as effective as composition in modifying thermal conductivity.

The effect of carbon content alone on thermoelectric power was determined by Samsonov (187) whose results are represented in Figure 58. The measured values (Figure 59) follow a

similar path. An examination of the phosphorous values printed next to each point shows that the thermoelectric power is also an inverse function of phosphorous content. In both the carbon and phosphorous comparisons, the samples with very low carbon content seem to be slightly out of place. A comparison of complete curves leaves no doubt, however, about the trends. High carbon content (above 20%) and probably high phosphorous content (above 30%) appear to reduce thermoelectric power considerably. Below these compositions, a low carbon, moderate phosphorous (10 to 20%) content sample will have a good thermoelectric power.

The thermoelectric figure of merit (Z) as reproduced in this equation is:

$$Z = \frac{\alpha^2 \sigma}{K} \qquad (16)$$

The thermal conductivity (K) for these samples can be modified about one order of magnitude at best. The thermoelectric power (α) can be changed by a factor of 2 to 5. If one is speaking in nundreds of microvolts, this is still only a six-fold improvement in spite of the square term in the expression (16).

The electrical conductivity at high temperatures, on the other hand, has a range of at least seven orders of magnitude in this study. It is, therefore, more important to select a

sample for thermoelectric application by its electrical conductivity than by either of the other two properties.

An examination of the figure of merit values presented in Figure 72 indicates that the composition $B_{12}C_3$ (P-54 and P-72) is best for thermoelectric use in the temperature range investigated (400°K to 850°K). The poorest sample (P-70B) in this range had the composition $B_{13}P_2$.

The figure of merit curve usually starts out with a slow increase, then increases sharply, and finally finishes with another slow increase. In spite of the straightening effect of the logarithmic scale, the sharp increase of the top (P-54 and P-72) curve is apparent. The mixed composition samples (P-43 and P-27A), the BP sample (P-22B), and the pure phosphide samples (P-70B and P-67B) do not yet indicate an upturn. For this reason, a useful zone at high temperature is possible for the four low samples.

Boron carbide ($B_{12}C_3$) appears to be a good thermoelectric material above 700°K. Boron phosphide ($B_{13}P_2$) in the pure form (P-70B) is poor. If 3% carbon is added to this sample, the high conductivity of P-64B (Figure 61) results. The extrinsic conductivity of P-64B and the K and α of P-70B would indicate that a figure of merit of 10^{-4} is possible for an impure boron subphosphide.

Except for those of the boron carbide sample, these figures are not too impressive until two factors are considered. In the first place, the electrical conductivity should be easily increased several orders of magnitude by suitable additions of impurities without a proportionate change in K and α. In the second place, the phosphide can be used to 1200°C or more and the carbide to perhaps 1800°C.

It would seem that excellent p-type thermoelectric materials with a boron carbide base could be made for use from 500°C to 1800°C. Probably good p-type thermoelectric materials for use from 500°C to 1200°C might be made with a boron phosphide base.

The figure of merit values reported for this study do not support those previously obtained (19)(45). This is because of the effect of surface moisture as seen in Figures 44 and 51. Samples preheated in vacuum gave reproducible results.

F. Conduction Mechanism The low potential obtained from the measurement of Hall coefficients indicates that these samples are compensated mixed conductors. If the formula,

$$\sigma = ne\mu \qquad (19)$$

is applied to sample P-70B, the purest $B_{13}P_2$ specimen, a total room temperature impurity concentration of $n = 4 \times 10^{14}$ car/cm^3

To calculate this requires the assumption of a mobility figure. An assumed mobility of 1 cm^2/vs would be in keeping with Shaw's (481) measured values for boron. Applying the same method to samples P-64B and P-56 for which Hall potentials were determined, produces total carrier concentrations of 5×10^{19} car/cm^3 and 7×10^{19} car/cm^3, respectively. These are the impure samples with the highest electrical conductivities of the compacts containing phosphorous. The magnitude of the Hall potential in $B_{13}P_2$ is approximately the same as that reported for boron.

The sign of the thermoelectric power and the sign of the Hall potential both indicate that boron subphosphide samples are p-type above 375°K. An element such as boron with a Group IV (C) or Group V (P) impurity would be expected to be n-type; yet boron and all of the borostitials are p-type at high temperature.

A surface effect might also account for the p-type conductivity through the mechanism of a p-type inversion layer on the surface. A similar p-type layer is reported by Dunlap (41) to be produced on n-type germanium by exposure to oxygen, ozone, or hydrogen peroxide.

A surface layer on a fine grained polycrystalline conductor could create a high impedance barrier between particles. If the particles were of high conductivity and if each particle were surrounded by a surface of altered composition, charge carrier passage could be impeded.

The concept of a p-type layer on an n-type crystalline particle is compatible with observations. Such a distribution would create p-n junctions around every particle. These surface p-n junctions have both the property of readily creating rectifying contacts with attached leads and also of creating insulating barriers between particles. Rectification at attached wire contacts was observed frequently during experiments.

Abeles (1) compared the resistivity of single crystalline and polycrystalline materials with the same concentration of impurity centers. The resistivity of the polycrystalline material was higher with increased boundary content because of the grain wall barrier action. Abeles pointed out that where resistance between grains is high, electrical resistance falls off rapidly as one increases the ac frequency. This is caused by a capacitive shorting effect at high frequencies.

Lagrenaudie (125) measured the conductivity of fused blocks of boron and AlB_{12} and obtained a similar response to frequency. He concluded that the central part of the crystal was more conductive than the intergranular part, particularly at low temperatures.

The high conductivity in the interior of the particle might be enhanced by conjugation through the crystal. The mobility of charge carriers would be markedly affected by both

conjugation and a high impedance surface layer. Mobility would be much greater within a well-formed crystal and the mean free path could extend to particle dimensions. The high impedance surface layer would be expected to limit strongly mobility by limiting mean free paths. Unless the two paths contributing to mobility can be separated, any estimate of mobility based on conductivity and Hall data is meaningless. Any great reduction in the mobility of a surface layer would also cause a corresponding increase in the concentration of impurity sites in the surface.

Etching experiments provide further evidence of a thick particle surface with properties different from those of the bulk crystals. High purity etching studies with CdTe revealed the difference in reactivity of p-type and n-type material. In the boron subphosphide compacts, as wide grain boundary or surface layers were removed by etching, well-developed crystalline cores were untouched.

The small negative magnetoresistance value obtained for boron subphosphide probably indicates a high level of inhomogeneity in the sample. Carmichael (24) has also obtained a reverse (negative) magnetoresistance effect in vacuum fused polycrystalline boron prepared from zone refined material. He

also reports a charge storage effect which is produced if conducting particles are separated by an insulating layer.

The gradually changing electrical conductivity curves obtained in this study and reported so frequently in the literature for boron and its derivatives are not uncommon. Such a curve represents an energy system of progressively changing barriers. As temperature is increased, more and more charge flows because it gradually becomes more plentiful or because it is more free to move as conductivity paths become more passable.

If the gradual change in conductivity were a function of the availability of charge carriers, a great many closely spaced extrinsic energy levels would be required. The concept of tunneling through a barrier might also explain enhanced movement with increased temperature. Higher temperatures would give the charge carriers an increased probability of barrier penetration.

Another way of looking at this is to consider the Arrhenius equation for activation energy:

$$\sigma = Ae^{\frac{-\Delta E}{kT}} \tag{20}$$

$$\ln\sigma = \frac{-\Delta E}{kT} + \text{constant} \tag{21}$$

In most semiconductor materials, the logarithm of the conductivity (σ) is a straight line function for particular activation energies (ΔE). In this case, A is a constant. If instead, A is a function

of temperature, a curved line results. The problem then is to determine if A is a function of temperature because of many extrinsic energy levels or because of a thermal enhanced penetration of a barrier to conduction between regions of high conductivity.

Shaw (198) stated that the gradual change in the conductivity curve for boron was due to Joule heating. This is a way of saying that the constant (A) in the Arrhenius equation is a function of temperature. Shaw suggested that heating introduced imperfections capable of contributing charge carriers.

Among the suggestions made to account for the sign change in boron, was the double-conduction-band theory mentioned by Putley (170). Another concept, proposed by Shaw (198), was that acceptor and donor levels alternately contributed carriers in increasing numbers. A third mechanism, suggested by Rupprecht (182) to account for sign change, is that of a surface effect. Sign change could be induced by chemically or mechanically treating the surface or by an anneal in an appropriate atmosphere. A surface mechanism is readily associated with a polycrystalline sample. A surface effect and a double-conduction-band theory might be adequate for explaining a single change of sign but not for a triple change. Shaw's (198) proposal is the most probable one because multiple impurities and phases are known

to be present. A single impurity in two similar phases of different composition might produce two closely spaced energy levels just as two different impurities might do so in one matrix.

At the high temperature end of the conductivity curves, a common intrinsic slope should be approached for samples of the same material. That this does not seem to happen with these samples indicates that several intrinsic slopes exist. The intrinsic activation energies listed in Table XXV are probably low since measurements to over 1000°K are needed to establish accurate slopes. The spread in the activation energies reported in Table VI emphasizes the difficulty in determining this slope. The difficulty is twofold. These curves are almost all gradually changing curves rather than joined straight segments. Electrically they represent a number of different compounds, not boron with impurities. At concentrations below those needed for compound formation, as the impurities are reduced, the properties approach those of pure boron.

A low temperature (150°K to 300°K) comparison of the electrical conductivity curves indicates three groups of curves. The group of four samples with the lowest conductivity consists of P-70B, P-67B, P-66B, and P-62B. The first three were made from ultrapure material. The fourth, P-62B, was made from low carbon material. Only P-70B has a phosphorous content equivalent to $B_{13}P_2$. The others have half this amount.

Two samples in the highest conductivity group are the $B_{13}C_2$ sample (P-71B) and the $B_{12}C_3$ sample (P-72). The two remaining samples in the highest conductivity group were expected to be in the very pure, low conductivity group. Apparently, the mold lining for sample P-64B cracked because its carbon content is 3.3%. Carbon or whatever else was picked up produced a straight extrinsic conductivity plot probably indicating a very high impurity concentration. This sample is essentially $B_{13}P_2$.

No obvious explanation exists for the high conductivity of sample P-56 (Figure 62). Emission spectroscopy indicates that it has a high manganese and silicon content, but sample P-62B also has these and is a low conductivity specimen. According to Figure 35, the 27.5% phosphorous content of sample P-56 falls on a eutectic composition. This could mean greater crystallization or grain growth and thus a higher conductivity.

The changes of sign of the Hall potential can best be accounted for by several extrinsic activation energy levels. Such a mechanism is proposed in Figure 76. The four extrinsic levels are shown in separate phases because of the probability of a surface layer of opposite sign from that of the bulk.

As temperature is increased, the extrinsic levels shown in Figure 76 first release electrons and then a slightly greater number of holes. This cycle takes place a second time. The

Band Picture

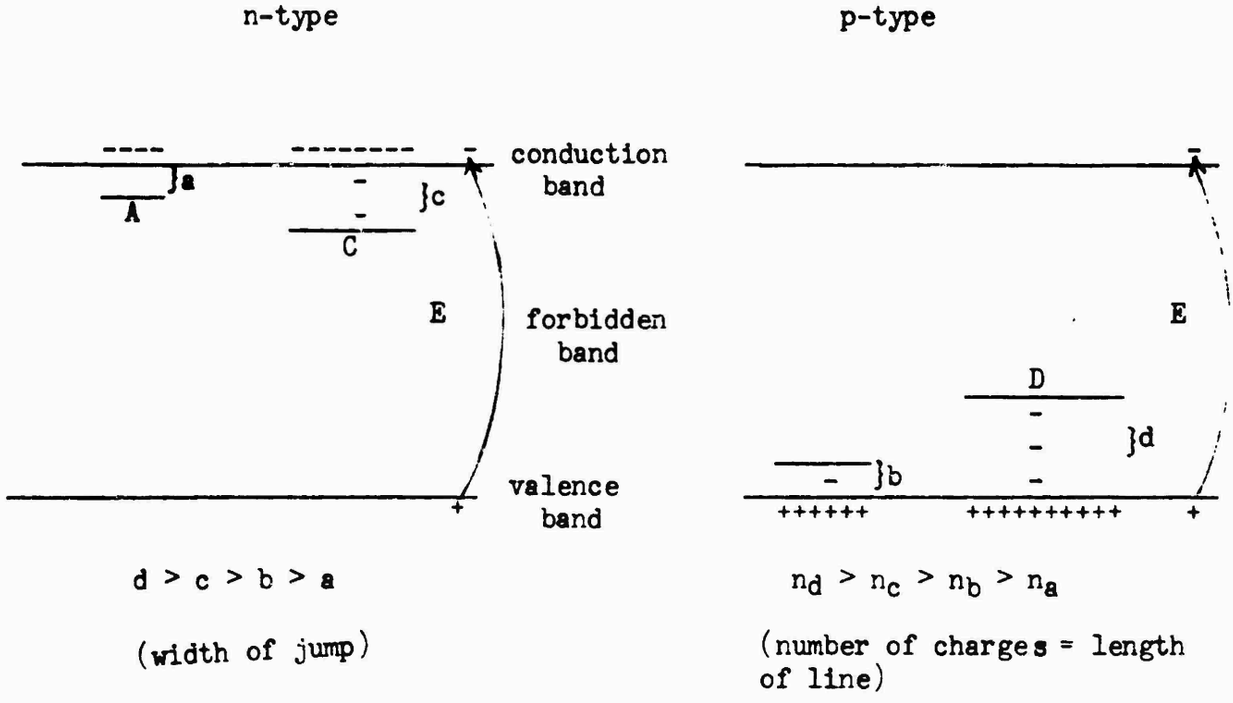

Sign Change

sign	−	→	+	→	−	→	+
conducting	A		A B		A B C		A B C D E

→ increasing temperature

Figure 76. Proposed Band Picture and Mechanism of Sign Change

third change of sign (P-6LB) occurs at the exhaustion point of the extrinsic portion of the conductivity curve. The p-type high temperature conductivity may be determined not only by the filling of the D level, but it may be augmented by having $\mu_h > \mu_e$. Throughout all of these changes, n_e and n_h remain almost the same.

The conductivity changes produced by the levels extrinsic to the material are probably further modified by a preparation-induced surface layer.

Speculation as to the nature of such a surface layer leads to a number of possibilities. Phosphorous is clearly present around the grains and in escape paths which can be seen with the aid of a microscope. Freshly fractured surfaces smell like phosphorous as do polished and ground surfaces. The thermoelectric potentials supplemented by electrochemical potentials is another possible indication of the existence of phosphorous between particles.

Phosphorous could also combine with an impurity such as silicon to produce a highly p-type material, phosphorous doped silicon. Reactions competing with the formation of such a layer would be the oxidation of phosphorous and the formation of a silicon boride. Giessen (58) has shown that phosphorous is soluble in silicon to only 1.3% by weight at 1250°C. This solubility decreases rapidly with temperature. If one thinks of compounds

instead of solubility, SiP, Si_5P_2, and Si_3P_4 might be formed. The compound SiP hydrolyzes readily and could account for the anomalous thermoelectric potentials.

Other impurity elements beside silicon could behave in a similar manner to promote a p-type layer.

In the decomposition of a crystalline grain, a concentration gradient is likely to be created. Such a gradient would exist both in phosphorous content and in defect content. A high concentration of defects at the surface would, according to Abeles (2), increase the resistance.

A situation paralleling that in organic semiconductors exists. Grains in this case are similar to the giant molecules of organic semiconductors. According to Clark (28) and Hoard (86), conjugation is possible in the crystal containing the boron lattice. Complete occupation of the three central sites would aid conductivity along conjugate paths. Vacancies would interrupt paths and reduce conductivity. The grain boundaries with the adjacent surface layer full of defects would then correspond to the jump distance between organic molecules. Many organic semiconductors do have curved line conductivity plots rather than straight ones.

Absorption measurements by Gaule (56) indicated that crystalline boron can accommodate a large concentration of gaseous impurities. Using unpublished results of experiments by Medcalf, Gaule showed that oxygen and nitrogen on the surface increased resistivity by 200% while hydrogen reduced it by 35%. This was also reported by Starks (206) who found that bars of boron heated in hydrogen at 1200°C had resistivities as low as 100 ohm cm at RT. The same figure increased to 10 megohms when the bars were heated in oxygen. Turovtseva (226) determined the gas content in powdered boron. He reported 0.09 to 0.25% hydrogen by weight, 0.21 to 1.04% oxygen by weight, and 0.011 to 0.08% nitrogen by weight. In the less carefully protected samples, carbon monoxide was thought to be responsible for much of the increase in carbon content. Thus one can consider a dynamic oxygen balance. Oxygen could be available from the boron starting material and carbon monoxide. Phosphorous and boron would compete for it. Oxygen then would form a boron suboxide or a layer of B_2O_3. The B_2O_3, according to Samsonov (187) is volatile between 1100°C and 1300°C.

Nitrogen and hydrogen could presumably be accommodated in the B_{12} lattice, but at the temperatures involved in hot-pressing, any impurity compounds might decompose. The boron suboxide, for instance, decomposes above 1750°C, according to Rizzo (175).

Gaseous impurities would be removed from the area around the sample by the helium flow or by the excess of phosphorous vapor.

Conductivity below 400°K depends on the effects of several extrinsic levels located close to the conduction and valence bands. The alternate release of extrinsic carriers is probably modified by a high impedance layer on the surface of the particles. Such a layer can be caused by a concentration of defects or impurities around the high conductivity particle cores and affects the conductivity curve at both high and low temperatures. A surface layer can cause a curved conductivity plot by the requiring of different energies for penetration of the barrier or by the providing of a disordered layer packed with many very close surface energy states. In either case, a surface layer probably exists.

If boron could be prepared with narrow grain boundaries and highly ordered regions on either side, straight line conductivity plots would be expected. A similar preparation with volatile interstitial elements in the borostitials would be many times more difficult to prepare. However, boron with almost straight line paths has been prepared by Eubank (47) from ultrapure samples that were vacuum hot-pressed.

One can only speculate on the nature of the extrinsic levels shown in Figure 76. The impurities detected by emission spectroscopy could account for them. Unknown surface states

from absorption or defects could also explain these levels and finally, natural phases from the phase diagram could act as impurities in the bulk material.

G. Properties of $B_{13}P_2$

The properties of the best sample of $B_{13}P_2$ are summarized in Table XXVIII. Values of BP, $B_{13}C_2$, and $B_{12}C_3$ are included for comparison.

A comparison of $B_{13}P_2$ and $B_{13}C_2$ reveals that the phosphide has a much lower electrical conductivity and about one third the thermal conductivity. The phosphide is not as hard as the carbide and exhibits slightly more elastic and plastic deformation. The thermoelectric power of the phosphide is higher as is its density.

Properties of the compacts produced in the boron-phosphorous-carbon system do not follow the same pattern. Hardness values appear to be determined mostly by the phases of the boron-carbon phase diagram with phosphorous content exerting a secondary influence.

Thermoelectric power depends on both phosphorous and carbon content apparently falling rapidly if either content becomes high. A wide range of composition with high thermoelectric power appears to exist.

Table XXVIII.

Summary of the Propertie. of $B_{13}P_2$

Property		$B_{13}P_2$ P-70B	BP(90%) P-22B	$B_{13}C_2$ P-71B	$B_{12}C_3$ P-72,P-54
Density g/cm^3		2.74	2.98	2.54	2.54
Electrical conductivity					
$ohm^{-1}\,cm^{-1}$	RT	6×10^{-5}	1.8×10^{-3}	3.3	3.3
	800°K	5×10^{-2}	0.8	100	4×10^{4}
Figure of merit					
$\frac{1}{°K}$	400°K	5×10^{-10}	5×10^{-7}	-	above 10^{-3}
	800°K	10^{-6}	5×10^{-6}	-	10^{-6}
Grain size microns		3-40	1-13	5-7	13-30
Knoop hardness					
kg/mm^2	peak	4795	-	-	7456
	30 g m	3700	-	-	4000
	100 g m	2720	-	-	2934
Thermal conductivity cal/cm°C sec					
	400°K	0.049	(0.047)	-	(0.15)
	800°K	0.028	(0.048)	-	0.07
Thermoelectric power					
µv/°C	400°K	210	(60)	-	68
	800°K	328	283	-	155

Thermal conductivity values probably increase with carbide content and decrease with phosphide content, but this is difficult to establish. Structure effects tend to obscure composition effects.

Electrical conductivity in the boron-phosphorous-carbon system is so complex that little can be said about it. Carbide content appears to increase it while phosphide content appears to decrease it. Bulk composition effects, however, may be obscured by general impurity effects.

H. Further Investigations

Any further investigation of the boron-phosphorous system should begin with the construction of a high temperature furnace and a hot-press. This unit or these units should be capable of subjecting a sample to vacuum before pressing and capable of maintaining a desired pressure of phosphorous while pressing or reacting.

Impurity control would be greatly aided if graphite were not needed inside the preparation unit and if higher purity boron nitride parts could be obtained.

Test equipment (K, α, σ) capable of extremely high temperature is needed to evaluate properly the thermoelectric properties of these compacts.

A phase diagram study of the boron-phosphorous system using Cohen's method and carefully analyzed samples should confirm the presence of other compounds besides $B_{13}P_2$. If, as indicated, other compounds exist, these should be prepared in pure form and their X-ray properties determined.

To evaluate the indications of a surface effect, samples should be first checked for a photo effect at p-n junctions. The electrical conductivity should then be determined for samples in various atmospheres (e.g., oxygen, vacuum, etc.) and at various frequencies.

Reaction hot-pressing is recommended for future sample preparation in the boron-phosphorous system.

Any equipment improvement made to facilitate the study of probable new phases such as $B_{10}P$ would also be suitable for the investigation of new borostitials, in particular, the possible existence of a boron subnitride. The untouched borostitials such as those containing germanium, selenium, and heavier elements should also be the subject of research.

VI. SUMMARY AND CONCLUSIONS

Hot-pressing BP produces a decomposition product, boron subphosphide, with a preferred composition of $B_{13}P_2$. Since this is an interstitial compound, a wide range of phosphorous content is possible. Preparation between 2000°C and 2100°C produces the best results. The same material can be prepared by reaction hot-pressing the elements.

Addition of carbon will produce preferred compositions such as $B_{13}C_2$ and $B_{12}C$, but a wide range of carbon content is also possible. The compound reported as B_4C or $B_{12}C_3$ melts peritectically. A solid solution range exists about each of the congruently melting compounds mentioned in the B-P-C system. Fine grained, very hard, strong compacts can be prepared from compositions in the B-$B_{13}P_2$-$B_{13}C_2$ system. These have high thermoelectric power, moderate thermal conductivity, and an electrical conductivity ranging from 10^{-5} $ohm^{-1}cm^{-1}$ up to semi-metallic behavior.

The compound BP can be hot-pressed, but bonding is poor without particle decomposition or the addition of a binding agent. A sample prepared with 10% decomposition had thermal and electrical properties midway between those of $B_{13}P_2$ and $B_{13}C_2$.

By taking special precautions, pure $B_{13}P_2$ can be prepared with total impurities below 0.1% by weight. This material has the proper boron to phosphorous ratio by analysis. The solid solution range around this compound is from 26.5 to 34% phosphorous. The compound has a density of 2.74 g/cm^3 and, under the conditions of hot-pressing, usually retains the grain size (1-14 microns) of the starting material (BP). The pure material has a thermal conductivity of 0.049 cal/cm °C sec at 400°K and a thermoelectric power of 210 μv/°C at 400°K. The electrical conductivity of the pure material at room temperature is low, 6×10^{-5} ohm^{-1}cm^{-1}.

The peak hardness of $B_{12}C_3$ (7456 kg/mm^2) is much higher than the peak hardness of $B_{13}P_2$ (4795 kg/mm^2). On the other hand, $B_{13}P_2$ has a slightly better resistance to fracture as seen by comparison of the 1000 gram load values. The $B_{13}P_2$ also has more elastic and plastic deformation at very low loads. The hardness vs. load curves were analyzed and the meaning of the various features was explained.

The $B_{12}C_3$ compact is more suitable for use as a thermoelectric generator than $B_{13}P_2$ in the temperature range from 400°K to 850°K. Mixed phosphide-carbide compacts are also less effective than the pure carbide. Good performance at temperatures above 850°K is likely even for the $B_{13}P_2$.

Measurements of electrical conductivity and Hall effect establish that a very small Hall potential changes sign three times before the materials become p-type even though they might be expected to be n-type. These effects with that of a non-linear thermal response of the electrical conductivity are explained on the basis of a dual conduction picture. Mixed conduction depends on the contribution of a number of extrinsic energy levels for charge carriers. The movement of these is probably hindered by a surface layer of opposite sign to that of the bulk material.

The existence of the phase $B_{10}P$ is sufficiently well established in the boron-phosphorous system to warrant further study. It probably exists with a solid solution range from 20 to 26.5% phosphorous.

While no boron subnitride has been shown to exist, the experimental observations require further study before they can be explained.

From this study, the following may be concluded:

1. The composition $B_{13}P_2$ is not as good a thermo-element as $B_{13}C_2$ which appears to be worthy of further investigation as a high temperature thermoelectric material.

2. The conduction mechanism in $B_{13}P_2$ is of mixed polarity and probably involves a surface inversion effect and multiple extrinsic levels. The electrical conductivity of pure $B_{13}P_2$ is four to seven orders of magnitude below that of $B_{13}C_2$ from 190°K to 1000°K.
3. The hardness of $B_{13}P_2$ at low loads is only slightly less than that of $B_{13}C_2$. An entire series of compositions with a wide range of hardness values can be produced in the B-P-C system. An even greater range should be possible in the borostitial family leading to a family of hard abrasives.
4. Although carbon is the major impurity in the boron subphosphide samples, pure $B_{13}P_2$ powders and theoretical density compacts of high purity can be prepared.

VII. BIBLIOGRAPHY

1. Abeles, F., "Resistivity and Thermoelectric Power of Metals Containing Grain Boundaries," Journal de Physique et le Radium, 16 (7), 34-35 (1955).

2. "Additional Electrical Resistance and Thermoelectric Power Caused by Lattice Defects in Metals," 237, 796-798 (1953).

3. Accary, A. and Caillat, R., "Study of Mechanism of Reaction Hot Pressing," J. Am. Ceram. Soc., 45 (7), 347-351 (1962).

4. Adamsky, R. F., "Unit Cell and Space Group of SiB_6," Acta. Cryst., 11, 744-745 (1958).

5. Adamsky, R. F. and Cline, C. F. (Carborundum Company), Hard, Refractory Crystalline Material, Germ. Pat. 1,115,634, October 19, 1961 (U. S. Appl. December 29, 1958).

6. Aftergut, S. and Brown, G. P., "Electronic Properties of Organic Compounds," in Organic Semiconductors, pp. 79-99, edited by J. J. Brophy and J. W. Buttrey, Macmillan Company, New York, 1962, 243 pp.

7. Allen, R. D., "The Solid Solution Series, Boron-Boron Carbide," J. Am. Chem. Soc., 75, 3582-3583 (1953).

8. Atoda, T., Boron Carbide, Japanese Pat. 13,910, August 21, 1961.

9. Austin, J. B., "Factors Influencing the Thermal Conductivity of Non-Metallic Materials," in Symposium on Thermal Insulating Materials, pp. 3-67, ASTM, Philadelphia, 1939, 123 pp.

10. Badar, L. J. and Jacobsmeyer, V. P., "Some Electrical Characteristics of Polycrystalline Boron," Phys. Rev., 94, 808 (1956).

11. Bean, K. E.; Starks, R. J.; and Medcalf, W. E., "Research Investigations in the Physical Chemistry and Metallurgy of Semiconducting Materials," Eagle-Picher Research Laboratory, Quarterly Report No. 5, 1961, Contract No. DA 36-039-SC-85131, ASTIA AD No. 264 303.

12. Becher, H. J., "Preparation and Structure of an Aluminum Beryllium Boride," Z. Anorg. Allgem. Chem., 317 (5-6), 346-352 (1962).

13. Best, P. and Twigg, S. R., "The Fabrication of Boron by Powder Metallurgical Techniques," Metallurgia, 62, 146-152 (1960).

14. Bonfiglioli, G. and Malvano, R., "Further Experiments on Surface Conductivity of Metallic Thin Films," Instituto Electrotechnico Nazionale Galileo Ferraris, Technical Note No. 5, Contract No. AF 61(052)-328, July 1961, ASTIA AD No. 266 537.

15. Bredt, J. H., "Thermopile Generator Feasibility Study, Part II Materials Investigation," General Electric Company, Final Report, August 1960, Contract No. AF 33(616)-5281, ASTIA Ad No. 265 599.

16. Briggs, C., "Heat Conduction in Solids, A Bibliography 1958-1962," The Martin Company, Literature Search No. 22, Denver, ASTIA AD No. 293 822.

17. Brosset, C. and Magnusson, B., "The Silicon-Boron System," Nature, 187, 54-55 (1960).

18. Bruzs, B., "The Theory of Thermoelectricity," Z. Electrochem., 38, 777-779 (1932).

19. Buchanan, R. C., Thermoelectric Measurements of Hot-Pressed and Simple Crystal Samples of Bismuth and Cadmium Tellurides and Selenides, Bachelor of Science Glass Technology Thesis, Alfred University, Alfred, N. Y., June 5, 1960.

20. Callen, H. B., "Thermoelectric and Thermomagnetic Effects," Natl. Bur. Standards (US), Circ. No. 524, 131-141 (1953).

21. "The Application of Onsager's Reciprocal Relations to Thermoelectric, Thermomagnetic, and Galvanomagnetic Effects," Phys. Rev., 73, 1349-1358 (1948).

22. Campbell, I. E., High Temperature Technology, John Wiley and Sons, Inc., New York, 1956, p. 526.

23. Canon, J. R. and Duffey, G. H., "Cuboctahedral Bonding," J. Chem. Phys., 35, 1657-1660 (1961).

24. Carmichael, C. H. and Dore, M., "Electrical Effects Observed in Polycrystalline Boron," Nature, 191, 485-486 (1961).

25. Caspari, M. E., "Investigation of Physical Properties of Semiconductors," University of Pennsylvania, April 1960, ASTIA AD No. 283 273.

26. Chasmar, R. P. and Stratton, R., "The Thermoelectric Figure of Merit and Its Relation to Thermoelectric Generators," J. Electronics and Control, 7 (1), 52-72 (1959).

27. Chretien, A. and Laveant, P., "The Borides of Gallium, the Boride GaB_{12}," Compt. Rend., 252, 134-135 (1961).

28. Clark, H. K. and Hoard, J. L., "The Crystal Structure of B_4C," J. Am. Chem. Soc., 65, 2115-2119 (1943).

29. Clawson, A. R.; Knorr, B.; and Wider, H. H., "Bibliography on the Hall Effect," Naval Ordnance Laboratory, Corona, California, Navweps Report 7233, September 1, 1962, ASTIA AD No. 283 808.

30. Cline, C. F., "The Compound SiB_6," J. Electrochem. Soc., 106, 322-325 (1959).

31. "Preliminary Investigations of the Silicon Boride, SiB_6," Nature, 181, 476-477 (1958).

32. Cohen, M. U., "Precision Lattice Constants from X-ray Powder Photographs," Rev. of Scientific Instruments, 6 (3), 68 (1935).

33. Colton, E., "Hexaboron Silicide: Promising Material in Nuclear Control Devices," Ceram. Ind., 76 (3), 70-71 (1961).

34. "Two Boron Silicides," Materials in Design Eng., 53, (6), 9-10 (1961).

35. "Preparation of B_4Si," J. Am. Chem. Soc., 84 (4), 1002 (1960).

36. Cotter, P. G., "Microhardness of Aluminum Boride Monocrystals," Am. Mineralogist, 43, 781-784 (1958).

37. Decker, B. F. and Kasper, J. S., "The Crystal Structure of a Simple Rhombohedral Form of Boron," Acta. Cryst., 12, 503-506 (1959).

38. DeGroot, S. R., Thermodynamics of Irreversible Processes, North-Holland Publishing Company, Amsterdam, 1952, 510 pp.

39. Domenicali, C. A., "Irreversible Thermodynamics of Thermoelectricity," Rev. Mod. Phys., 26, 237-275 (1954).

40. Drabble, J. R. and Goldsmid, H. J., Thermal Conduction in Semiconductors, Pergamon Press, New York, 1961, 233 pp.

41. Dunlap, W. C., An Introduction to Semiconductors, John Wiley and Sons, Inc., New York, 1957, 417 pp.

42. Ehrenberg, W., Electric Conduction in Semiconductors and Metals, Oxford University Press, Clarendon, 1958, 389 pp.

43. Engelke, J. L.; Halden, F. A.; and Farley, E. P., "Synthesis of New High Temperature Materials," Stanford Research Institute, WADC Tech. Rept., 59-654, February 1960.

44. Epelbaum, V. A.; Gurevich, M. A.; and Ormont, B. F., "Phase Composition of the Boron-Carbon System," Zhur. Neorg. Khim., 1, 2149-2154 (1956).

45. Erikson, C. V., Thermoelectric Properties of Hot Pressed Boron Phosphide, Bachelor of Science Ceramic Engineering Thesis, Alfred University, Alfred, N. Y., June 1961.

46. Esposito, R. J. and Gottlieb, A. D., "Bibliography of the III-V Semiconductors," Frankford Arsenal, Memo Rept. No. M61-10-1, Contract No. TS 4-4024 and 50201008, ASTIA AD No. 253 604.

47. Eubank, W. R.; Pruitt, I.E.; and Thurnaur, H., "Observations on Boron and Some Borides," in Boron, Synthesis, Structure and Properties, edited by J. A. Kohn, W. F. Nye, and G. K. Gaule, Plenum Press, Inc., New York, 1960, 189 pp.

48. Feigelson, R. S., "Some Physical Properties of Polycrystalline Silicon Boride," Watertown Arsenal Laboratories, Report No. WAL TR 853/1, May 1962, ASTIA AD no. 277 686.

49. Feigelson, R. S. and Kingery, W. D., "Physical Properties of Polycrystalline Silicon Borides," Am. Ceram. Soc. Bull., 42 (11), 688-693 (1963).

50. Finn, J. M.; Jr., Nelson, E.M.; and Mercuri, R. A., Union Carbide Company, High Purity Finely Powdered Boron, Brit. Pat. 857,060, December 29, 1960.

51. Formstecher, M. and Ryskevic, E., "Preparation of Boron Carbide in the Gaseous Phase," Compt. Rend., 221, 558-560 (1945).

52. Fredericks, W. J., Keneshea, F. J.; and Craigg, F., "A Bibliography of Group III-V Compounds, Vol. III," Stanford Research Institute, ASTIA AD No. 294 727.

53. Frederikse, H. P. R.; Hosler, W. R.; and Roberts, D. E., "Electrical Conduction in Magnesium Stannide at Low Temperatures," Phys. Rev., 103, 67-72 (1956).

54. Friedrich, L. W. and Jacobsmeyer, V. P., "Some Electrical Properties of Elementary Boron," Phys. Rev., 91, 492 (1953).

55. Garrett, C. G. B., "Organic Semiconductors," in Semiconductors, pp. 634-675, edited by N. B. Hannay, Reinhold Publishing Corp., New York, 1959, 767 pp.

56. Gaule, G. K., and others, "Optical and Electrical Properties of Boron and Potential Applications," in Boron, Synthesis, Structure, and Properties, pp. 159-174, edited by J. A. Kohn, W. F. Nye, and G. K. Gaule, Plenum Press, Inc., New York, 1960, 189 pp.

57. Giardini, A. A., and others, "Vector Hardness Properties of Boron and Aluminum Borides," in Boron, Synthesis, Structure and Properties, pp. 140-158, edited by J. A. Kohn, W. F. Nye, and G. K. Gaule, Plenum Press, New York, 1960, 189 pp.

58. Giessen, B. and Vogel, R., "The System Si-P," Z. Metallk., 50, 274-277 (1959).

59. Glaser, F. W.; Moskowitz, D.; and Post, B., "An Investigation of Boron Carbide," J. Appl. Phys., 24, 731-733 (1953).

60. Granville, J. W. and Hogarth, C. A., "A Study of Thermoelectric Effects at the Surfaces of Transistor Materials," Proc. Phys. Soc. (London), 64B, 488-494 (1951).

61. Gray, T. J., The Defect Solid State, Interscience Publishers, Inc., New York, 1957, 511 pp.

62. "Semiconductor Materials," Annual Report, December 1960-November 1961, Contract No. Nonr 1503(01), State University of New York College of Ceramics at Alfred University, Alfred, N. Y.

63. "Semiconductor Materials," Annual Report, December 1958-November 1959, Contract No. Nonr 1503(01), State University of New York College of Ceramics at Alfred University, Alfred, N. Y.

64. Greene, R. F., "Theory of Surface Thermoelectricity," Naval Ordnance Lab., December 15, 1960, Navord No. 6294, ASTIA AD No. 247 452.

65. Greiner, E. S. and Gutowski, J. A., "Electrical Resistivity of B-P Alloys," J. Appl. Phys., 30, 1842-1843 (1959).

66. "Electrical Resistivity of Boron," J. Appl. Phys., 28, 1364-1365 (1957).

67. Grodzinski, P., "Experiences in Low Load Hardness Testing," Microtechnic, 12 (4), 197-205 (1958).

68. "Testing Indentation and Abrasion Hardness of Hard Metals," Industrial Diamond Review, 16, 191-195, 228-233 (1956) and 17, 7-14, 29-35, 47-50, 70-74, 87-96, 106-114, 133-137 (1957).

69. "Micro-Indentation Hardness, Its Elastic, Plastic, and Fracture Components," Metallurgia, 50, 125-131 (1954).

70. "Micro-Indentation Hardness, A New Definition," Industrial Diamond Review, 12 (143), 209-218 (1952).

71. Gruber, B. A. (Monsanto Chemical Company), Process of Stabilizing Boron Phosphide and Resultant Article, U.S. Pat. 3,009,230, November 21, 1961.

72. Gruber, B. A.; Ruehrwein, R. A.; and Williams, F. V. (Monsanto Chemical Company), Boron Phosphide Articles and Coatings, U.S. Patent 3,090,703, May 21, 1963.

73. Gurevich, L., "The Phonon Drag in Metals," J. Phys. (USSR), 9, 477 (1945) and 10, 67 (1946).

74. Gurevich. M. A.; Epelbaum, V.A.; and Ormont, B. F., "Formation of the SiB_3 Phase in the Si-B System," Zhur. Neorg. Khim., 2, 206-208 (1957).

75. Hagenlocher, A. K., "Semiconductor Properties of Boron", in Boron, Synthesis, Structure, and Properties, pp. 128-134, edited by J. A. Kohn, W. F. Nye, and G. K. Gaule, Plenum Press, Inc., New York, 1960, 189 pp.

76. Hagg, G., "Powder Photographs of a New Iron Carbide," Z. Physikal Chem., B12, 33 (1931) and B44, 433 (1930).

77. Henderson, C. M. and Harris, D. M. (Monsanto Chemical Company), Thermoelectricity, U.S. Pat. 3,081,361, March 12, 1963, and U.S. Pat. 3,081,364, March 12, 1963.

78. Henisch, H. K., "Thermo-Electric Measurements on Semiconductors," Proc. Phys. Soc. (London), 64B, 1014 (1951).

79. "The Activation Energy of Disordered Semiconductors," Z. Physik. Chem., 198, 41-51 (1951).

80. Henry, N. F. M.; Lipson, H.; and Wooster, W. A., The Interpretation of X-ray Diffraction Photographs, MacMillan and Co., Ltd., London, 1951, 258 pp.

81. Herring, C., "Theory of the Thermoelectric Power of Semiconductors," Phys. Rev., 96, 1163-1187 (1954).

82. Hill, D. E. and Epstein, A. S. (Monsanto Chemical Company), Thermoelectricity, U.S. Pat. 3,077,506, February 12, 1963.

83. Hilsum, C. and Rose-Innes, A. C., Semiconducting III-V Compounds, Pergamon Press, New York, 1961, 239 pp.

84. Hoard, J. L. and Newkirk, A. E., "An Analysis of Polymorphism in Boron Based upon X-ray Diffraction Results," J. Am. Chem. Soc., 82, 70 (1960).

85. Hoard, J. L.; Geller, S.; and Hughes, R. E., "The Structure of Elementary Boron," J. Am. Chem. Soc., 73, 1892-1893 (1951).

86. Hoard, J. L.; Hughes, R.E.; and Sands, D. E., "The Structure of Tetragonal Boron," J. Am Chem. Soc., 80, 4507-4515 (1958).

87. Holden, S. J., Monsanto Research Fellowship Reports, Alfred University, Alfred, N. Y., 1958-1959, 5 pp.

88. Horn, F. H., "Simple Rhombohedral Boron: Preparation and Properties," in Boron, Synthesis, Structure, and Properties, pp. 110-115, edited by J. A. Kohn, W. F. Nye, and G. K. Gaule, Plenum Press, Inc., New York, 1960, 189 pp.

89. "Electrical and Optical Properties of Simple Rhombohedral Boron," J. Appl. Phys., 30, 1611-1612 (1959).

90. "The Crystallization of Simple Rhombohedral Boron from Platinum," J. Electrochem. Soc., 106, 905-906 (1959).

91. Hume-Rothery, W. and Raynor, G. V., The Structure of Metals and Alloys (Fourth Edition), Institute of Metals, London, 1962, 380 pp.

92. Ioffe, A. F., Physics of Semiconductors, Infosearch Ltd., London, 1960, 436 pp.

93. Semiconductor Thermoelements and Thermoelectric Cooling, Infosearch Ltd., London, 1957, 184 pp.

94. "Thermal Conduction in Semiconductors," Nuovo Cimento, 3 (10), Supplement No. 4, 702-715 (1956).

95. "Estimation of the Heat Conductivity of Semiconductors," Doklady Akad., Nauk, SSSR., 87, 369-372 (1952).

96. Jackson, J. S., "Hot Pressing High Temperature Compounds," Powd. Met., 8, 73-100 (1961).

97. Jacobs, H., and others, "Electrodeless Measurement of Semiconductor Resistivity at Microwave Frequencies," IRE Proc., 49, 928-932 (1961).

98. Jan, J. P., "Galvanomagnetic and Thermomagnetic Effects in Metals," in Solid State Physics (Volume V), pp. 1-96, edited by F. Seitz and D. Turnbull, Academic Press, Inc., New York, 1957, 455 pp.

99. Johnson, V. A. and Whitesell, W. J., "Theory of the Magnetoresistive Effect in Semiconductors," Phys. Rev., 89, 941-947 (1953).

100. Johnstone, H. L.; Hersch, H. N.; and Kerr, E. C., "Low Temperature Heat Capacities of Inorganic Solids V The Heat Capacity of Pure Elementary Boron in both Amorphous and Crystalline Conditions between 13° and 305°K," J. Am. Chem. Soc., 73, 1112-1117 (1951).

101. Kalinina, A. A. and Shamray, F. I., Abstracts of Papers and Communications to the Section on the Chemistry of Metals and Alloys of the Eighth Mendeleyev Congress of General Chemistry, Acad. Sci., USSR Press, 1958, 80 pp.

102. Kammerer, K., "The Description of Thermoelectric Phenomena by a Temperature-Entropy Diagram," Ann. Physik., 85, 948-958 (1928).

103. King, I. R., and others, "Preparation and Characterization of High-Purity Single-Crystal Boron," Texaco Experiment Inc., Final Report, March 1961-February 1962, Contract No. AF 33(616)-7884, Wright-Patterson AFB, January 1963, 47 pp.

104. Kingery, W. D., Property Measurements at High Temperatures, John Wiley and Sons, Inc., New York, 1959, 416 pp.

105. Kingery, W. D.; Woulbroun, J.M.; and Charvat, F. R., "Effects of Applied Pressure on Densification During Sintering in the Presence of a Liquid Phase," J. Am. Ceram. Soc., 46 (8), 391-395 (1963).

106. Kirk, R. E. and Othmer, D. F., Encyclopedia of Chemical Technology (Volume II), p. 585, Interscience Encyclopedia, Inc., New York, 1949.

107. Kittel, C., "Interpretation of the Thermal Conductivity of Glasses," Phys. Rev., 75 (6), 972-974 (1949).

108. Kmetko, E. A., "Effect of Ambients on the Thermoelectric Power and Conductance of Germanium Particle Aggregates," Phys. Rev., 99, 1642-1643 (1955).

109. Knarr, W. A., "Silicon Boron Phases and Determination of the Enthalpy of Vaporization and Formation of SiB_6," Univ. Microfilms, Mic. 60-1853, 1960, 131 pp.

110. Knoop, F.; Peters, C.G.; and Emerson, W. B., "A Sensitive Pyramidal-Diamond Tool for Indentation Measurements," J. Research NBS, 23, 39-61 (1939).

111. Knowlton, J. W. and May, M. S., "Manufacture of Boron Carbide by the Hot Mold Process," Ind. Heating, 26 (1), 142-150 (1959).

112. Kohn, J. A., "Crystallography of the Aluminum Borides," in Boron, Synthesis, Structure, and Properties, pp. 75-82, edited by J. A. Kohn, W. F. Nye, and G. K. Gaule, Plenum Press, Inc., New York, 1960, 189 pp.

113. "Survey of the Study of Hardness," Industrial Diamond Review (Volume 12), Supplement No. 1, 1952, 13 pp.

114. Kohn, J. A. and Eckart, D. W., "Aluminum Boride, AlB_{12}," Z. Krist., Bd 116, 134-142 (1961).

115. Kohn, J. A.; Gaule, G. K. and Giardini, A. A., High-Temperature Semiconductor Materials: Boron and Aluminum Borides, Proc. Second Army Sci. Conf., West Point, New York, 1959, 189 pp.

116. Kohn, J. A., Katz, G. and Giardini, A. A., "AlB_{10}, a New Phase, and a Critique of the Aluminum Borides," Z. Krist., 111 (1), 53-62 (1952).

117. Kohn, J. A.; Nye, W. F.; and Gaule, G. K., editors, Boron, Synthesis, Structure, and Properties, Plenum Press, Inc., New York, 1960, 189 pp.

118. Kraft, R., "Bibliography on the Measurement of the Hall Effect," Lawrence Radiation Laboratory, Livermore, California, Contract No. W-7405-eng-48, August 21, 1961, 40 pp.

119. Kranz, R., "Preparation and Properties of Boron Carbide," Keram. Z., 15 (8), 459-464 (1963).

120. "Boride Carbide," Hamburger Beitr. Angew. Mineral u. Kristall Physik., 2, 99-115 (1959).

121. Kroll, W., "Preparation of Amorphous Boron," Z. Anorg. Allgem. Chem., 102, 1-33 (1918).

122. Krumbein, W. C. and Pettijohn, F. J., Manual of Sedimentary Petrography, p. 325, Appleton-Century-Crofts, Inc., New York, 1938, 549 pp.

123. Kudryavtsev, V. I. and Sofronov, G. V., "Precision Lattice-Parameter Determination of Boron Carbide from $B_{2.75}C$ to $B_{8.75}C$ by X-ray Exposures Obtained in the Region of Large Angle Scattering (0 → 90°)," Trudy Seminara po Zharostoikim Materialam Akad. Nauk, Ukr. SSR. Inst. Mettallokeram i. Spetsial Splavov Kiev., No. 5, 52-64 (1960).

124. Lachman, J. C., "Thermocouples for Ultrahigh Temperatures," Metal Progr., 80 (1), 73-76 (1961).

125. Legrenaudie, J., "Dispersion in Frequency of the Conductivity of Boron and AlB_{12}," J. Phys. Radium, 16, 731-732 (1955).

126. "Properties of Boron," J. Phys. Radium, 14, 14-18 (1953).

127. "Semiconductor Compounds of Boron with Carbon and Aluminum," J. Chim. Phys., 50, 352-355 (1953).

128. "Electrical and Optical Properties of Boron," J. Phys. Radium, 13, 554-557 (1952).

129. LaPlaca, S. and Post, B., "The Boron Carbide Structure Type," Planseeber. Pulvermet., 9, 109-112 (1961).

130. Laubengayer, A. W.; Newkirk, A. E.; and Brandaur, R. L., "Progress in the Preparation and Determination of the Properties of Boron," J. Chem. Educ., 19, 382-383 (1942).

131. Lawson, W. D. and Nielson, S., Preparation of Single Crystals, p. 241, Academic Press, Inc., New York, 1958, 255 pp.

132. Lipscomb, W. N. and Britton, D., "Valence Structures in the Higher Borides," J. Chem. Phys., 33, 275-280 (1960).

133. Longuet-Higgins, H. C. and Roberts, M., "The Electronic Structure of an Icosahedron of Boron Atoms," Proc. Roy. Soc. (London), A230, 110-119 (1955).

134. McCarty, L. V. and Carpenter, D. R., "The Preparation of a New Crystalline Modification of Boron, and Notes on the Synthesis of Boron Triiodide," J. Electrochem. Soc., 107, 38-42 (1960).

135. McCarty, L. V., and others, "A New Crystalline Modification of Boron", J. Am. Chem. Soc., 80, 2592 (1958).

136. McClelland, J. D., "Plastic Flow Model of Hot Pressing," J. Am. Ceram. Soc., 44 (10), 526 (1961).

137. McQuarrie, M., "Thermal Conductivity VII Analysis of Variation of Conductivity with Temperature for Al_2O_3, BeO, and MgO," J. Am. Ceram. Soc., 37 (2), 91-95, Part II (1954).

138. Magnusson, B. and Brossett, C., "The Crystal Structure of $B_{2.89}Si$," Acta. Chem. Scand., 16, 449-455 (1962).

139. Matkovich, V. I., "Interstitial Compounds of Boron," J. Am. Chem. Soc., 83, 1804-1806 (1961).

140. "Unit Cell, Space Group, and Composition of a Lower Boron Sub-Phosphide," Acta. Cryst., 14, 93 (1961).

141. "A New Form of Boron Silicide, B_4Si," Acta Cryst., 13, 679-680 (1960).

142. Matkovich, V. I. and Economy, J., Aluminum Borides and Their Relation to Other Structures Involving Boron Icosahedra, 146th National ACS Meeting, Denver, Janusry 19-24, 1964. (Complete reference is not available at present.)

143. Mellor, J. W., A Comprehensive Treatise on Inorganic and Theoretical Chemistry (Volume 8), p. 844, Longmans Green and Co., New York, 1931, 1110 pp.

144. Meyerson, G. A. and Samsonov, G. V., "Fusibility Diagram of the B-C System and the Character of the Phases in this System," Izvest. Sektora Fiz-Khim. Analiza Inst. Obshchei i Neorg. Khim. Akad. Nauk. SSSR, 22, 92-103 (1953).

145. Meyerson, G. A., and others, "Solid Solutions in the B-Si-C System," Izvest. Akad. Nauk. SSSR. Otdel. Tekh. Nauk. Met. i Tophivo, No. 4, 90-94 (1961).

146. Mikheeva, V. I.; Shamrai, F.I.; and Krylova, E. Y., "Preparation of Amorphous Boron of a High Degree of Purity, I Reduction of Boric Anhydride by Light Metals, and III Refining of Amorphous Boron," Zhur. Neorg. Khim., 2, 1223-1231, 1242-1247 (1957).

147. Moissan, H. and Stock, A., Compt. Rend., Acad. Sci. Paris, 131, 139 (1900).

148. Moss, T. A., Photoconductivity in the Elements, pp. 75-95, Academic Press, Inc., New York, 1952, 263 pp.

149. Mott, B. W., Micro-Indentation Hardness Testing, Butterworths Scientific Publications, London, 1956, 272 pp.

150. Murray, P.; Livery, D.T.; and Williams, J., "The Hot Pressing of Ceramics," Chapter 17 in Ceramic Fabrication Processes, edited by W. D. Kingery, John Wiley and Sons, New York, 1958, 235 pp.

151. Naray-Szabo, St. V., "X-ray Investigation of AlB_{12}," Z. Kristallogr., 94, 367-374 (1936).

152. Naray-Szabo, St. V. and Tobias, C. W., "X-ray Powder Patterns of Boron Coated Mo and W Filaments," J. Am. Chem. Soc., 71, 1882 (1949).

153. Newkirk, A. E., "Preparation and Chemistry of Elementary Boron," in Symposium - From Borax to Boranes, pp. 27-41, Advances in Chemistry Series, American Chemical Society, Washington, D. C., 1961, 244 pp.

154. Niemyski, T. and Olempska, Z., "The Preparation of Pure Boron for Semiconductor Investigations," J. Less Common Metals, 4, 235-243 (1962).

155. Niemyski, T.; Olempska, Z.; and Sosnowski, F., "High Purity Boron for Semiconductor Research," in Ultrapurification of Semiconductor Materials, pp. 67-79, edited by M. S. Brooks and J. K. Kennedy, Macmillan Co., New York, 1962, 655 pp.

156. Nies, N. P.; Morgan, C.A.; and Jones, G. P. (U.S. Borax and Chemical Corporation), Borides by Electrolysis of Fused Salts, Brit. Pat. 861,743, February 22, 1961.

157. Norton, F. H. and Kingery, W. D., "Thermal Conductivity," J. Am. Ceram. Soc. (Part II), 37, 66-110 (1954).

158. Nowotny, H., "Advanced Experiments on Metal-Silicon-Boron and Metal-Carbon-Boron Systems," Technische Hochschule, Vienna, Final Technical Report, Contract No. DA 91-591-EUC-1810, June 30, 1962, ASTIA AD No. 278 041L.

159. Nyberg, D. W., "Electrodeless Techniques for Semiconductor Measurement," Canadian Jour. of Physics, 40, 1962, ASTIA AD No. 404 981.

160. O'Connor, J. R. and Smiltens, J., Silicon Carbide, Pergamon Press, New York, 1960, 521 pp.

161. Onsager, L., "Reciprocal Relations in Irreversible Processes," Phys. Rev., 37, 405 (1931).

162. Parthe, E. and Norton, J. T., "The Cell and Symmetry of So-Called Monoclinic AlB_{12}," Z. Krist., 110, 167-168 (1958).

163. Pasternak, R. A., "Crystallographic Evidence for the Existence of B_7O," Acta. Cryst., 12 (8), 612-613 (1959).

164. Pellekaan, T., Apparatus for Fusing Contacts onto Semiconductors, U.S. Pat. 2,979,024, April 11, 1961.

165. Peret, J. L., "Preparation and Properties of the Boron Phosphides," J. Am. Ceram. Soc., 47 (1), 44-46 (1964).

166. Perri, J. A.; LaPlaca, S.; and Post, B., "New Group III-Group V Compounds, BP and BAS," Acta. Cryst., 11, 310 (1958).

167. Pohl, H. A.; Bornmann, J.A.; and Itoh, W., "Semiconductors in Polymers," in Organic Semiconductors, pp. 134-158, edited by J. J. Brophy and J. W. Butrey, Macmillan Co., New York, 1962, 243 pp.

168. Popper, P. and Ingles, T. A., "Boron Phosphide, A III-V Compound of Zinc Blende Structure," Nature, 179, 1075 (1957).

169. Portnoi, K. I.; Samsonov, V.; and Solonnikova, L. A., "Alloys in the System B-Si-C," Zhur. Neorg. Khim., 5, 2032-2041 (1960).

170. Putley, E. H., The Hall Effect and Related Phenomena, Butterworths Scientific Publications, London, 1960, 263 pp.

171. Raybold, R. L., "Electroless Contacts on BP," Rev. Sci. Inst., 31, 781-782 (1960).

172. Ridgway, R. R., "Boron Carbide", J. Electrochem. Soc., 66, 1-16 (1934).

173. Ridgway, R. R. and Bailey, B. L. (Norton Company), Apparatus Suitable for Molding Boron Carbide, etc. under the Action of Heat and Pressure, U.S. Pat. 2,150,884, March 14, 1939.

174. Rizzo, H. F., "Oxidation of Boron between 400°C and 1300°C in Air," in Boron, Synthesis, Structure, and Properties, pp. 175-189, edited by J. A. Kohn, W. F. Nye, and G. K. Gaule, Plenum Press, Inc., New York, 1960, 189 pp.

175. Rizzo, H. F.; Simmons, W.C.; and Bielstein, H. O., "Existence and Formation of the Solid B_6O," J. Electrochem. Soc., 109 (11), 1079-1082 (1962).

176. Rizzo, H. F.; Wever, B.C.; and Schwartz, M. A., "Refractory Compositions Based on Si-B-O Reactions," J. Am. Ceram. Soc., 43, 497-504 (1960).

177. Rollier, M. A., "Lattice Dimensions of Elementary Boron," Proc. XIth Int. Cong. Pure Appl. Chem. (London), 5, 135-137 (1947). (Published 1953).

178. Ruehrwein, R. A. and Williams, F. V.(Monsanto Chemical Company), Crystallization of Boron Phosphide, U.S. Pat. 2,966,424, December 27, 1960.

179. Ruh, E. and McDowell, J. S., "Thermal Conductivity of Refractory Brick," J. Am. Ceram. Soc., 45 (4), 189-195 (1962).

180. Rundqvist, S., "Crystal Structure of BP," Cong. Intern. Chim. Pure et Appl. 16e Paris 1957 Mem. Sect. Chim. Minerale, 539-540 (Published 1958).

181. "Two Borides with the Cementite Structure," Nature, 181, 259-260 (1958).

182. Rupprecht, H., "Abnormal Temperature Dependence of Hall Coefficient of Slightly p-doped InAs," Z. Naturf., 13a, 1094 (1958).

183. Samsonov, G. V., Handbook on the Properties and Applications of High Melting Point Compounds, Literature on Ferrous and Nonferrous Metallurgy, State Scientific and Technical Press, Moscow, 1963.

184. "Thermophysical Properties of Alloys in the B-C-Si System," Poroshkovaya Met., No. 3, 53-62 (1961).

185. "The Modern Status of B-C System, Equilibrium Diagram," Zhur. Fiz. Khim., 32, 2424-2429 (1958).

186. Samsonov, G. V. and Neshpor, V. S., "Alloys of Rare Metals with Boron and Silicon for Some Radio and Electrotechnical Applications," Redkie Metally i Splavy Trudy Pervago Vsesoyuz; Soveshchaniza po Splavam Redkikh Metal., Akad. Nauk. SSSR, Inst. Met. im A. A. Baikov, Moscow, 392-417 (1957). (Published 1960).

187. Samsonov, G. V. and Portnoy, K. I., Alloys Based on High Melting Compounds, Translation by Foreign Technology Division WP-AFB, Ohio, FTD-62-430/1 & 2, July 24, 1962, ASTIA AD No. 283 859, 387 pp.

188. Samsonov, G. V. and Synelnykova, V. A., "On the Width of the Forbidden Gap in Boron Carbide," Ukrayinskyy Fizchnyy Zhurnal, 6 (5), 687-689 (1961).

189. Samsonov, G.V.; Zhuravlev, N.N.; and Amnuel, I. G., Fiz. Metal i Metalloved Akad. Nauk. SSSR. Ural Filial, 3, 309-313 (1956).

190. Sands, D. E. and Hoard, J. L., "Rhombohedral Elemental Boron," J. Am. Chem. Soc., 79, 5582-5583 (1957).

191. Schossberger, F. V., "Thin Films for Composite Molecular Electronics," Armour Research Foundation, IIT, Chicago, Final Report, December 1961, Contract No. AF 33(616)-6445, ASTIA AD No. 271 645.

192. Schulze, R., "Maximum Curves as Results of Sources of Error in Microhardness Testing," Metallober Flaeche, 8, A52-A54 (1954).

193. Secrist, D. R., "Phase Equilibria in the System Boron Carbide-Silicon Carbide," J. Am. Ceram. Soc., 47 (3), 127-130 (1964).

194. Serebryanskii, V. T. and Epelbaum, V. A., "Phase Diagram for the System Aluminum-Boron," Zhurnal Strukturnoy Khimii, 2 (6), 748-750 (1961).

195. Serebryanskii, V. T.; Epelbaum, V. A.; and Zhdanov, G. S., "Phase Diagram of the Al-B System," Dokl. Akad. Nauk. SSSR., 141, 884-886 (1961).

196. Shaw, M. C., "A Yield Criterion for Ductile Metals Based upon Atomic Structure," Journal of the Franklin Institute, 254, 109-126 (1952).

197. Shaw, W. C.; Hudson, D.E.; and Danielson, G. C., The Electrical Properties of Crystalline Boron, U.S. Atomic Energy Commission, ISC-380, 1953, 152 pp.

198. "Electrical Properties of Boron Single Crystals," Phys. Rev., 107, 419-427 (1957).

199. "Some Electrical Characteristics of Crystalline Boron," Phys. Rev., 89, 900 (1953).

200. Shilliday, T. S., "Thermoelectric Power Generation and Related Phenomena," Battelle Institute, Final Report, May 15, 1961, Contract No. Nobs-77034, ASTIA AD No. 265 147.

201. Sizelove, J. R., "Band Gap and Mobility Arrays for Binary Compounds," Electronic Technology Laboratory, Wright-Patterson AFB, November 1961, Project 4159, Contract No. ASDTN 61-149, ASTIA AD No. 271 955.

202. Slaughter, J. I. and Margrave, J. L., "Temperature Measurement," Aerospace Corporation, Report No. TDR-169 (3240-20) TN-1, October 30, 1962, Contract No. AF 04(695)-169, ASTIA AD No. 298 142.

203. Small, L., Hardness-Theory and Practice (Part I: Practice), Service Diamond Tool Company, Ferndale, Michigan, 1960, 549 pp.

204. Spinar, L. H. and Wang, C. C., "The Crystal Structure of Tridecaboron Diphosphide," Acta. Cryst., 15, 1048 (1962).

205. Stadelmaier, H. H. and Yun, T. S., "Concerning Ternary Borides with Chromium Carbide, $Cr_{23}C_6$, Structure," Z. Metallk., 53, 754-756 (1962).

206. Starks, R. S., in "Research Investigations in the Physical Chemistry and Metallurgy of Semiconducting Materials," edited by J. F. Musgrave, Eagle-Picher Research Laboratories, Final Report, Contract No. DA 36-039-SC-85131, May 15, 1962, ASTIA AD No. 277 480.

207. Stone, B. D. (Monsanto Chemical Company), Process for the Production of Large Single Crystals of Boron Phosphide, U.S. Pat. 3,009,780, November 21, 1961.

208. (Monsanto Chemical Company), Cubic-Crystalline Boron Phosphide, Germ. Pat. 1,105,858, U.S. Appl. June 29, 1960.

209. Stone, B. D. and Hill, D., "Semiconducting Properties of Cubic Boron Phosphide," Phys. Rev. Letters, 4, 282 (1960).

210. Stone, B. D. and Ruehrwein, R. A. (Monsanto Chemical Company), Production of Single Crystal Boron Phosphide, U.S. Pat. 3,073,679, January 15, 1963.

211. (Monsanto Chemical Company), Production of Single Crystal Boron Phosphide, U.S. Pat. 3,073,679, January 15, 1963.

212. Stone, B. D., and others, Thermodynamic Properties of Cubic BP and of Rhombohedral B_6P, Ultrapurif. Semicond. Mater. Proc. Conf., Boston, 1961, pp. 645-651, MacMillan Co., New York, 1962, 655 pp.

213. Stroh, A. N., "The Formation of Cracks in Plastic Flow II," Proc. Roy. Soc. (London), 223A (1191), 548-560 (1955).

214. "The Formation of Cracks as a Result of Plastic Flow," Proc. Roy. Soc. (London), 223A (1191), 548-560 (1955).

215. Stuckes, A. D. and Chasmar, R. P., "Measure of Thermal Conductivity of Semiconductors," in the Report of the Rugby Conference on Semiconductors, pp. 119-125, Phys. Soc., London, 119, 119-125 (1956).

216. Talley, C. P., "Preparation of Single Crystal Boron," J. Appl. Phys., 32, 1787-1788 (1961).

217. "Th mal Conductivity of Polycrystalline Boron," J. Phys. Chem., 63, 311 (1959).

218. Talley, C. P.; LaPlaca, S.; and Post, B., "A New Polymorph of Boron," Acta. Cryst., 13, 271 (1960).

219. Talley, C. P.; Line, L.F.; and Overman, Q. D., "Preparation and Properties of Massive Amorphous Elemental Boron," in Boron, Synthesis, Structure, and Properties, p. 94, edited by J. A. Kohn, W. E. Nye, and G. K. Gaule, Plenum Press, Inc., New York, 1960, 189 pp.

220. Talley, C. P.; Post, B.; and LaPlaca, S., "A New Modification of Elemental Boron," in Boron, Synthesis, Structure, and Properties, pp. 83-85, edited by J. A. Kohn, W. F. Nye, and G. K. Gaule, Plenum Press, Inc., New York, 1960, 189 pp.

221. Tarasov, N. D., Hot Molded Carbide Articles Free of Pores, USSR Pat. 116,456, January 19, 1959.

222. Taylor, R. E., "Thermal Conductivity and Expansion of Beryllia at High Temperatures," J. Am. Ceram. Soc., 45 (2), 74-78 (1962).

223. Taylor, W. J., and others, "Electrical Properties of High-Purity Boron," The Ohio State University Research Foundation, Columbus, Ohio, July 1961, 170 pp., ASTIA AD No. 265 266.

224. Thomas, A. G. and Jones, H. J., "Hot Pressing of Ceramic Powders," Powder Met., 6, 160-169 (1960).

225. Tipton, C. R., editor, Reactor Handbook, p. 1159, Interscience Publishers, Inc., New York, 1960, 1207 pp.

226. Turovtseva, Z. M. and Kunin, L. L., Analysis of Gases in Metals, Consultants Bureau, New York, 1959, 374 pp.

227. Tweet, A. G., "Properties of Grain Boundaries in Gold-Doped Germanium," Phys. Rev., 99, 1182-1189 (1955).

228. Uno, R., "On the Electrical Properties of Polycrystalline Boron," J. Phys. Soc. (Japan), 13 (7), 667-675 (1958).

229. VanBueren, H. G., Imperfections in Crystals, North-Holland Publishing Company, Amsterdam, 1960, 675 pp.

230. VanWazer, J. R., Phosphorous and Its Compounds, Volume I, Chemistry, Interscience Publishers, 1961, 954 pp.

231. Vickery, R. C., "Synthesis of Boron Phosphide and Nitride," Nature, 184, Suppl. No. 5, 268 (1959).

232. Vuillard, C., "Boron Carbide Crystals," Compt. Rend., 257 (25), 3927-3929 (1963).

233. Weibull, W., "Investigations into Strength Properties of Brittle Materials," Proc. Ing. Vetenskaps Akademien, Stockholm, No. 151, 1939.

234. Weintraub, E., "Boron: Its Properties and Preparation," J. Ind. & Eng. Chem., 5, 106-115 (1913).

235. Welker, H. and Weiss, H., "Group III-V Compounds," in Solid State Physics (Volume III), edited by F. Seitz and D. Turnbull, Academic Press, Inc., New York, 1956, 588 pp.

236. Wentorf, R. H., "Synthesis of the Cubic Form of Boron Nitride," J. Chem. Phys., 34, 809-812 (1961).

237. "Cubic Form of Boron Nitride," J. Chem. Phys., 26, 956 (1957).

238. Westgren, A., "Crystal Structure and Atomic Properties of Alloys Containing Transition Elements," J. Franklin Institute, 212, 577 (1931).

239. Whelan, J. M., "Properties of Some Covalent Semiconductors," in Semiconductors, pp. 389-436, edited by N. B. Hannay, Reinhold Publishing Co., New York, 1959, 767 pp.

240. Will, G., "On the Crystal Structure of AlB_{12}," J. Am. Chem. Soc., 85, 2335 (1963).

241. Willardson, R. K. and Goering, H. L., editors, Compound Semiconductors, Volume I - Preparation of III-V Compounds, Reinhold Publishing Co., New York, 1963, 576 pp.

242. Williams, D. N., Properties of Boron, U.S. Dept. Comm., Off. Tech. Services, PB Rept. 161 191, 1960, 9 pp.

243. Williams, F. V. (Monsanto Chemical Company), Process for Preparing Boron Phosphide, U.S. Pat. 3,094,387, June 18, 1963.

244. (Monsanto Chemical Company), Process for the Production of Boron Phosphide, U.S. Pat. 2,984,577, May 16, 1961.

245. "High Temperature Transistors," Ceramic and Engineering News, 37 (16), 60, April 20, 1959.

246. (Monsanto Chemical Company), Crystalline Boron Arsenide, Germ. Pat. 1,109,655, U.S. Appl. July 18, 1959.

247. Williams, F. V. and Ruehrwein, R. A. (Monsanto Chemical Company), Boron Phosphide, U.S. Pat. 2,966,426, December 27, 1960.

248. "Preparation and Properties of Boron Phosphides and Arsenides," J. Am. Chem. Soc., 82, 1330-1332 (1960).

249. Williams, F. V.; Ruehrwein, R.A.; and Hill, D. E. (Monsanto Chemical Company), Diodes, U.S. Pat. 3,022,452, February 20, 1962.

250. Williams, F. V.; Ruehrwein, R.A.; and Moeller, T. (Monsanto Chemical Company), Boron Phosphide, U.S. Pat. 2,974,064, March 7, 1961.

251. Williams, S. R., Hardness and Hardness Measurements, Am. Soc. Metals, Cleveland, 1942, 558 pp.

252. Wood, C. and Bocciarelli, C. V., "Intermetallic Compounds," Philco Corporation, Quarterly Progress Rept. No. 2, ASTIA AD No. 146 065P.

253. Wray, K. L. and Connolly, T. J., "Thermal Conductivity of Clear Fused Silica at High Temperatures," J. Appl. Phys., 30 (11), 1702-1705 (1959).

254. Zhdanov, G. S. and Sevast'yanov, N. G., "X-ray Investigation of the Structure of B_4C," J. Phys. Chem. (USSR), 17, 326-335 (1943).

255. "Crystal Structure of B_4C," Compt. Rend. Acad. Sci. (URSS), 32, 432-434 (1941).

256. Zhdanov, G. S.; Zhuravlev, N.N.; and Zevin, L. S., "Rontgenographic Establishment of Formation of Solid Solution in Boron Carbide," Doklady Akad. Nauk. SSSR., 92, 767-768 (1953).

257. Zhdanov, G. S., and others, "Solubility of Boron and Carbon in Boron Carbide $B_{12}C_3$ (B_4C)," Zhur. Fiz. Khim., 28, 1076-1082 (1954).

258. Zhuravlev, N. N., and others, "Properties and Phase Composition of Alloys of Boron with Carbon," Izvest. Akad. Nauk. SSSR. Otdel. Tekh. Nauk. Met. i Toplivo, No. 1, 133-141 (1961).

DISTRIBUTION LIST FOR FINAL REPORT -- CONTRACT Nonr 1503(01)
Alfred University, Alfred, New York

Director 6
Advanced Research Projects Agency
The Pentagon
Washington, D. C. 20025

Institute of Science and Technology
The University of Michigan
Box 618
Ann Arbor, Michigan 48103
ATTN: IRIA

J. Jerger
Servo Corporation
Hicksville, New York 11800

N. J. Kreidl
Bausch and Lomb Optical Company
Rochester, New York 14602

Department of the Navy
Chief, Bureau of Ships
Washington, D. C. 20025
ATTN: Code 687 C, Mr. Woodside

Commanding General
Signal Corpos Engineering Laboratories
Belmar, New Jersey 07719
ATTN: Physical Optics, Mr. Daniel F. Kelly

A. Smakula
Massachusetts Institute of Technology
Cambridge, Massachusetts 02139
Laboratory for Insulation Research

Commander
Aeronautical Systems Division
/ASRNRS-3/
Wright-Patterson Air Force Base, Ohio 45433

Commander
Air Force Space Systems
Division /SSPRE/
Air Force Unit Post Office
Los Angeles, California 90045

Commanding General
U. S. Combat Surveillance Agency
1124 N. Highland Street
Arlington, Virginia 22200
ATTN: Mr. A. L. Webb

Prof. Bruce Crawford
Department of Chemistry
University of Minnesota
Minneapolis, Minnesota 55414

Commanding Officer
Diamond Ordnance Fuze Lab
Washington, D. C. 20025
ATTN: Mr. Charles Ravitsky

Commanding General
Engineer R and D Labs
Fort Belvoir, Virginia 22060
ATTN: Far Infrared Branch
Dr. W. Weihe

Battelle Memorial Institute
505 King Avenue
Columbus, Ohio 43201
ATTN: BMI-DEFENDER

Chief, Naval Ordnance Lab
White Oak
Silver Spring, Maryland 20900
ATTN: L. C. Lanahan

Research Division
Eastmand Kodak Hawkeye Works
St. Paul Street and Avenue E
Rochester, New York 14600

G. J. Su
University of Rochester
Rochester, New York 14620
Chemical Engineering Dept.

R. J. Sneed
Section Head
Physics and Infrared Section
General Dynamics/Pomona
Pomona, California 91766

Commanding Officer
U. S. Naval Ordnance Lab
Corona, California 91720

Director
U. S. Army Engineering R and D Labs
Fort Belvoir, Virginia 22060
ATTN: Technical Documents Center

Office of the Director of Defense 2
Defense Research and Engineering
Information Office Library Branch
Pentagon Building
Washington, D. C. 20025

U. S. Army Research Office 2
Box CM, Duke Station
Durham, North Carolina 27700

Defense Documentation Center 20
Cameron Station
Alexandria, Virginia 22314

Director 6
U. S. Naval Research
Technical Information Officer
Code 2000, Code 2021
Washington, D. C. 20025

Commanding Officer
Office of Naval Research Branch Office
230 N. Michigan Avenue
Chicago, Illinois 60600

Commanding Officer
ONR Branch Office
207 W. 24th Street
New York, New York 10011

Chief of Naval Research 3
Office of Naval Research
ATTN: Physics Branch
Washington, D. C. 20025

Commanding Officer
ONR Branch Office
1000 Geary Street
San Francisco, California 94109

Air Force Office of Scientific Research
Washington, D. C. 20025

Director
National Bureau of Standards
Washington, D. C. 20025

Director
Research Department
U. S. Naval Ordnance Laboratory
White Oak, Silver Spring, Maryland 20900

Commanding Officer
ONR Branch Office
1030 East Green Street
Pasadena, California 91101

Commanding Officer
ONR Branch Office
495 Summer Street
Boston, Massachusetts 02110

Dr. Gerard F. W. Mulders
Head, Astronomy Section
National Science Foundation
1951 Constitution Ave., NW
Washington, D. C. 20550

Dr. Robert Fleischer
Program Director for Solar-
Terrestrial Res.
National Science Foundation
Washington, D. C. 20550

Head
Section for Atmospheric Sciences
National Science Foundation
Washington, D. C. 20025

Commanding Officer
U. S. Army Materials Research Agency
ATTN: Technical Library
Watertown, Massachusetts 02172

Boulder Laboratories
National Bureau of Standards
ATTN: Library
Boulder, Colorado 80301

Dr. A. R. Hilton
Texas Instruments, Inc.
Research Building
13500 North Central Expressway
Dallas, Texas 75200

Chief, Bureau of Naval Weapons
Department of the Navy
Washington, D. C. 20025
ATTN: S. J. Gorman, RRRE-31

AF Cambridge Res. Laboratories
ATTN: CRXL-R, Research Library
Lawrence G. Hanscom Field
Bedford, Massachusetts 01730

ONR Branch Office
Federal Building
Church and Fitzhugh Streets
Rochester, New York 14614